Dependent Degradation-based Maintenance Modelling of Offshore Wind Turbine Pitch Systems

MSc SET Thesis

Akshay Antrolia

Delft University of Technology

TNO innovation for life

Dependent Degradation-based Maintenance Modelling of Offshore Wind Turbine Pitch Systems

by

Akshay Antrolia

to obtain the degree of Master of Science in Sustainable Energy Technology
at Delft University of Technology.
To be defended publicly on Monday 26th August, 2024 at 13:00.

Research carried out at:

Wind Energy Group, Faculty of Aerospace Engineering, Delft University of Technology

Wind Energy Group, TNO (Netherlands Organisation for Applied Scientific Research)

Project Duration: December 2023 - August 2024
Student Number: 5779286

Thesis Committee:

Prof. Dr. Simon Watson	Wind Energy, Aerospace Engineering
Dr.ir. Xiaoli Jiang	Transport Engineering and Logistics, Mechanical Engineering
Dr. Donatella Zappalá	Wind Energy, Aerospace Engineering
Dr. Simone Mancini	Wind Energy, TNO

An electronic version of this thesis is available at https://repository.tudelft.nl/

TU Delft

Abstract

A key hurdle to meet the ambitious renewable energy targets is the high levelized cost of offshore wind energy. With Operations and Maintenance (O&M) actions making up more than a quarter of the total costs, substantial research efforts have been undertaken to optimize these actions. In line with this overarching goal, this project focuses on O&M actions, specifically optimizing time-based maintenance strategies to minimize costs. Literature reveals a variety of methods developed, such as Remaining Useful Life (RUL) models, degradation models, reliability models and maintenance models to simulate Wind Turbine (WT) lifetimes, O&M actions and calculate costs. A majority of these studies only look at single failure modes (FM) or multiple independent FMs. In the field of wind energy, there is a significant lack of research on failure interactions and degradation dependence between different components or FMs. This project aims to build a model that accounts for dependencies in degradation between different FMs. This model is further combined with a maintenance model to simulate maintenance actions and estimate corresponding O&M costs.

The proposed degradation-based maintenance model builds on a simplified in-house model developed by the Wind Energy group at TNO. A Markov model, built in Python, is used to represent the degradation process. This is further combined with copula functions to represent degradation dependencies, using available copula packages in Python. Inspection and maintenance functions are then integrated into the degradation model to simulate O&M actions within the WT lifetime. Each action incurs either one or a combination of costs due to inspection, maintenance or operation, from WT downtime. An extensive number of time-based strategies are modelled, with varying inspection intervals for each. Finally, the accumulated lifetime costs are calculated and compared for the various maintenance strategies. The inspection interval with the minimum lifetime costs is selected as the optimum maintenance strategy. In order to verify the validity of the proposed model, the results of an existing research paper on degradation modelling for WT blades are first replicated.

After successful verification, case studies are carried out to apply the model to the degradation processes of offshore wind turbine (OWT) hydraulic pitch systems. This is an extremely critical system, crucial for both WT operation and safety with the highest failure rates among all WT systems. The case studies selected in this work cover two pitch FMs: hydraulic fluid leakage and hydraulic valve wear. The model is applied to the case of single FMs and the case of multiple FMs, both independent and dependent. For both the single FM models, different optimum inspection intervals and lifetime costs are obtained. A higher failure rate for one of the FMs is the basis for the increased optimum lifetime cost and the decreased optimum inspection interval. Comparing the direct summation of the results of two single FM models with the multiple FM independent model outputs dissimilar results. The independent model leads to a reduced inspection interval and slightly higher lifetime costs. For the dependent case, a 39% reduction in the lifetime costs and an increase in the optimal inspection interval is observed compared to the independent case. This results in cheaper and less frequent O&M actions for the dependent case.

This work shows that, compared to the other case studies, modelling dependency between FMs allows for improved O&M actions, resulting in lower costs. This methodology has the potential to be used in future multi-component or multi-FM studies. The inclusion of degradation dependencies between components would better model the inter-dependencies between FMs and hence allow for improved optimization of O&M strategies.

Delft, August 2024

Acknowledgements

I cannot begin to express my thanks to my supervisors Dr. Donatella Zappalá, Dr. Yichao Liu and Dr. Simone Mancini. From hiring me for this thesis position to brainstorming with me every step of the way, I am deeply indebted to you - for your time, efforts and patience. I have also had the pleasure of working with some amazing people at TNO with whom I've had many interesting conversations; from birds hitting wind turbines to camping in the Norwegian wilderness.

As I bring an important chapter in my life to a close, I now understand how difficult it is to write a thank-you speech. To anyone I might miss, know that I hold dear the times we spent together. To my family, I'm extremely grateful for your support with all that I decide to do. To my friends, both here and back home, thank you for all the laughs, the phone calls, the hugs - both real and virtual and the love. Special mentions to Rishikesh, Jayant, Aravind, Anand, Tanya, Savion, Pushkar, Esha, Samiksha, Achintya and Shubh. Thank you for your relentless support, helpful advice and guidance. To my housemates, Vibhor, Vanshika and Aparna, I appreciate the house over my head while I write this, the food on my plate these last few days and your constructive criticisms.

Delft, August 2024

Contents

List of Figures

List of Tables

Nomenclature

Abbreviations

Abbreviation	Definition
AEP	Annual Energy Production
AGAN	As Good As New
CI	Confidence Interval
CM	Corrective Maintenance
CdM	Condition based Maintenance
COP	Conference of Parties
CTMC	Continuous Time Markov Chains
CTV	Crew Transfer Vessel
CV	Coefficient of variation
DT	Downtime
DTMC	Discrete Time Markov Chains
FM	Failure Mode
LCOE	Levelized Cost of Electricity
MCMC	Markov Chain Monte Carlo
MTTF	Mean Time to Failure
O&M	Operations and Maintenance
OPEX	Operational Expenditure
OWT	Offshore Wind Turbine
PDF	Probability Density Function
PM	Preventive Maintenance
RUL	Remaining Useful Life
SSM	System State Matrix
TM	Time based Maintenance
WT	Wind Turbine

Symbols

Symbol	Definition	Unit
C_{CM}	Corrective Maintenance costs	[€]
C_e	Cost of electricity	[€]
C_I	Cost of inspection	[€]
C_l	Cost of technicians	[€]
C_M	Cost of maintenance	[€]
C_O	Cost of operation	[€]
$C_{PM,m}$	Minor preventive Maintenance costs	[€]
$C_{PM,M}$	Major preventive Maintenance costs	[€]
C_r	Cost of component repair or replacement	[€]
C_v	Costs of labour	[€]
cf	Capacity factor	[-]
$E[X]$	Expectation of function	[-]
S	System state	[-]
m, n	Time	[*Years*]

Symbol	Definition	Unit
n	Monte Carlo sample size	[-]
n_l	Number of technicians	[-]
P	Transition probability matrix	[-]
P	Wind turbine power rating	[*MW*]
P_{ij}	Transitional probability from state i to state j	[-]
$P(X\|Y)$	Conditional probability of event X given event Y	[-]
T_d	Downtime duration	[*hours*]
T_{hor}	Simulation horizon	[*years*]
T_i	Inspection intervals	[*years*]
T_I	Inspection duration	[*hours*]
T_{lead}	Lead time duration	[*days*]
T_{Mi}	Maintenance duration for state i	[*hours*]
t_n	Time event n	[*years*]
T_{Si}	Sojourn time in state i	[*years*]
T_{travel}	Travel time	[*hours*]
$T_{weather}$	Harsh weather condition duration	[*days*]
w	Weight factor	[-]
X	Markov process	[-]
δ	Discount rate	[*%*]
λ	Transition rate	[*1/years*]
$\lambda_{i,j}$	Transition rate from state i to state j	[*1/years*]
μ	Mean	[-]
π_i	Probability of incorrect detection	[-]
π_{ri}	Probability of incorrect repair	[-]
$\pi_{weather}$	Probability of harsh weather conditions	[-]
σ	Standard deviation	[-]
θ	Copula correlation coefficient	[-]

1 Introduction

1.1. Climate Change & Wind Energy

Climate change issues were first raised at the United Nations Scientific Conference, held in Stockholm in 1972 (UN Chronicle, 2007). However, the issue was not the central concern of the United Nations, with the focus being water resources, deforestation, and marine mammals, among others. It was in 1988 that climate change took centre stage with the formation of the Intergovernmental Panel on Climate Change. From key Conference of the Parties (COP) events in Kyoto 1997 to Paris 2015, climate targets have been updated and policies have been reformed. (Climate Brief, 2020). One of these was the Paris Agreement, a legally binding international treaty to limit global temperature rise in this century to well below 2° C above pre-industrial levels and to pursue efforts to limit the temperature increase even further to 1.5°C. While the agreement required countries to submit and meet their individual nationally determined contributions in the short term, the long-term low greenhouse gas emission development strategies were not mandatory to be met (UNFCCC, 2021). In July 2021, the European Climate law came into effect, legally obliging the European Union countries to meet their 2030 and 2050 climate goals (European Council, 2024b). A target of at least 40% renewable energy in Europe's energy market by 2030 has been established (European Council, 2024a). However, in reality, this still seems a long way away. According to Reuters (2023), the world climate is on track to warm by nearly 3°C this century, largely missing the goal set by the Paris Agreement. Despite this, the recent 2023 COP28 held in Dubai remains hopeful of meeting the Paris Agreement targets (UNFCCC, 2023a). The conference concluded that a 43% reduction in greenhouse gas emissions, compared to 2019 levels, is required by 2030 to limit global warming to 1.5° C. The United Nations Climate Change Executive Secretary Simon Stiell mentioned in his closing speech for COP28, "Tripling renewable and doubling energy efficiency [...] need to turn these pledges into real economy outcomes" (UNFCCC, 2023b). The International Energy Agency further doubles down on this target stating that the "single most important lever to bring about reduction in carbon dioxide emissions is to triple the global installed renewable power by the end of 2030" as shown in Figure 1.1 (IEA, 2023b).

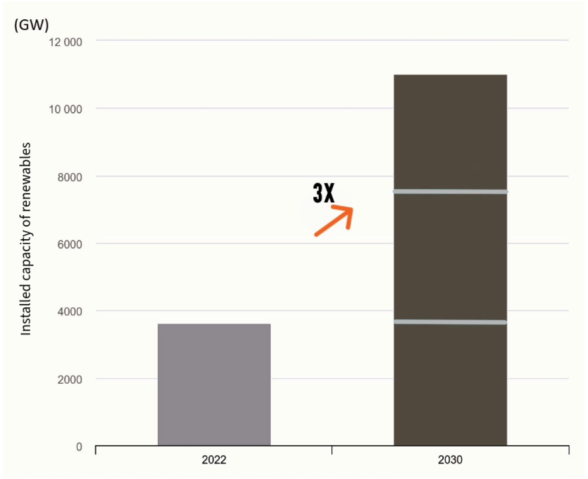

Figure 1.1: Global renewable power capacity in 2022 and 2030, as per Net Zero Emissions by 2050 scenario (IEA, 2023b)

In order to meet this target, large strides have been made in expanding renewable energy capacity. In 2022, the renewable power capacity added worldwide increased by almost 13% (IEA, 2023b). This

growth rate was expected to reach up to 33% in 2023 but has only increased to approximately 15%. Furthermore, renewable electricity generation is set to overtake energy generation by coal in early 2025. Solar and wind energy lead the current rapid global expansion of renewable power capacity with solar photovoltaic accounting for two-thirds of the increase in 2023 (IEA, 2023a). Solar photovoltaic production capacity is set to double to almost 550 GW by 2028 compared to 2022. This growth is adequate to meet the annual solar energy demand as envisioned in the International Energy Agency's Net Zero Emissions by 2050 Scenario. However, the same cannot be said for wind power. Compared to solar photovoltaics, Wind turbine (WT) installation growth is not fast enough to meet the current demand. Although 2020 saw the highest increase of 95.3 GW in year-on-year wind power installations, Figure 1.2 shows that this growth has slowed down in the last couple of years. This is primarily due to COVID-19 and supply chain issues (GWEC, 2023). Increased commodity prices and supply chain challenges are reducing the profitability of WT manufacturers. Despite these factors, the market still has a positive outlook, with wind power additions rebounding sharply to a value of 116 GW in 2023 (WWEA, 2024). A total of 1221 GW of new wind power capacity is expected to be built between 2023-2030. This ambitious goal comes with its own set of challenges.

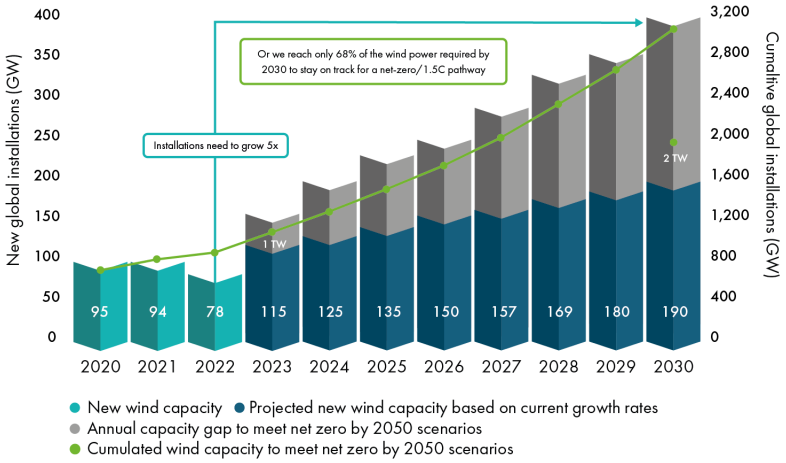

Figure 1.2: Wind energy growth trends (GWEC, 2023)

Veers et al. (2019) and Veers et al. (2023) discuss the grand challenges associated with wind energy, particularly in the design, manufacturing and operation of future WT systems. Multiple key challenges are articulated such as:

1. Improved understanding of the physics of atmospheric flow
2. Integration of wind power into the future electricity grid
3. Reassessing design processes against limits of applicability for the size of future turbines
4. Additional motion and hydrodynamic loads on Offshore Wind Turbines (OWTs)
5. Uncertainty in turbine wakes
6. Integration of improved materials in the manufacturing of larger-than-ever components

In addition to the challenges, key goals that must be a part of WT development are also delved into (Veers et al., 2023).

1. Economic optimization across all stages in holistic life cycle assessment
2. Designing with nature to minimize the negative impacts on the environment
3. Seamless integration with alternative energy generation and storage sources
4. Shortening the design cycle

Most of the challenges described above can be boiled down to the key goal of economic optimization across all life-cycle stages for a WT. In the design phase, a clearer understanding of the physics of the

atmospheric flow will allow for the design of larger turbines, which, in turn, reduces the Levelized Cost of Electricity (LCOE) of wind energy. Similarly, an in-depth study on WT wakes and wake interactions will aid in improving the control strategy during the operation stage of WTs. An improved control strategy will output higher annual energy production (AEP) and thus, a reduced LCOE. Advanced maintenance strategies aid in reducing the costs associated with the maintenance of WTs and reduce the LCOE of wind energy. It is evident that one of the main objectives for improving wind energy is economic optimization. In line with this goal, this thesis aims to contribute to diminishing the LCOE of wind energy.

1.2. Cost of Wind Energy

The entire process of wind farm design has enormous costs associated with it. As a result, most wind farms are currently built with the help of government subsidies. However, with increasing economies of scale and continuous improvements in the field, wind energy costs are declining. By the end of 2023, the world's first-ever subsidy-free wind farm, Hollandse Kurt Zuid, become operational in the North Sea, off the coast of the Netherlands (Government of the Netherlands, 2020).

Equation 1.1 presents the equation for LCOE of wind energy (C. Dao et al., 2019).

$$LCOE = \sum_{n} \frac{\frac{CAPEX + OPEX_n}{(1+\delta)^n}}{\frac{AEP_n}{(1+\delta)^n}} \tag{1.1}$$

where CAPEX is the capital expenditure, OPEX is the operational expenditure, AEP is annual energy production, δ is the discount rate and n is the year. It is observed that along with capital and operational costs, AEP also affects the LCOE. To reduce the LCOE, either the costs can be lowered or the AEP can be increased. Reduction in costs can be undertaken in a diverse number of ways. For example, utilising alternative materials which are cheaper or less prone to deterioration will reduce material costs. Manufacturing costs can be decreased with enhanced manufacturing techniques to reduce expensive labour work. Quick logistics of spare parts can successfully minimize delays in installation and maintenance actions and reduce operation costs. On the other hand, the AEP is maximised by ensuring that a WT remains functional and produces energy as often as feasible. This can be achieved by improving the reliability of a WT. Reliable systems require fewer maintenance actions which reduces the OPEX as well as increases the AEP, which contributes to a reduced LCOE.

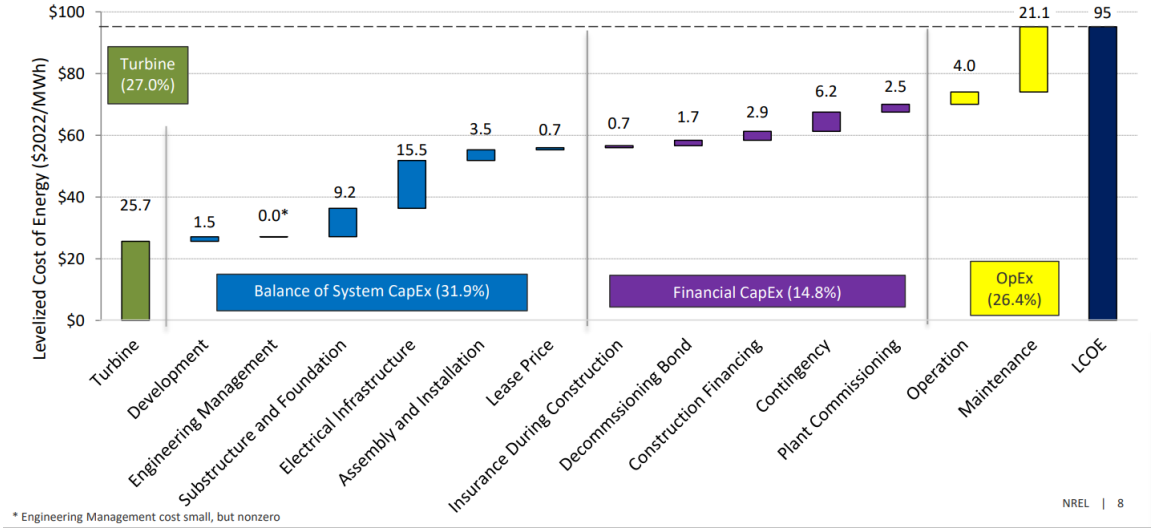

Figure 1.3: LCOE breakdown for fixed-bottom offshore wind plants (NREL, 2022)

Accounting for the different life-cycle stages, a comprehensive breakdown of LCOE for bottom-fixed

OWT is shown in Figure 1.3 (NREL, 2022). It is seen that Operations and Maintenance (O&M) activities correspond to a large proportion of the total cost, slightly higher than 25%.

A detailed review conducted by Welte et al. (2018) showed that O&M costs make up 12-32% of wind farm costs, with an average value of 25%. Shafiee and Sørensen (2019) equated this cost to around 75-90% of the initial investment for a wind farm. These are only direct O&M costs and do not include indirect costs due to wind farm unavailability which would lead to even higher figures. Analysing these costs further, NREL (2022) provides a breakdown of the OPEX for bottom-fixed and floating offshore wind farms, shown in Table 1.1. The OPEX are seen to have the largest contribution from the equipment and vessels required to perform maintenance. Vessels usually have high renting rates and include Crew Transfer Vessels (CTVs), cable lay vessels, diving support vessels and jack-up vessels. Other costs include labour costs for all technicians who carry out inspection and maintenance actions, material costs for repairs and spare parts, insurance fees for all assets and port fees for usage of the port for all O&M actions.

Table 1.1: OPEX breakdown for fixed-bottom and floating offshore wind plants (NREL, 2022)

Parameter	Fixed Value ($/kW-yr)	Floating Value ($/kW-yr)
Maintenance	**91**	**56**
Labor(technicians)	4	4
Materials	2	3
Equipment (vessels)	85	49
Operations	**17**	**30**
Management administration	2	2
Port fees	1	14
Insurance	15	15
Total OpEx	**108**	**87**

Furthermore, with quick advancements in WT design, turbine sizes are rapidly increasing. Wind farms are steadily being shifted to far-offshore locations for the advantages of higher wind speeds and lower public resistance. However, OWTs face higher degradation from the higher wind speeds and have lower accessibility as compared to their onshore counterparts (C. Dao et al., 2019). This means maintenance actions will get even more costly and complex in the future. With increasing WT sizes, larger and higher lifting capacity vessels are required. Such state-of-the-art vessels are limited in number and there are often delays in arranging for and renting them. Despite these increases in costs, wind farm owners and operators are coming under increasing pressure to reduce O&M costs (Shafiee and Sørensen, 2019). Thus, to minimize operation and maintenance delays and to lower the LCOE of wind energy, effective planning of maintenance activities and management of offshore wind energy assets plays a key role. Minimization of these costs is the need of the hour to make wind energy more viable for the future (C. D. Dao et al., 2021). This is the overarching goal of this thesis project: to contribute to the reduction of O&M costs through improved maintenance strategies.

1.3. Degradation & Failure

A WT is a complex system consisting of thousands of components, all of which are subject to degradation throughout WT operation. From the foundations exposed to recurring wave loads to the blades continuously eroded by rain, hail and strong winds, degradation is a perpetual phenomenon. Examples include fatigue cracking and leading-edge corrosion on WT blades, scour on WT foundations and thermal fatigue for gearboxes and generators (C. D. Dao et al., 2021,Shafiee and Sørensen, 2019).

Degradation is quite a complex process with numerous dependencies on physical and environmental factors. As a result, there have been numerous efforts in degradation modelling using a variety of techniques and approaches. Advanced techniques use live sensor data from OWTs as indicators to estimate the health of a component. With the health estimate, the amount of degradation and the remaining useful life (RUL) can be determined. This is visualized in Figure 1.4 which shows degradation accumulation in a component over its lifetime, measured via the indicators of vibration and temperature. This example could apply, for example, to the gearbox. Sensors measuring the vibrations of the gearbox shaft and the temperature of the gearbox oil act as indicators of gearbox health. Excessive vibrations or temperature, if detected, indicate deterioration from normal working conditions. Both are detrimental to gearbox health and lead to a reduced RUL. Failure of the gearbox occurs when its accumulated degradation reaches a certain threshold, i.e. the Functional Failure shown in Figure 1.4. Usually, this threshold is when the component can no longer function or represents a very high risk to the overall system condition if operated further. Abid et al. (2019) presents a few other examples of sensors and health signals for fault prognostics and RUL calculations for a WT. Monitored signals such as the turbine power curve, the vibrations of a bearing, the gearbox oil temperature and acoustic signals from blades or cooling fans can be utilised for degradation modelling. (J. Andrawus et al., 2006, Mammadov, 2024).

Alternative degradation modelling techniques involve the use of past failure or degradation data. Usually, past failure data exists as the number of failures and their time of occurrence for different components. By analysing the average time taken for a component to fail over a large dataset, failure rates can be calculated. The failure rate of a component is defined as the number of failures observed in a particular period (usually a year) and is represented as the number of failures per year. On the other hand, degradation data is more detailed, going beyond failure instances to representing component health across its entire lifetime. However, such degradation datasets are quite scarce in the literature. Failure rate or degradation data can then be used to model component degradation and determine its maintenance strategies.

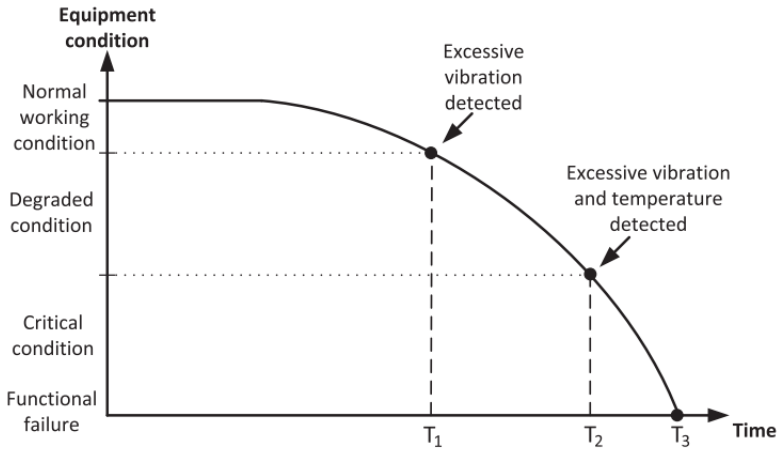

Figure 1.4: Example of a degradation process and condition thresholds triggered by vibration and temperature sensors (Le and Andrews, 2016)

Among the various WT systems, the largest contributor to failure rates for OWTs is seen to be hydraulic pitch systems with a failure rate of 1.076 failures per year (Carroll et al., 2016). Furthermore, an in-depth review of the failure analysis and modelling field shows that a lot of research has already been carried out for subsystems like gearboxes (Byon and Ding, 2010), drivetrains, blades (Besnard and Bertling, 2010) and bearings (J. Li et al., 2019). On the other hand, while failures of pitch systems have been studied, their degradation has not been modelled in detail despite having a high failure rate and considerable downtime (DT). In order to fill this gap, this thesis will focus on modelling the degradation of pitch systems.

1.4. Multiple Degradation Processes & Dependencies

Modern mechanical systems have become increasingly complex and consist of thousands of components interacting with each other (Meango and Ouali, 2018). Additionally, most real-life components face multiple degradation processes occurring simultaneously due to different failure modes (FMs). Subsequently, mutual influence or interactions between components or FMs within a system cannot be ignored (Shen et al., 2020). The analysis of this interaction makes a great difference in more accurate estimates of a component's health (Zeng et al., 2023). The increased accuracy achieved helps improve predictions for degradation and failure of the component. This information can be subsequently used in efficient maintenance planning. For example, oil contamination within a gearbox may lead to increased degradation and wear of the gears which in turn, further contaminates the oil lubricant. Degradation of an internal bearing component, such as the crushing of a ball may lead to an imbalance in the force distribution and increased degradation of one of the bolts holding the bearing (Z. Wang et al., 2022).

This dependence among components or FMs is called stochastic dependency (Shen et al., 2020). This can further be categorized into failure dependence and degradation dependence. Failure dependence means that the failure of a component induces the failure or affects the rate of degradation of another component. This can be further extended to degradation dependence if the rate of degradation of a component is not only dependent on another component's failure but also its degradation process. Hence, if two components are degradation-dependent, the degradation of one induces a quicker degradation of another. Shahraki et al. (2017) conducted a review of approaches for modelling multiple degradation processes and concluded that dependent degradation modelling is becoming an increasingly important research topic among researchers. While most studies assumed independence between the degradation processes, this study conceded that this may not always be realistic and could lead to ineffective models. Such dependent-degradation relations between multiple FMs are quite common in most systems, however, they are not always easy to study and analyze.

Most of the current research in the field of maintenance modelling focuses either on individual components with a specific FM (Welte et al., 2006), individual components with multiple independent FMs (Besnard and Bertling, 2010) or on multiple components with multiple FMs linked by a network structure (H. Li et al., 2020). A network structure connects multiple components of a system in a particular configuration using series, parallel or other connections. While the network structure does entail a certain degree of dependency based on the connections, this only represents the dependency upon the occurrence of failure, i.e. failure dependence. The degradation processes before the failure event, for each component or FM, are still independent. Thus, the degradation associated with an FM has no impact on the degradation related to another FM. This topic is further delved into in Section 2.5.

While dependent degradation and failure modelling is implemented in aerospace and nuclear fields, it is yet to be studied specifically for WTs. Considering dependencies in the degradation process allows a more accurate estimation of component health. This improves maintenance planning, making it efficient and reducing O&M costs. Subsequently, one of this study's objectives is to model dependent degradation processes. For this study, stochastic degradation dependencies and economic dependencies as explained in Section 2.5 are modelled.

1.5. Maintenance

According to C. D. Dao et al. (2021), maintenance refers to any activity that keeps the WT operating satisfactorily throughout its lifetime. Maintenance of WTs is a complex and expensive activity as seen in Figure 1.3. Shafiee and Sørensen (2019) provided a clear overview of the tasks carried out when offshore maintenance is scheduled. The required spare parts are ordered from wind farm depots, service vessels and transportation vessels are hired and maintenance technicians are allocated for the repair. Delays in any of these processes lead to extra costs. Metocean conditions, such as wind speeds and wave heights, also play an important role in scheduling these maintenance actions as they affect vessel workability and subsequently, production losses (McMorland et al., 2022).

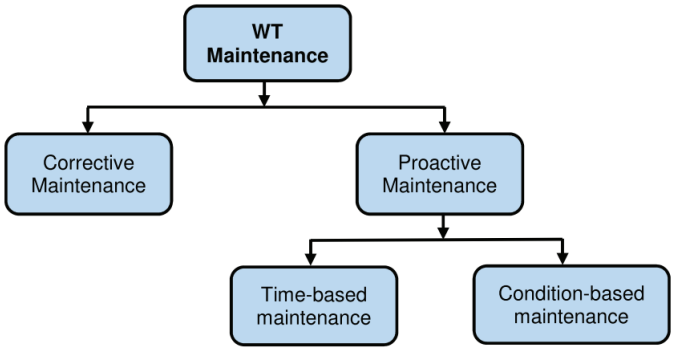

Figure 1.5: Types of maintenance activities (C. D. Dao et al., 2021)

Figure 1.5 shows the broad classification of maintenance activities into the strategies of corrective maintenance (CM) and proactive maintenance. Proactive maintenance strategies are further classified into time-based maintenance (TM) and condition-based maintenance (CdM). CM is performed only after component failure or upon a severe decline in power production (Shafiee and Sørensen, 2019). On the other hand, proactive maintenance is performed before a failure occurs to prevent it from happening. A CdM strategy focuses on the repair or replacement of damaged components based on their health condition (J. Andrawus et al., 2006). Alternatively, a TM strategy follows predefined maintenance intervals without considering the component's health. Degradation models coupled with various maintenance strategies are usually tested computationally to decide the optimum strategy. Finding the cost-optimal strategy that minimizes costs is critical in planning efficient O&M actions.

Each maintenance strategy and finding the optimum among them is dealt with in detail in Section 2.6. The benefits and limitations of each strategy and the reason for choosing a combined TM-CM strategy for this study are outlined.

1.6. Research Motivation

As explained in Section 1.2, the primary aim of this study is to contribute to the ongoing research in reducing O&M costs for the offshore wind energy industry. This is done by improving the degradation and maintenance modelling for the critical components of pitch systems. The lack of research covering the topic of degradation modelling of pitch systems provides impetus to this study. Another important focus of this study is dependent degradation modelling. Most degradation approaches proposed in this field model only independent FMs. The interactions and dependencies between multiple FMs are largely ignored. Thus, the inclusion of degradation dependency is aimed at improving the modelling of interactions in real-life systems. Zeng et al. (2023) further identifies an opportunity to validate the added value of considering dependencies, which is not yet well-addressed in the literature. Subsequently, analysing the effect of considering dependencies forms an important research question for this study. Hence, the objective is to apply the dependent-degradation model to inspection and maintenance actions to understand the impact of dependencies on O&M costs and achieve efficient O&M planning.

From a socioeconomic and system integration perspective, this research will further push the inclusion of dependency modelling in the field of wind energy science. Based on the model built for this study, a larger model integrating all the key WT components and the dependencies in their degradation processes could be developed. After accounting for dependent degradation, O&M strategies can be optimized for minimizing O&M costs. Besides reduction in costs, improved maintenance strategies, featuring a reduction in time spent out at sea, directly benefit the lives of the technicians and the vessel crew and improve their social conditions.

In a broader perspective, advancements in wind energy O&M strategies directly contribute to reduc-

ing the LCOE. This reduction further strengthens energy independence and energy security for all. This is a positive step in building towards the United Nation's Sustainable Development Goals of universal access to clean and affordable energy. With increased deployment of wind energy, greenhouse gas emissions will reduce leading to reduced air and water pollution and increased biodiversity. Furthermore, the increasing number of projects on wind energy has a positive impact on the economy. Such large-scale projects create many jobs, boost the Gross Domestic Product and encourage energy trade with foreign countries (KPMG, 2019).

To conclude, this thesis will focus on modelling multiple dependent degradation processes in WT pitch systems and developing cost-effective, well-planned inspection and maintenance strategies.

1.6.1. Research Questions

The main research objective of this thesis is:

Model multiple degradation processes of offshore wind turbine pitch systems for optimising their maintenance strategies.

To achieve the goal of this thesis, the following key research questions need to be addressed:

1. How does the process of degradation occur in OWT pitch systems? Which are the most common failure modes?
2. How to model the degradation of a system across its entire lifetime?
3. How to model inspection and maintenance actions for a subsystem of an OWT?
4. How to incorporate a degradation model into an inspection and maintenance model and create a degradation-based maintenance model?
5. What is the optimum maintenance schedule for an offshore wind turbine pitch system in the case of multiple independent FMs?
6. How to introduce and model dependency between multiple failure modes in degradation models?
7. What are the impacts of modelling dependent degradation processes on the O&M strategy and costs for OWT pitch systems?
8. Which input parameters of the degradation-based maintenance model have the largest impact on O&M costs and strategy?

1.7. Outline

This report is organised in the following order. Chapter 2 covers an in-depth literature review of the various topics involved in this project. This is followed by Chapter 3 which details out the necessary theoretical background of the concepts used. Next, the modelling approach and the proposed model are presented in Chapter 4. The verification of the model with existing literature and its application to the case study of OWT pitch systems is then described in Chapter 5. The results from this case study and the comparison between the adoption of independent and dependent degradation processes are presented and discussed in Chapter 6. Chapter 7 concludes this thesis, discussing key takeaways and providing recommendations for future work.

2
Literature Review

In the field of component degradation and maintenance, a few research topics have been studied in detail. Numerous papers in the literature analyse Failure Modes (FMs) and failure rates for various Wind Turbine (WT) components, either theoretically or using field data. This data form the basis of degradation models built for cost estimations, reliability analyses and maintenance optimization. Degradation models are often coupled with Remaining Useful Life (RUL) estimations and reliability analysis to predict the time to failure. These results are then used to plan maintenance strategies. A variety of maintenance strategies are also coupled with degradation models to compare maintenance actions and perform lifetime cost analyses. Several studies focus on simulating the degradation model to analyze availability, Downtime (DT) and failure events. These results are key in identifying critical systems which might require further attention. A wide collection of research papers, textbooks, master thesis and other literature is reviewed in this chapter to develop an understanding of the research field and state-of-the-art developments.

First, O&M modelling is briefly introduced in Section 2.1. Next, WT subsystems are analyzed and critical subsystems are identified in Section 2.2. Section 2.3 further elaborates on the selected critical system - WT pitch system, its components and FMs. Section 2.4 discusses degradation modelling and provides a classification of the various methodologies available. Next, dependencies in modelling are introduced in Section 2.5 and available methodologies in the literature are presented. Section 2.6 discusses key maintenance strategies and presents the maintenance strategy optimization problem.

2.1. O&M Modelling

As seen in Section 1.2, O&M actions are extremely costly, with large amounts of uncertainty associated with them. Hence, O&M models aim to accurately replicate O&M activities to assess various solutions and select the best ones (Welte et al., 2018). For example, Ren et al. (2021) presents optimization problems of LCOE minimization, maintenance strategy optimization and schedule planning. Welte et al. (2018) presents vessel path optimization and vessel fleet optimization problems. McMorland et al. (2022) conducted a thorough review of existing O&M modelling literature for floating offshore wind turbines. The following key inputs for an O&M model were identified:

1. Metocean conditions: Weather data (usually wave heights and wind speeds) is typically input into the model as a time series. These conditions determine the operability of the vessel and the crew.
2. Taxonomy and Reliability: Information about WT subsystems and components, including their classification, failure rates and repair times.
3. Maintenance: Type of maintenance strategy and its schedule.
4. Transport: Information about the vessel required for O&M activities, including cost, speed, capacity and operational limits
5. Site logistics: Details of the turbines and the site such as distance to shore, number of turbines, water depth and power curves.
6. Cost data: All possible costs such as costs of vessel, labour, repair, electricity price and other indirect O&M costs such as spare parts, tax, rent and balance of plant
7. Crew: Availability and capacity of the crew to carry out O&M activities.

As discussed in Section 1.6, this study mainly focuses on degradation modelling (Section 2.2 to 2.5), which is a part of the taxonomy and reliability category, on maintenance modelling (Section 2.6) and on cost modelling (Section 2.6.1). While the other inputs are not modelled in detail, they are still an integral part of an O&M model and will be considered while building the proposed model.

2.2. Wind Turbine Subsystems

A WT is made of many subsystems, with each subsystem consisting of multiple components interacting with each other, as shown in Figure 2.1. Le and Andrews (2016) provide a detailed understanding of the main subsystems, the involved components and their health indicators. While the explanation does not cover every component of every system, it is useful for a general understanding of the entire WT. It is also important to note that each study might not group the same WT components under the same subsystem. Figure 2.1 presents the main subsystems, which are:

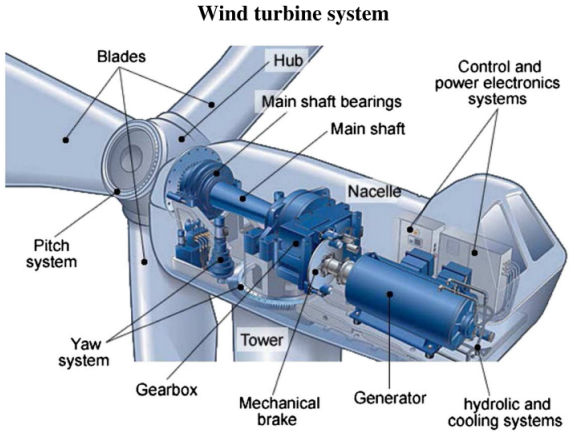

Figure 2.1: Wind turbine main subsystems (Le and Andrews, 2016)

1. Drivetrain, consisting of gearbox, bearing and shaft
2. Hydraulic, consisting of hydraulic pump and valve
3. Braking, Yaw, Pitch, consisting of brake discs, callipers, hydraulic actuator, gear and bearing
4. Rotor, consisting of hub and blades
5. Power, consisting of generator, frequency controller and transformer
6. Structure, consisting of tower, nacelle and foundation

Akin to all mechanical components, these subsystems undergo degradation and suffer from failures. Various studies analyse Offshore Wind Turbine (OWT) data and compare the different subsystems over their failure rates, DT and maintenance costs. Figure 2.2 shows the analysis of failure rates and Operations & Maintenance (O&M) costs for OWTs performed by Carroll et al. (2016). A population of 350 WTs operating for 15.5 million hours was studied. Failures were defined as unscheduled visits to the WT which consumed material. They were further classified as minor repairs with material costs less than € 1,000, major repairs with material costs between € 1,000 and € 10,000 and major replacements for material costs over € 10,000. The results showed that the largest contributor to failure rates for OWTs were pitch and hydraulic systems with a failure rate of 1.076 failures per year, followed by auxiliary components and the generator with a failure rate of just over 1 failure per year. In terms of repair times, the hub, the blades and the gearbox had the largest contributions. Since the failure rates of hubs and blades were low, they were unlikely to contribute greatly to the overall O&M costs. The highest repair costs were associated mainly with the gearbox, with almost twice the repair costs associated with the hub and blades. A large difference in rates and costs was observed in the results of this paper compared to expert data. This was attributed to varying definitions for failure rates and maintenance costs. Further, the authors highlighted the uncertainty associated with failure rates. Even with the same definition, failure rates will vary for each population based on the manufacturer, supplier, technology and quality standards used.

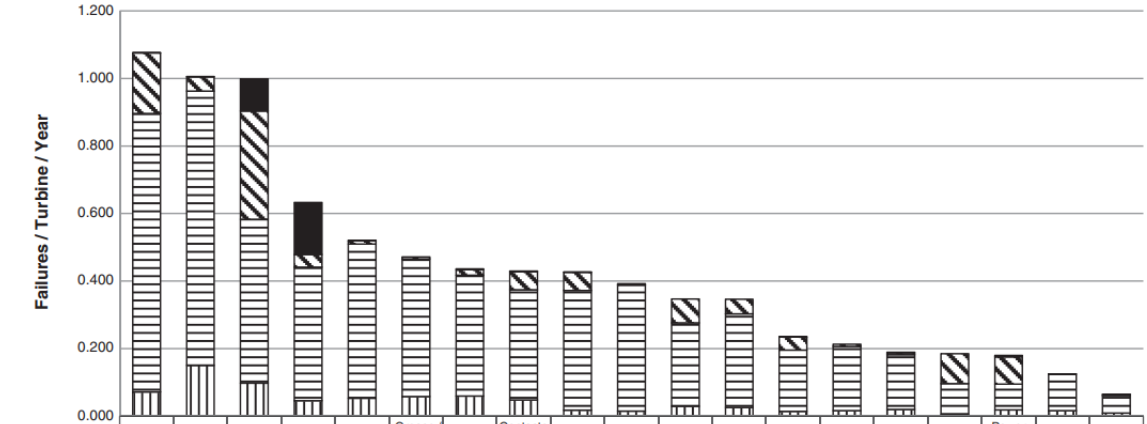

	Pitch / Hyd	Other Components	Generator	Gearbox	Blades	Grease / Oil / Cooling Liq.	Electrical Components	Contactor / Circuit Breaker / Relay	Controls	Safety	Sensors	Pumps/ Motors	Hub	Heaters / Coolers	Yaw System	Tower / Foundation	Power Supply / Converter	Service Items	Transformer
Major Replacement	0.001	0.001	0.095	0.154	0.001	0.000	0.002	0.002	0.001	0.000	0.000	0.000	0.001	0.000	0.001	0.000	0.005	0.000	0.001
Major Repair	0.179	0.042	0.321	0.038	0.010	0.006	0.016	0.054	0.054	0.004	0.070	0.043	0.038	0.007	0.006	0.089	0.081	0.001	0.003
Minor Repair	0.824	0.812	0.485	0.395	0.456	0.407	0.358	0.326	0.355	0.373	0.247	0.278	0.182	0.190	0.162	0.092	0.076	0.108	0.052
No Cost Data	0.072	0.150	0.098	0.046	0.053	0.058	0.059	0.048	0.018	0.015	0.029	0.025	0.014	0.016	0.020	0.004	0.018	0.016	0.009

Figure 2.2: Failure rates for wind turbine subsystems (Carroll et al., 2016)

One of the earliest attempts at analysing WT reliability data, the ReliaWind project (Gayo, 2011) investigated the reliability of large WTs and recommended methods to raise WT availability and lower costs. Data from 350 WTs operating for 450 months with 35,000 DT events was studied. Critical subsystems for a modern WT and their FMs were identified. The project concluded that the pitch system had the highest failure rates (21% of the total failure rate) as well as the highest DT (23% of the total DT) followed by the frequency controller, control system, generator and gearbox. Le and Andrews (2016) conducted WT system analysis for condition, maintenance and failure prediction. The WT was segregated into a few important subsystems and Weibull degradation distributions for key WT components were used as input. Logistic, repair and travel durations were also modelled as Weibull distributions. The results showed that the highest number of failures were observed in electrical components, such as the frequency converter and transformer, followed by the hydraulic pumps and valves. While applying the CdM strategy, the pitch bearing or gear and the pitch actuator were the two components with the highest average number of component replacements before failure. C. Dao et al. (2019) reviewed both onshore and OWT component reliability data from over 18,000 WTs with over 90,000 operational years and analysed its impact on the Levelized Cost of Electricity (LCOE). Variations in reliability data were studied to identify critical sub-assemblies. The paper also drew similar conclusions to Le and Andrews (2016) with the highest failure rates observed in pitch systems of 0.938 failures per year followed by the electric system with 0.9 failures per year. The components with the highest DT were observed to be gearboxes and generators. Further, it was observed that uncertainties in failure rate data were smaller for large surveys compared to surveys with short operation durations or small WT populations. Zheng et al. (2020) developed analytical methods to analyse the reliability of WT systems. Failure data was classified and processed to identify the critical subsystem. Using a single wind farm data from China (13 2.5 MW WTs operating for a year), similar results as Le and Andrews (2016) were obtained with the highest number of failures observed in the electrical system, specifically the control system, followed by the pitch system. However, due to the small population size, quite large failure rates were obtained. Over the entire year, approximately 79 and 58 failures were reported for the electronic control and pitch system respectively.

The systems with the most frequent failures directly contribute to the DT and impact the reliability of the entire WT (Zheng et al., 2020, Padman et al., 2016). Thus, it is necessary to focus specifically on the degradation of these systems. While electrical components are seen to have high failure rates, Kerres et al. (2015) explained that they are usually modelled as binary systems, with one functioning state and one failed state. This is because the physical condition of such systems is hard to detect and deterioration is usually not observed before failure. Thus, the next most critical pitch system is selected

for this study.

2.3. Pitch System

The oldest WTs used blades set at a fixed angle throughout their operation. Improvements in WT design introduced pitchable blades, i.e. blades which can be rotated over their axes. This motion is visualized in Figure 2.3. The dashed circle represents the blade root with the airfoil representing a single cross-section of the blade. The blade is shown to be linked with a hydraulic piston by a connecting rod. With the feathering and operating motions of the piston within the hydraulic cylinder, the airfoil and hence the blade can be pitched within a large range of angles.

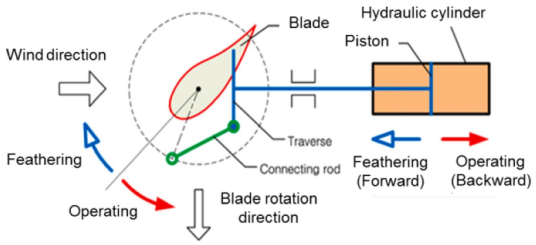

(a) Feathering and operating position of the blade

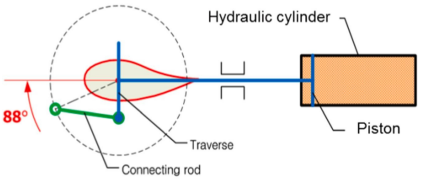

(b) Feathering position

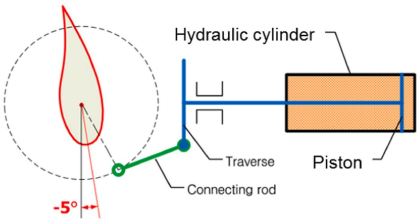

(c) Maximum pitching status

Figure 2.3: Position control of blade pitch angle control (Lee et al., 2020)

To understand the working of WT blades, Figure 2.4 shows how lift force is generated from a single airfoil. Incoming wind speeds are denoted as $U(1-a)$ after accounting for the induction factor. The plane of rotation of the blade lies perpendicular to the plane of this paper and is shown by a dashed black line. The relative wind speed originating from WT rotation is Ωr_1 directed towards the airfoil. The resultant of these two wind speeds is shown as $V_{res,1}$. $V_{res,1}$ lies at a particular angle to the chord line of the airfoil. This angle is referred to as the angle of attack α_1. Depending on the value of α_1, the airfoil generates a lift force and a drag force. For each airfoil, there exists an ideal angle of attack that produces the highest lift-to-drag ratio. The life force is shown in Figure 2.4, perpendicular to the resultant wind direction. θ_1 is the angle between the chord line and the plane of rotation and φ_1 is the sum of θ_1 and α_1.

The pitch system of a WT is extremely critical to its operation as well as safety. The angular control of blades, called blade pitch angle control, varies the angles mentioned above, specifically the angle of attack. The blade angles are regulated depending on the wind speed and turbine operation. This allows control over the lift generated by the airfoil and subsequently, the power generated by the WT. This is understood with a power curve, which can be separated into the partial-load region, i.e. the region between cut-in wind speed and rated wind speed and the full-load region, i.e. the region between the rated wind speed and the cut-out wind speed. In the partial-load region, power generation is maximised. Thus, as wind speeds increase, maximum power generation is achieved by increasing the rotational speed of the blades to maintain a constant angle of attack for the airfoil. The blades are not pitched, i.e. the pitch angle is 0°. Subsequently, the power generated by the WT increases for higher wind speeds.

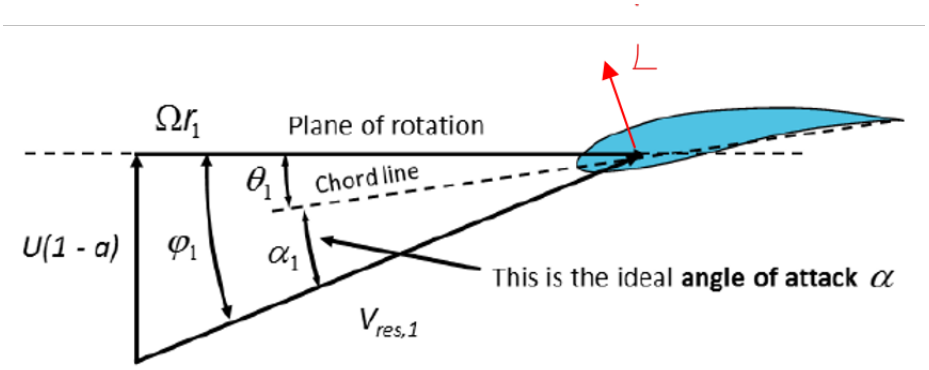

Figure 2.4: Velocity triangle and lift generation airfoil (Zaaijer and Viré, 2022)

However, for the full-load region, the objective is to maintain constant power. This is achieved by pitching the blades to 'vane', i.e. pitching towards the incoming wind. Figure 2.5 shows the original grey airfoil and the pitched blue airfoil. The pitching action reduces the angle of attack from α to α_{new}. This action reduces the lift generated by the airfoil. A lower lift corresponds to a lower power coefficient and lower power generation. Thus, WT blades act as aerodynamic brakes to limit power production to the turbine's maximum capacity. This reduction in power coefficient opposes the increase in the power that would have occurred because of the increasing wind speed.

Figure 2.6 shows pitch angles as a function of wind speeds. It is seen that the pitch angle is zero in the partial-load region and is steadily increasing in the full-load region. When the wind speeds are too low or too high for the WT to generate any energy, the blades are pitched fully in vane position. In case of emergencies and extreme wind speeds, this is done to reduce aerodynamic loading and to safeguard the system (Wei et al., 2022). For safety requirements, each blade has its independent pitch system (Walgern et al., 2023). If this system fails, the turbine is required to be brought to an emergency shutdown (Jiang et al., 2014).

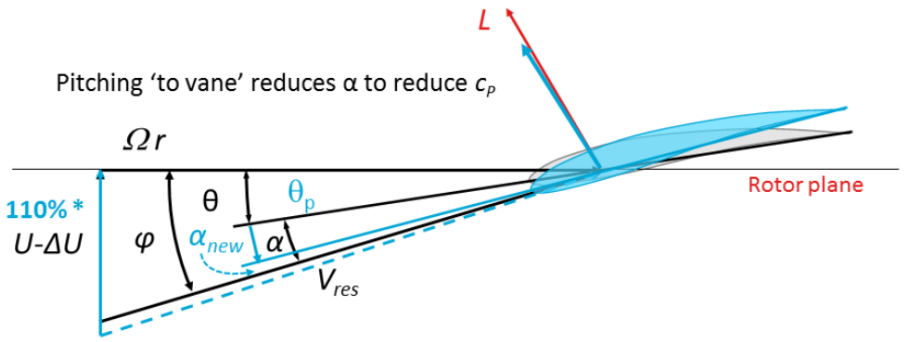

Figure 2.5: Pitching airfoil to vane (Zaaijer and Viré, 2022)

The pitch system is mounted inside the rotating hub of a turbine, protecting it from adverse environmental conditions (Padman et al., 2016). It further acts as an interface between the blades and the hub. Bearings are used to support the rotation of the blade. The pitch angle is controlled by pitch brakes and speed and position sensors (Zaaijer and Viré, 2022). Most pitch systems used in the industry are either hydraulic or electric systems (Padman et al., 2016). Figure 2.7 shows a schematic of the two systems, the different sub-components and their connections. The mechanism of pitching of the blade is the primary distinction between the two systems. In electric pitch systems, electric motors provide the driving force. On the other hand, hydraulic systems are driven by pumps which circulate hydraulic fluid throughout the system.

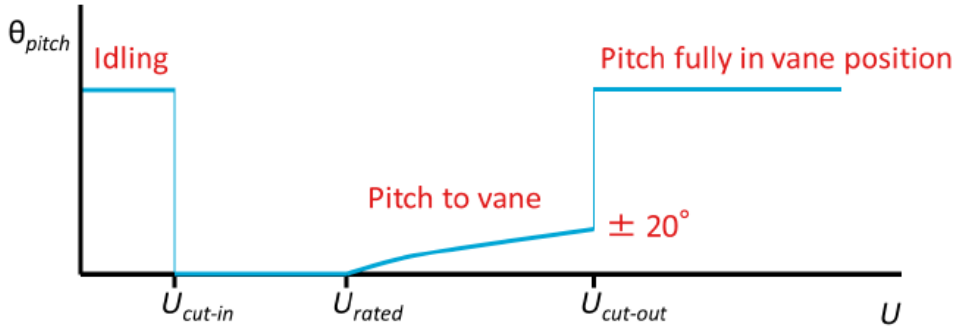

Figure 2.6: Pitch angle as a function of wind speed (Zaaijer and Viré, 2022)

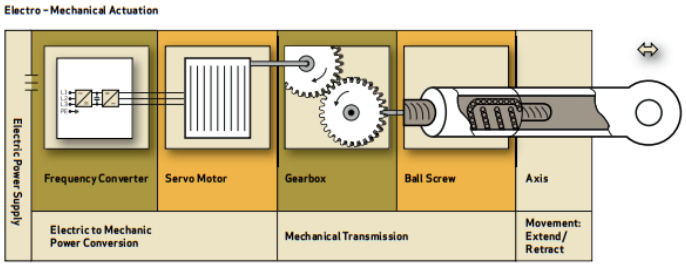

(a) Electrical pitch system

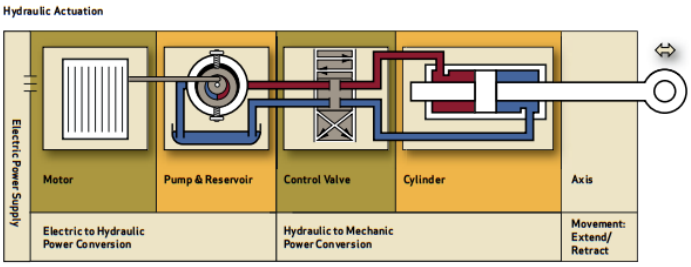

(b) Hydraulic pitch system

Figure 2.7: Comparison of pitch systems (a) electrical and (b) hydraulic configurations (Padman et al., 2016)

An electric pitch system works based on electric power supplied to a motor which is used to rotate or pitch the blades. The major elements of this system are listed here.

1. Power source
2. Backup power source
3. Motor
4. Controller
5. Brake
6. Gearbox
7. Bearing

Here, the main power source powers the entire system with electrical energy. A backup battery ensures safe operation in the event of an emergency. The pitch controller receives control signals and accordingly, sends commands to the pitch motor. The reduction gearbox reduces the speed while increasing the torque of the motor. This drives the internal gear in the pitch ring, which then rotates the blades (Wei et al., 2022).

A hydraulic pitch system works similarly to the electric counterpart, with the end objective of pitching the WT blades. Here, pressurized hydraulic fluid provides the required force to the blades. The major elements of such a system are listed here.

1. Power source
2. Pump
3. Hydraulic supply lines
4. Hydraulic valve and slip ring
5. Reservoir or Accumulator
6. Actuator
7. Bearing

The hydraulic power unit performs a function similar to the power source in electric pitch systems. Electrical energy from the power unit drives the pump which is responsible for circulating the hydraulic fluid. The pump pushes the hydraulic fluid through the hydraulic lines and the hydraulic valves into the hydraulic piston. Here the fluid drives the actuator which is mechanically connected to the blades. The pistons are mounted in a way that allows for the blade's rotational motion. For emergencies, such as pressure drops due to leakages, there usually exists an emergency fluid storage tank.

Both systems have their benefits and drawbacks. Electric systems do not have risks of leakages and consume less energy. However, backup batteries within the electric pitch system are a drawback with short life cycles. Thus, frequent maintenance is required to replace the battery pack. On the other hand, hydraulic systems hold a clear advantage in terms of system speed and reliability. Since a lower number of technical components are used, maintenance and diagnostics are also easier (El-Henaoui, 2009).

Pitch system components face large inertial loads in the form of heavy blades and strong but variable wind forces. Within the hub, the pitch system faces high temperatures, vibrations and humidity. Centrifugal forces and gravitation forces, combined with complex and aggressive aerodynamic flows, further accelerate the ageing of the system (Zhang et al., 2019). In order to understand and compare the failure mechanisms of the two systems, their FMs are discussed in the next section, Section 2.3.1.

2.3.1. Failure Modes for Pitch Systems

Electric pitch systems are analysed first. With the highest failure rates observed for pitch systems in the ReliaWind project, the components with the most failures were observed to be the battery, motor and converter (Gayo, 2011). Padman et al. (2016) studied pitch system reliability by analysing data from 1330 WTs located in North America, Europe and China, covering 4 million turbine days. An average failure rate of 0.7 failures per turbine per year was observed for 1.5 MW- 3 MW sized onshore WTs. The study concluded that frequent failures occur in motors, electronics and backup power sources. Walgern et al. (2023) used segregated onshore WT hydraulic and electric pitch system field data for reliability analysis. A wide variety of pitch systems from 6 original equipment manufacturers with a total of around 2700 turbine operation hours was considered. For the electric pitch system, results showed high failure rates for components such as the motor relay, the controller and the power source (battery) as shown in Figure 2.8a. Since Walgern et al. (2023) analysed onshore WTs, smaller failure rates of 0.56 for electric pitch systems were obtained.

For hydraulic systems, Gayo (2011) obtained hydraulic fluid leakages and sensor failures as the most important FMs. Padman et al. (2016) observed that notable sources of failure were valve joint wear, fluid leaks and fluid contamination. These issues contributed the most to lowering the reliability and increasing the DT. According to Walgern et al. (2023), the hydraulic reservoir, hydraulic valve and actuator showed the highest failure rates as shown in Figure 2.8b. As discussed in Section 2.2, Carroll et al. (2016) obtained hydraulic pitch system failure rates to be 1.076 failures per turbine per year. Key FMs were associated with oil issues, such as leakages and contaminations, hydraulic valve wear issues, accumulator or reservoir failures, sludge sensor failures and pump failures, as shown in Figure 2.9 in terms of percentage of the overall failure. The individual failure rates for the various FMs

can be obtained by multiplying these percentages by the total failure rate for the entire pitch system.

Z. Wang et al. (2022) performed an in-depth failure mode, effects and criticality analysis specifically focused on OWT pitch systems. However, no segregation for hydraulic or electric pitch systems was made. Seven main malfunctions were analyzed and critical links were identified. It was concluded that the FMs with the highest ranking across severity, occurrence and detectability were bearing internal component failures, short/open circuits of motor windings, gear failures of the gearbox and bolt fractures. Z. Wang et al. (2022) also observed higher rankings for failure of mechanical components compared to electrical components. Accordingly, the suggestion of allocating higher reliability for mechanical components was given.

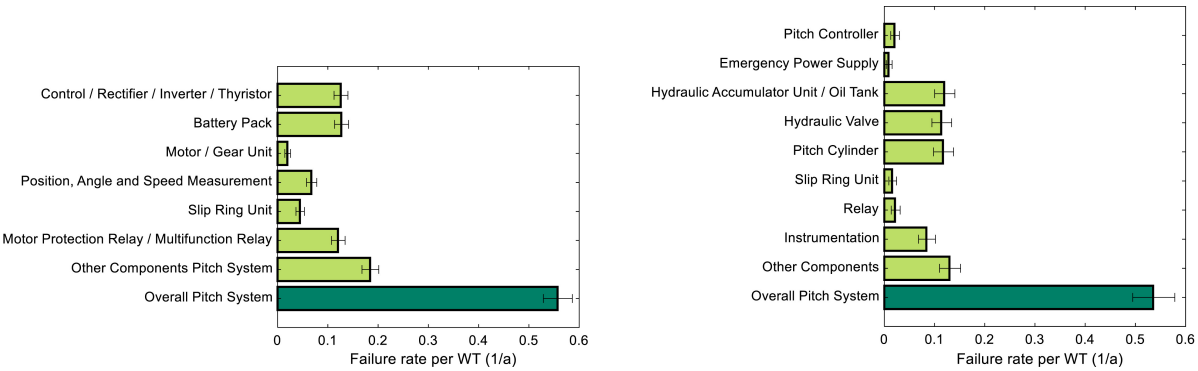

(a) Electric pitch system

(b) Hydraulic pitch system

Figure 2.8: Average failure rates for onshore WT (a) electric and (b) hydraulic pitch systems (Walgern et al., 2023)

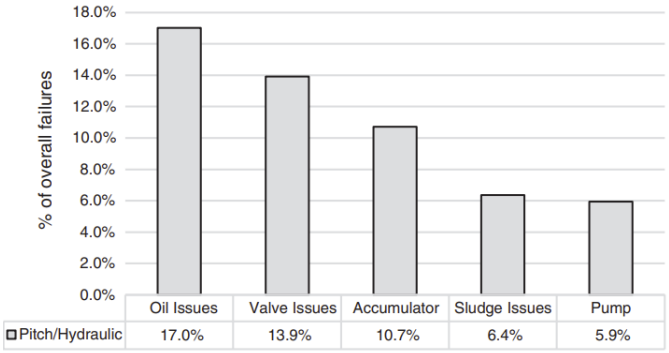

Figure 2.9: OWT hydraulic pitch failure modes (Carroll et al., 2016)

As discussed in Section 2.2, the physical condition of electric systems is usually hard to detect and deterioration is usually not observed before failure. This applies to electrical pitch systems, with its primary FMs associated with electrical components. Further, most of the higher failure rates and higher severity rankings occur in hydraulic pitch systems (Z. Wang et al., 2022). Hence, hydraulic pitch systems will be focused on in this study.

2.4. Degradation Modelling

Component health and maintenance models are classified into three categories: similarity models, survival models and degradation models (MATLAB, 2019). Similarity models are used when complete historical datasets exist with run-to-failure data, from start through degradation to failure. These datasets are used to train the similarity model. Based on the current state of the system, the model looks at the closest trajectories and predicts the future state. On the opposite end of the spectrum, survival models require only failure data, such as the time of machine failure. Using this data for a

large number of components, a probability distribution is created and parameters such as the RUL can be estimated. Degradation models are a combination of both these models. They are utilized when the user has some degradation data between start and failure and an estimate of a safety threshold beyond which the component must not operate. Curve fitting is carried out for the existing data, where a mathematical function is constructed that best fits the data points. This curve is then extrapolated until the threshold value beyond which a component must not be operated. Outputs such as the RUL or the future system state can be gleaned from these models. Abid et al. (2019) performed a study on WT fault prognostics for predictive maintenance and discussed various approaches for calculating the RUL of components. A broad classification into two types of approaches was proposed: experience-based approaches and degradation modelling-based approaches. The first type of approach requires run-to-failure data, similar to similarity models previously discussed. On the other hand, degradation modelling-based approaches use online monitoring data to establish the current health of the system. Using this data, the degradation evolution over time is predicted and the RUL is estimated.

For many applications, including WTs, collection of run-to-failure data is not feasible. Such detailed and comprehensive degradation datasets require the system to be under observation for long periods which is difficult. Welte et al. (2006) stated that repair time and inspection interval data is usually much easier to collect than sojourn time or degradation data. Sojourn time is defined as the amount of time an object is expected to spend in a state before leaving it. For example, if component health is segregated into a finite number of states, the time spent in each state before degrading to the next state is sojourn time. With scarce data available in the literature, this study focuses on degradation modelling-based approaches which require less data. Abid et al. (2019) and Shahraki et al. (2017) classified these approaches into two categories: physics or model-based approaches and data-driven-based approaches. Physics-based approaches use physical and mathematical relations to describe a component's degradation process, taking into account component-specific failure mechanisms. Some of the existing models are, among others, the Paris Law (C. D. Dao et al., 2021), the Arrhenius model (Chang and Mosleh, 2017) and the Inverse Power (Kececioglu and Jacks, 1984). Such models require an in-depth understanding and accurate modelling of the component loads and their primary failure mechanisms. They are useful for capturing a physical phenomenon and better at explaining the behaviour of a system under varying operating conditions. Due to these characteristics, it is quite difficult to develop such models for complex systems, such as multi-component systems or multiple competing failure mechanisms within a single component. On the other hand, when the physics behind a degradation process becomes complex, data-driven models become quite useful. These can be either statistical or artificial intelligence models which act as black-box models, where the relation between input and output is unknown.

2.4.1. Data-Driven Models

Data-driven models are easier to implement when the physics behind the failure mechanisms becomes complex. However, such models lack physical meaning and are less interpretable than physics-based models, specifically regarding physical forces, stresses and failure mechanisms. Other drawbacks include the need for the existence of historical data and the subsequent high level of dependency on it. Despite these shortcomings, such models are becoming increasingly popular for modelling component degradation. Their advantage lies in the fact that understanding the degradation mechanisms is not required. Further, these models are widely applicable to any component and quite effective in describing the uncertainties associated with a degradation process (Abid et al., 2019).

A variety of data-driven degradation models were reviewed by Shahraki et al. (2017) including general path models, stochastic process models, finite state models and artificial intelligence models. General path models are simple and capable of modelling continuous processes. They describe the degradation process with two terms, a mathematical function and an error term. The function can be obtained from existing data or engineering experience and captures the degradation trend. The error term is modelled as a normal distribution and introduces randomness (Lin and Ding, 2022). However, the inherent degradation in these models is considered to be deterministic and thus, capturing the temporal variability is not possible and this limits their applications. Abeygunwardane (2012) highlighted the suitability of probabilistic or stochastic models for the purposes of maintenance and reliability stud-

ies. Their simplicity and the ability to include and model uncertainties make them the preferred choice. Uncertainties can include uncertainties with equipment deterioration or even outcomes of inspection and maintenance actions. Stochastic process models include, among others, Petri-net models, Wiener or Gaussian processes, gamma processes and inverse Gaussian processes. A Petri-net model is used by Le and Andrews (2016) to model WT degradation and maintenance. The model uses places to represent the condition of the component and transitions for dynamic processes of inspection, maintenance and degradation. Degradation transitions degrade the system from a healthy state to a deteriorated state, while maintenance transitions reverse this degradation and bring the system back to a healthy state. These models can deal with dynamic processes and modelling dependent degradation processes between different subsystems. However, Petri-net models are graphical models and require a detailed graph of each subsystem and its relations. As a result, a single model built for one system is limited in its application beyond that system. Wiener processes are not considered suitable for modelling monotonic degradation processes. Thus, such process models are not applicable for wear or cumulative damage processes. Gamma processes are quite suitable for modelling fatigue, corrosion and crack growth. Welte et al. (2006) proved that Gamma processes represent a good choice for modelling a series of randomly occurring shocks. The Weibull distribution is suitable in the case of competing deterioration mechanisms. Inverse Gaussian processes are predominantly used to model monotonic degradation when other processes do not fit the data very well. A key shortcoming of these stochastic process models is the requirement of long-term data and a large number of historical data points which is essential in regression analysis and curve fitting techniques. This disadvantage is overcome by finite-state Markov models which require less historical degradation data.

2.4.1.1. Finite State Markov Processes

A finite state Markov process is defined as a stochastic process that evolves through a finite number of states (Shahraki et al., 2017). These states are used to represent the health of the component and can vary from new condition to functional failure. The degradation from the new condition through the degraded states to failure is modelled as transitions between the states. The inherent Markov property is defined as follows: the future state of the system is dependent only on its current state and is independent of the past states. Many physical processes comply with this property, especially component degradation and hence, Markov processes are suitable for degradation modelling. A detailed understanding of Markov processes and their associated theory is covered in Chapter 3.

Markov processes are used extensively in literature due to their ability to accurately represent component degradation. Besnard and Bertling (2010) used Markov models to model WT blade degradation and maintenance. Inspection-based and condition-based maintenance strategies were compared to identify the optimum inspection interval for each strategy. Adumene and Okoro (2020) used Markov models to predict the reliability of WTs comprising multiple components. The components were linked using logic gates allowing for one-sided dependency between them. The research aimed to identify the critical system vulnerability path to assist in management and remedial action. A similar study by Ossai et al. (2016) focused on WT failure rates and DT to model various WT component degradation and maintenance using Markov models. Based on the results, critical components were identified and advised to be focused on for future research.

The main limitations of Markov processes lie in the choice of the steps defining the discrete system states and in the calculation of the transition rates between the states (Shahraki et al., 2017). Segregating system health into discrete states with self-defined boundaries for each state is by itself an assumption. Further, most datasets only contain failure rates of a component which signifies the time from start to failure. To convert this into deterioration transition rates between individual states also requires some assumptions. Another limitation is that the transition rates are constant which limits the model to exponentially distributed transitions. In order to counter these drawbacks, a number of variations exist within Markov processes. Shahraki et al. (2017) provided an overview of the different approaches: Semi Markov processes, Partially Observable Markov processes and Hidden Markov processes. Further, the distinction between discrete time or continuous time processes and homogeneous or non-homogeneous processes exists within each category.

For example, the drawback of constant transition rates can be easily eliminated with the implementation of Semi Markov processes which allow for varying rates. Beyond exponential distributions, existing research also proposes the use of the Weibull distribution to represent the degradation distributions of WT systems (J. Andrawus et al., 2006, Kerres et al., 2015, Le and Andrews, 2016, Ossai et al., 2016). Welte et al. (2006) explained that two-parametric distributions like the Gamma or the Weibull distribution usually perform better due to higher flexibility. To avoid the stark segregation of the health of a system into states, Partially Observable Markov processes and Hidden Markov processes have been developed. Here, the degradation level or health of the component is not directly accessible which is valid for many complex degradation processes and specific systems with directly unobservable system health. For instance, Byon and Ding (2010) applied the Partially Observable Markov process to develop season-dependent condition-based maintenance strategies for a WT gearbox. J. Li et al. (2019) focused on the reliability assessment of WT bearings based on the Hidden Markov model. The health states of the WT were assumed to be hidden and unobservable with the observable parameters being temperature, pressure and flow.

2.5. Dependencies in Modelling

Interactions in the literature are mainly modelled in three ways, stochastic dependence, economic dependence and structural dependence (Laggoune et al., 2010). Olde Keizer et al. (2017) further extends this classification by introducing resource dependence. An overview of these dependencies is provided here.

1. Stochastic dependence implies dependencies between the health or state of components. This is seen when one component's state influences another component's degradation process. For components which share the same load, the failure of one increases the load on the remaining components, increasing their failure rates. As discussed in Section 1.4, stochastic dependencies are further classified as failure-dependent and degradation-dependent.
2. Economic dependence implies dependence on inspection and maintenance costs between multiple FMs or components. This is applicable when the combined system maintenance costs are not simply the sum of the individual maintenance costs, for example, due to fixed set-up costs (Oakley et al., 2022). For OWT, fixed set-up costs can include vessel, equipment and transport costs to the offshore location. These costs do not vary whether maintenance occurs for one component or the entire system. Subsequently, cost savings can be achieved by joint maintenance of multiple components.
3. Structural dependence implies dependence between components linked structurally. Originally, this dependence was mainly studied from a technical point of view. For instance, if the maintenance of one component either requires or prohibits the maintenance of another component, they are structurally dependent. This dependence is extended by Olde Keizer et al. (2017) by analysing the performance point of view. Performance structural dependence exists when the performance of multiple components linked together in a particular configuration affects the overall system performance. The configuration can represent the system as components connected in series, parallel, k-out-of-n or a mixed structure.
4. Resource dependence applies when a common set of resources is shared between multiple components or FMs, e.g., a shared set of tools or a limited number of maintenance workers.

A more recent and detailed study into dependent failure behaviour modelling was carried out by Zeng et al. (2023). A classification framework was developed for different methodologies across both stochastic (statistical) models and physics-based (mechanistic) models as shown in Figure 2.10. While Zeng classifies all models as part of dependent failure modelling, both degradation and failure-dependent models are included in the classification. Further, the models included cover both stochastic and structural dependencies.

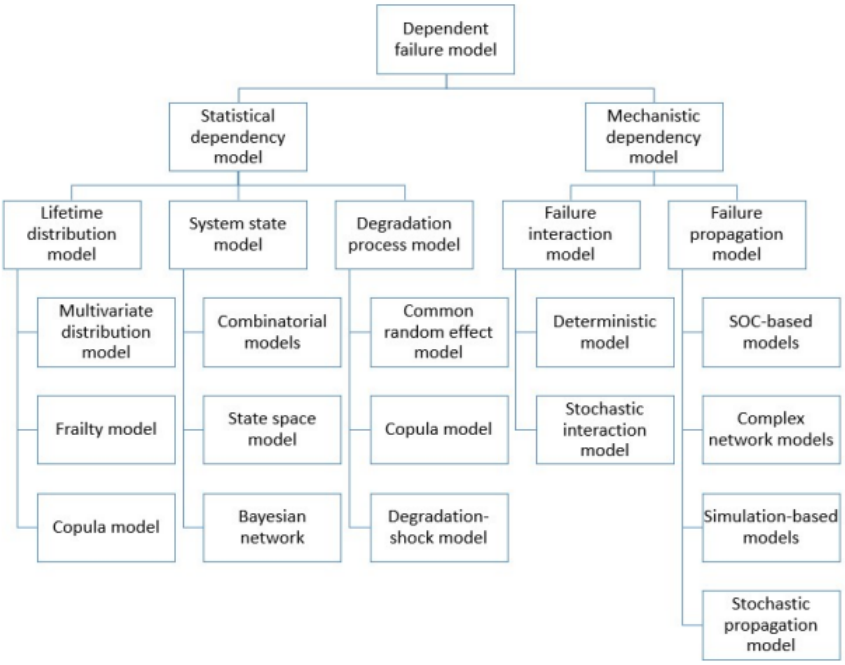

Figure 2.10: Classification framework for dependent failure behavior models (Zeng et al., 2023)

Focusing on statistical models for this study, three categories of lifetime distribution models, system state models and degradation process models are presented by Zeng et al. (2023). Lifetime distribution models focus on modelling statistical dependency between lifetime distributions. This can be done via multivariate distributions which create a joint distribution from individual lifetime distributions. However, the parameters of the joint distribution are difficult to obtain as they need to be estimated from lifetime data, which is scarce. Frailty models simplify this by allowing for the creation of a joint distribution based on individual lifetime distributions (called marginal distribution) and shared frailty terms. Although frailty models work well with failure-dependent models, they cannot directly be applied to degradation-dependent models. Finally, copula models are similar to frailty models and require only the marginal distributions and a copula function. However, using these models involves some mathematical complexity. Further, the copula function's selection is also quite critical to the model. A review conducted by Shahraki et al. (2017) on modelling multiple degradation processes concluded that new multivariate degradation models (P. Wang and Coit, 2004) or copula-based models (Sari, 2008, Y. Li et al., 2021) are gaining attention and many studies on this topic have been proposed.

In case lifetime distributions are unknown, system state models can be used. These models incorporate statistical dependencies between variables which represent component health (also called state). System State models mainly include combinatorial models, state space models and Bayesian networks. Combinatorial models, such as reliability block diagrams and fault trees are used to represent structural dependencies between components of a system. A network structure (components connected in series, parallel, etc. connections) is used which limits each model to the particular case for which it is developed. Further, combinatorial models are limited to representing failure-dependent systems without capturing degradation dependencies. State space models, such as Petri Net and Markov models can model dependencies between component states capturing degradation dependencies. However, these systems face the state space explosion problem for large systems (Zeng et al., 2023). A large system requires many states which makes the model computationally cumbersome to solve. Bayesian networks are graphical methods to represent system states and their failure logic. These models can capture many dependencies between components. However, they are also mainly limited to failure dependencies. To incorporate degradation dependencies, dynamic Bayesian networks need to be implemented. However, these are simply individual Bayesian networks at discrete time events. Subsequently, degradation behaviour in continuous time cannot be captured. Similar to combinatorial models, Bayesian networks also require a network structure which is difficult to create

for large systems.

Finally, degradation process models specifically cover degradation-dependent models, which can model dependence between multiple degradation processes. These models include common random effect models, copula models and degradation shock models. However, as discussed earlier, degradation dependencies can also be modelled by state space models such as Markov processes. Common random effect models are similar to frailty models. Multiple individual degradation processes are modelled separately and linked by shared common parameters. However, the estimation of these shared parameters is often a challenge. Copula models, as discussed earlier, can also be used to model dependencies between the degradation processes. Their strength lies in allowing the separation between the marginal distributions and the copula function. Finally, degradation-shock models model the dependencies between random shocks and a primary degradation process. Shocks are modelled as abrupt increases in degradation levels which might occur due to sudden stresses or impulses acting on the component.

Most of the studies discussed in this chapter only consider single degradation processes. A few studies venture into multiple degradation processes which are primarily limited to stochastic failure dependencies. For example, Besnard and Bertling (2010) proposed multi-failure modelling by considering the degradation of WT blades due to cracking and coupling it with the effects of lightning as shocks to the blades. However, both FMs and their effects were considered to be independent of each other. Consequently, the failure rates for both the degradation process and the shocks were simply summed up. Lyu et al. (2023) modelled dependent behaviour between degradation and shocks. This is similar to the degradation-shock model mentioned in Figure 2.10. A reliability analysis for multi-state systems was conducted by modelling non-linear degradation. The degradation process was defined based on the magnitude and the number of shocks affecting the system state. Here, only a one-sided dependency was seen with shocks affecting the degradation state of the system.

There have also been several research papers incorporating structural dependencies by modelling entire WTs or entire systems comprising multiple components, each with its own FMs. H. Li et al. (2020) used Bayesian networks to conduct a reliability analysis of floating OWTs while including all key components and possible FMs. Zheng et al. (2020) used the fault tree in Figure 2.11 for the reliability analysis of WT pitch systems by connecting failure events with AND and OR gates. Adumene and Okoro (2020) also used a fault tree analysis method including more FMs from individual WT components for reliability prediction in harsh environments. Le and Andrews (2016) used a Petri Net model to model the degradation of all key WT components and their FMs to analyse maintenance actions. Fault trees, which are combinatorial models, and Bayesian networks inherently assume independence of basic events. For example, in Figure 2.11, events X1 and X2 are considered to be independent and are related via an OR gate while contributing to FM M1. Only when either X1 or X2 fails, M1 fails. It is assumed that the individual FMs and their subsequent degradation processes before the failure event occurs are independent of the other FMs. Thus, events X1 and X2 are seen to be failure-dependent but degradation-independent. Such modelling methods consider multiple FMs along with their failure dependencies, which are accounted for within the overall network structure by the hierarchy and the linkages between events. Dependency is included via series or parallel (AND or OR gates) positioning of the FMs which affect the ultimate failure event. However, this dependency is only unidirectional with one failure event (M1) depending on multiple independent FMs (X1, X2). The inherent degradation dependency between the multiple FMs is unaccounted for.

A few other ways to model dependent degradation are also seen in the literature. Tuning the degradation rates (Shen et al., 2020) or sojourn times (Y. Wang and Pham, 2012) of one component based on the degradation state of another adds dependency in an otherwise standard independent model. This dependency, however, is only triggered by a change in the state. A drawback of such models is the requirement of extensive data for each state which requires experimentation or field-tests. For example, different degradation rates or sojourn times must be specified based on each state of a dependent process.

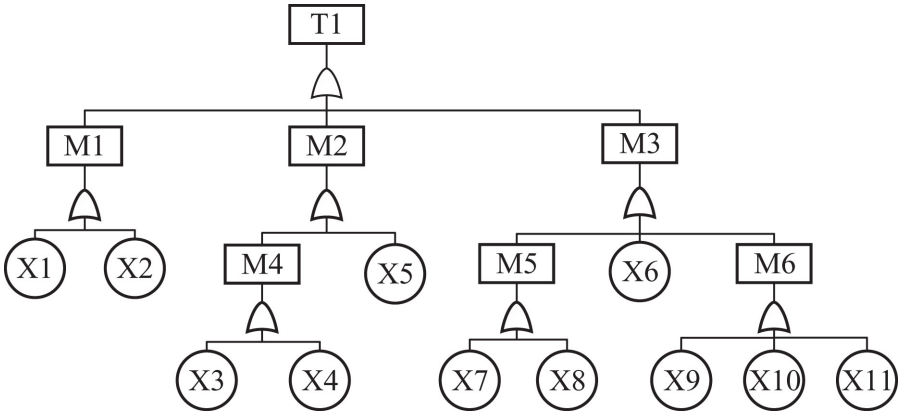

Figure 2.11: Pitch system fault tree analysis (Zheng et al., 2020)

2.6. Maintenance Modelling

Corrective Maintenance (CM) - The strategy only involves the replacement of failed components and is often the simplest for implementation. However, it also leads to large DT from the extensive replacement and repair work undertaken only after a component fails. Subsequent production losses directly translate to unsold energy and substantial monetary losses in the revenue that could be generated. These are referred to as operation costs throughout the study. In addition, procuring new parts and associated lead time add up to the total costs. Further, maintenance costs associated with CM are quite high as component replacement is often, much more expensive than repair. While this strategy might be viable for small onshore WTs, it is no longer cost-effective for large offshore, multi-MW wind farms (Shahraki et al., 2017). With high power ratings, high costs and DTs are associated with every component, leading to considerable operation costs (Ren et al., 2021).

Condition-based Maintenance (CdM) - This strategy is similar to the example in Figure 1.5. It requires continuous monitoring and inspection techniques to determine the current health of the component and schedule any maintenance if required. Sensors are deployed for different WT components and various indicators are measured throughout the operation. These indicators are used to estimate the level of degradation or the health of a component. Based on these outputs, maintenance action is scheduled for when the component's degradation reaches a predetermined threshold and failure is prevented from occurring. Such techniques also consider current metocean conditions and account for bad weather delays while scheduling maintenance actions. CdM strategies are becoming quite popular recently with many ongoing research studies and improvements in the field (Byon and Ding, 2010, Besnard and Bertling, 2010, Le and Andrews, 2016, Abid et al., 2019, C. D. Dao et al., 2021, N. Li et al., 2022). However, they are still quite expensive. Adequate sensors need to be installed and health indicators need to be assessed to ensure precise forecasts for the health of a component. Robust sensors, which can withstand harsh offshore conditions and operate for sufficiently long periods must be deployed, which is expensive. Additionally, data obtained from the sensors can be inaccurate, containing biases and noise, resulting in false positives. Apart from these issues, the sensor used to estimate health might fail making the entire procedure invalid (Ren et al., 2021). Thus, CdM is not entirely economical for all components yet.

Time-based Maintenance (TM) - For TM strategies, inspections and maintenance actions are carried out at predetermined fixed intervals. Thus, regular repairs and maintenance are carried out, unplanned maintenance is eliminated, adequate availability of vessels is maintained and efficient use of resources is achieved (J. Andrawus et al., 2006). However, if a failure occurs between two inspection intervals, the WT remains out of operation until the next planned inspection (Ren et al., 2021). This can lead to large DTs and operational costs. Maintenance intervals for such strategies are often determined based on historical field data such as failure or degradation rates as discussed in Section 1.3. Such strategies depend on the accuracy of the input rates data and the choice of the inspection interval. Too frequent inspections increase WT DT from inspection actions while too-long intervals lead to unexpected failures

between inspections, also increasing WT DT (J. Andrawus et al., 2006). The selection of the inspection interval is often modelled as an optimisation problem to minimize costs and DT (Ren et al., 2021). This is further discussed in Section 2.6.1.

To improve on the limitations of TM strategies, a combined TM-CM strategy is implemented in the literature (Besnard and Bertling, 2010). All maintenance actions are carried out at predetermined inspection intervals, except when failures occur. In case of failures, instead of waiting till the next scheduled inspection, CM tasks are started immediately. Thus, spare parts are ordered, vessels are hired and technicians are allocated. Then, based on the weather conditions, CM is carried out as soon as possible.

Based on the discussion above, the combined TM-CM strategies are selected to be modelled within this study. Once optimised, such strategies are very useful and applicable for extended periods of WT lifetime.

2.6.1. Cost Modelling for Maintenance Strategy Optimization

For most studies in the literature, the objective of maintenance optimization is to find the optimum maintenance strategy. The optimum can be defined as minimum O&M costs (Besnard and Bertling, 2010, Welte et al., 2006), maximum power generation (Arzaghi et al., 2020), minimum expected energy not supplied or minimum downtime (C. D. Dao et al., 2021). While maximising power generation or minimizing downtime might share the same optima, the same might not hold for O&M costs. For example, a strategy aimed at minimum DT and energy loss will focus on maximising WT availability. A very frequent TM strategy can achieve high WT availability but will also lead to extremely high O&M costs. Thus, it might be interesting to analyse both DT and costs while selecting an optimum maintenance strategy.

An overview of the various costs associated with inspection and maintenance actions was presented earlier in Section 1.5. Ren et al. (2021) and Shafiee and Sørensen (2019) provided a review of WT O&M actions with a detailed breakdown of the total costs. These costs consist of replacement component cost (the cost of the component which is to be replaced by a new one), logistics costs (for renting the service vessels and transportation cost), labour costs (for the technicians performing inspections and maintenance tasks on components), and production losses (due to WT failure and DT). For the purpose of this study, the above-mentioned costs are classified into three broad categories: maintenance costs (comprising component replacement, logistics and labour costs), inspection costs (comprising labour and logistics costs) and operation costs (comprising production losses).

Degradation models coupled with various maintenance strategies are usually tested computationally to decide the optimum strategy. For the selected TM-CM strategy, maintenance optimisation can be achieved by applying several different inspection intervals and calculating lifetime costs and downtime for each. An example of this inspection interval optimisation problem is shown in Figure 2.12 where lifetime costs are minimized. Inspection intervals are varied on the x-axis with each interval corresponding to one TM strategy. Each strategy is run for the entire WT lifetime, O&M actions are simulated and lifetime costs are accumulated. For long inspection intervals, inspection actions are carried out at a low frequency. Performing inspections infrequently will allow the system to degrade to a higher extent or even fail. Higher degradation or a high number of failures would require additional maintenance action, increasing maintenance costs. Simultaneously, due to the infrequent inspection actions, vessels and labourers are deployed to the OWT only a handful of times. Hence, the cost of performing inspections, which mainly comprises of vessel and labour costs, is relatively small. On the other hand, frequent maintenance actions for short inspection intervals improve the reliability of the turbine. The turbine degrades only slightly between consecutive inspections. This lowers the costs of repairs and maintenance to be conducted. However, frequent maintenance also includes renting vessels and contracting labourers quite frequently, which increases the cost of performing inspections exorbitantly (Shafiee and Sørensen, 2019, J. A. Andrawus et al., 2007). Due to the competing natures of inspection and maintenance costs, a minimum is seen in the total cost curve. Thus, finding the cost-optimal solution that minimizes the lifetime costs is critical for TM strategies.

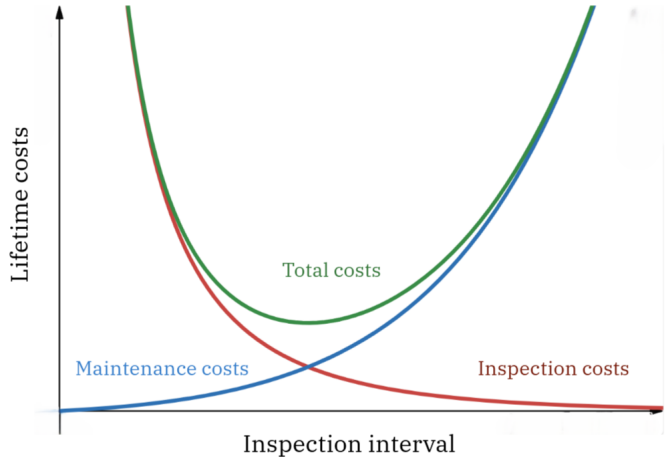

Figure 2.12: Example of inspection interval optimisation problem for TM strategies (Mammadov, 2024)

3
Theoretical Background

This chapter aims to provide a theoretical background for the concepts and approaches used throughout the study. First, Section 3.1 introduces the concept of Markov Chains and their analysis, including the types of Markov chains, transition probability calculations, sojourn times, transition rates and state transition diagrams. Next, the theory for the integration of Markov Chains with Monte Carlo simulations is presented in Section 3.2. In order to model dependent degradation, copula models will be used and are introduced in Section 3.3. Finally, using the concepts explained in the earlier sections, the theory of failure rate variation across component life and deterioration rate estimation is discussed in Section 3.4.

3.1. Markov Chain Analysis

3.1.1. Markov Property

The Markov property, as explained in Section 2.4.1.1, is defined as "the future state of the system is dependent only on its current state and is independent of the past states". This property holds true in many physical applications across various fields such as finance, economics, biology and engineering, to name a few. Consequently, this concept is immensely popular and widely used.

Mathematically, the Markov property is defined as (Pishro-Nik, 2014):

$$P(X(t_{n+1}) = j|X(t_n) = i, X(t_{n-1}) = i_{n-1}, ..., X(t_1) = i_1) = P(X(t_{n+1}) = j|X(t_n) = i) \tag{3.1}$$

where, t_n is time event n, X is the Markov process and i_n is the state of the system. Thus, $X(t_n) = i_n$ means that the process X at time event t_n is in the state i_n. $P(X)$ is the probability of the process being in a particular state. In line with the definition of the Markov property, Equation 3.1 states that the probability distribution of $X(t_{n+1})$ is determined solely by $X(t_n)$, the state of the process at time n, and does not depend on the past values of $X(t_k)$ for $k \leq n-1$.

3.1.2. Markov Chains

Based on the Markov property, a fundamental concept in probability theory called Markov processes has been developed. Privault (2018) explains that Markov processes are stochastic processes which follow the Markov property and are used as a mathematical tool to simulate time-dependent random phenomena. These processes describe systems that transition from one state to another, based on certain probabilistic rules. Here, a 'state' is defined as possible configurations or conditions or health of a system. For example, based on the problem to be modelled, states can be defined as healthy, degraded, critical and failure. The random evolution through the states, also called transitions between the states, is determined by transition rates or by transition probabilities.

3.1.2.1. Transition Probabilities

Initially introduced in Equation 3.1, the term $P(X(t_n) = j|X(t_{n-1}) = i)$ stands for conditional or more specifically for this case, transitional probability. These probabilities are:

$$P_{ij} = P(X(t_{n+1}) = j|X(t_n) = i) \tag{3.2}$$

Thus, if the process is in state i at time event t_n, it will make a transition to state j at time event t_{n+1} with the probability P_{ij}.

Since the transition probability will be different for each unique combination of states (transition from the state i to state j), this data can be represented in a matrix which is indexed by the state number. Assuming that for a particular system, the states S vary from 0 to n, such that $S \in (0, 1, 2..., n)$, the transition probability matrix can be defined as in Equation 3.3.

$$P = \begin{bmatrix} P_{00} & P_{01} & P_{02} & .. & P_{0n} \\ P_{10} & P_{11} & P_{12} & .. & P_{1n} \\ : & : & : & & \\ : & : & : & & \\ P_{n0} & P_{n1} & P_{n2} & .. & P_{nn} \end{bmatrix} \tag{3.3}$$

where P denotes the one-step transition probability matrix.

Transition probabilities are always nonnegative. Further, assuming that a process must always transition into some state, i.e. when the process leaves state i, it must enter another state j, (Ross, 2014), this results in:

$$P_{ij} >= 0,\ i, j >= 0; \tag{3.4}$$

$$P_{ii} = 0 \tag{3.5}$$

$$\sum_j P_{ij} = 1,\ i = 0, 1... \tag{3.6}$$

This translates to the condition that the sum of the probabilities in any particular row of the transition probability matrix must equal 1.

3.1.3. Types of Markov Chains

Markov processes are classified into two broad groups of Discrete Time Markov Chains (DTMC) and Continuous Time Markov Chains (CTMC) (Privault, 2018).

1. DTMCs consider each event happening at discrete time instants. Thus, the process transitions from one state to another only at discrete time events, after one unit of time for each transition.
2. In CTMCs, time is no longer assumed to be a discrete variable. The time spent in each state is a continuous random variable, also called sojourn time.

DTMCs are only useful in situations when the time spent in each state is constant. A DTMC, for instance, can be used to track an epidemic's monthly progression. In the context of this study, a DTMC would restrict WT component degradation to happen once a year or at other specified discrete time intervals. Degradation, however, is an unpredictable and random process which can occur at any time instant. CTMCs incorporate this randomness by allowing the time spent in each state to be a continuous random variable (Pishro-Nik, 2014). Further, CTMCs are used to represent the deterioration process in all research in the literature that uses Markov processes (Welte et al., 2006, Adumene and Okoro, 2020, Ossai et al., 2016). This thesis is concerned with the degradation and maintenance modelling of WTs across their lifetimes and thus, CTMCs are used to represent this process and will be discussed in more detail.

3.1.4. Continuous Time Markov Chains

CTMCs have two key components (Ross, 2014):

1. a discrete-time Markov chain along with its transition probabilities;
2. a holding time parameter for each state, called the transition rate, which determines the amount of time spent in that state.

The theory discussed in Section 3.1.2 is valid for DTMCs with process states, transitions and their probabilities defined at discrete time events of t_n, t_{n+1}. This can further be used for CTMCs.

Rewriting Equation 3.2 for continuous-time processes results in Equation 3.7. Here, time events are replaced with time values. Hence $X(t)$ now represents the value of the Markov process at time t. If Equation 3.7 is independent of r, then the transition probabilities are said to be stationary or homogeneous probabilities which do not vary with time. An alternate class of Markov processes are non-homogeneous processes with transition probabilities varying with time.

$$P_{ij} = P(X(t+r) = j | X(r) = i) \tag{3.7}$$

3.1.4.1. Sojourn Times

As discussed earlier, CTMCs simulate the process with sojourn times as continuous random variables instead of discrete time events. In order to satisfy the Markov Property, the sojourn times are represented by random variables which must be memoryless. Exponential random variables with an exponential Probability Distribution Function (PDF) satisfy this criterion (Ross, 2014). This is further explained here.

If λ is the transition rate which determines the amount of time spent in a state, the exponential PDF, for λ > 0, is defined by Equation 3.8 (Ross, 2014).

$$f(x) = \begin{cases} \lambda e^{(-\lambda x)}, \text{ if } x > 0 \\ 0, \text{ if } x < 0 \end{cases} \tag{3.8}$$

In order to satisfy the Markov property, the exponential probability distributions must be memoryless as seen in Equation 3.9.

$$P(X > (r+t) | X > (t)) = P(X > (r)), \quad \forall \textit{ r, t >= 0} \tag{3.9}$$

If X represents the lifetime of a component, Equation 3.9 states that the probability of the component surviving at least $r + t$ hours given that it has survived t hours is the same as the initial probability that the component survived r hours. This is similar to the component forgetting that it has already survived t hours.

Equation 3.9 is equivalent to

$$\frac{P(X > (r+t)) \cap P(X > (t))}{P(X > (t))} = P(X > (r)) \tag{3.10}$$

$$P(X > (r+t)) = P(X > (r)) P(X > (t)) \tag{3.11}$$

It can be seen that Equation 3.8 satisfies Equation 3.11 for $e^{-\lambda(r+t)} = e^{-\lambda r} e^{-\lambda t}$. Thus, it follows that exponential random variables are memoryless. This property makes exponential random variables suitable for Markov processes.

Exponential sojourn time PDFs are visualized for sample values of λ in Figure 3.1. The distributions show the probability of the sojourn times between transitions. An unexpected dip in the PDFs is seen for small values of sojourn times in all three curves. This is because the curves have been plotted using random value sampling of a million samples instead of the analytical function equation.

To conclude, a weighted random choice is made for the sojourn time using probabilities of the exponential distribution at each state. A weighted random choice function assigns weights or probabilities to each available choice. Then, random selection is carried out in a way that the results of a large number of random selections will replicate the probability curve.

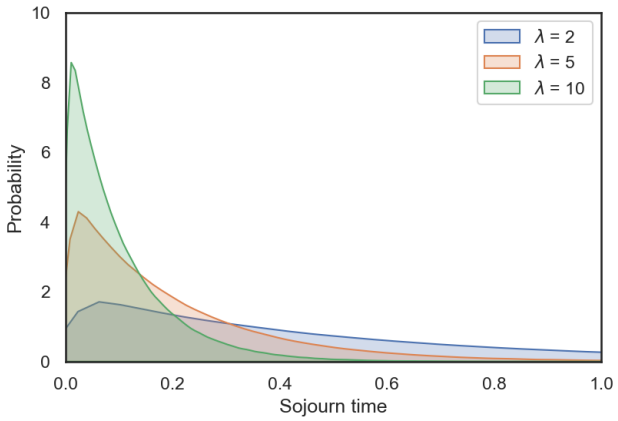

Figure 3.1: Exponential PDFs for λ = 2, 5, 10

3.1.4.2. Transition Rates

Transition rates govern the transitions between the various states of a Markov chain. The parameter λ introduced in Equation 3.8 represents the transition rate which also equals the inverse of the expectation (mean) of exponential distributions. The expectation of an exponential random variable is calculated as:

$$\begin{aligned} E[X] &= \int_0^\infty x f(x)\, dx \\ &= \int_0^\infty x\lambda e^{-\lambda x}\, dx \\ &= -xe^{-\lambda x}\Big|_0^\infty + \int_0^\infty e^{-\lambda x}\, dx \\ &= 0 - \frac{e^{-\lambda x}}{\lambda}\Big|_0^\infty \\ &= \frac{1}{\lambda} \end{aligned} \tag{3.12}$$

Thus, the sojourn times spent in each state are exponentially distributed, with the mean equal to the inverse of the transition rate. This property of having a constant transition rate (λ) being equal to the reciprocal of the mean is only valid for exponential distributions (Singh and Billinton, 1977). Based on the transition rate for each state, the exponential PDF defining the sojourn times can be varied, specific to each state and its properties. This property is useful to represent degradation across states, where the rate of degradation increases with the worsening health of the component.

Apart from being linked to sojourn times, transition rates are also inherently linked to transition probabilities (Pishro-Nik, 2014, Singh and Billinton, 1977). Consider a CTMC $X(t)$ with $X(0) = i$. The chain jumps to the next state at T_{Si} where T_{Si} is chosen randomly from an exponential distribution with mean λ_i. For a very small $\delta > 0$, following the Taylor Series expansion, the transition probability is calculated as:

$$\begin{aligned} P(T_{Si} < \delta) &= 1 - e^{-\lambda_i \delta} \\ &\approx 1 - (1 - \lambda_i \delta) \\ &= \lambda_i \delta \end{aligned} \tag{3.13}$$

Thus, the probability to leave state i within time δ is approximately $\lambda_i \delta$. Consequently, λ_i is called the transition rate out of state i and it is defined as:

$$\lambda_i = \lim_{\delta \to 0^+} \left[\frac{P(X(\delta) \neq i | X(0) = i)}{\delta} \right] \tag{3.14}$$

Similarly, when transitioning from states i to j, we get $\lambda_{ij} = \lambda_i P_{ij}$ where λ_{ij} is the transition rate from state i to j. Similar to Equation 3.14,

$$\begin{aligned} \lambda_{ij} &= \lim_{\delta \to 0^+} \left[\frac{P(X(\delta) = j | X(0) = i)}{\delta} \right] \\ &= \frac{d}{d\delta} P_{ij} \end{aligned} \tag{3.15}$$

Using this transition rate, a square transition rate matrix, also called generator matrix, can be built. Similar to the transition probability matrix, it has a size equal to the number of states for the rates corresponding to each unique combination of states. This matrix's diagonal elements are chosen so that the sum of the rows equals zero (Privault, 2018) as follows:

$$\begin{aligned} \sum_{j \in S} \lambda_{ij} &= \frac{d}{d\delta} \sum_{j \in S} P_{ij} \\ &= \frac{d}{d\delta} 1 \\ &= 0 \end{aligned} \tag{3.16}$$

where S is the state space of the Markov process. Using Equation 3.16, the diagonal elements are obtained to be equal to the negative of the rate of leaving the state as follows:

$$\begin{aligned} \lambda_{ii} &= -\sum_{j \neq i} \lambda_{ij} \\ &= -\sum_{j \neq i} \lambda_i P_{ij} \\ &= -\lambda_i \sum_{j \neq i} P_{ij} \\ &= -\lambda_i \end{aligned} \tag{3.17}$$

Given the transition rates, the transition probabilities can be calculated by applying the Laplace-Stieltjes transform and its inverse to Equation 3.14. Assuming that δ is small, we can alternatively use $\lambda_{ij} = \lambda_i P_{ij}$. The transition probabilities can be then defined as:

$$P_{ij} = \frac{\lambda_{ij}}{\lambda_i} \tag{3.18}$$

By using Equation 3.17, Equation 3.18 can be rewritten as:

$$\begin{aligned} P_{ij} &= \frac{\lambda_{ij}}{-\lambda_{ii}} \\ &= \frac{\lambda_{ij}}{\sum_j \lambda_{ij}} \end{aligned} \tag{3.19}$$

3.1.5. State Transition Diagrams

State Transition Diagrams are a graphical method to represent the different states of a component (or a system) along with the transitions between them. These are usually represented by circles with the number or the name of the state inside. Each transition in the state transition diagram is accompanied by a transition rate specific to that transition. State diagrams are widely used to represent probabilistic

maintenance models (Abeygunwardane, 2012). This is due to two key advantages. First, state diagrams can provide a concise and clear representation of all processes of deterioration, inspection and maintenance of a component and the connections between these states. Second, these diagrams can be converted directly into Markov models and parameters of rates and probabilities can be calculated easily as described earlier.

To better understand Markov chains, an example of a three-state Markov chain state diagram is shown in Figure 3.2. A three-state $S = \{1,2,3\}$ Markov chain is considered with transitions amongst the different states. This Markov chain represents the degradation of a component from 'Normal' state to 'Degraded' state and finally to the 'Failed' state. The transition diagram for this Markov chain is shown in Figure 3.2.

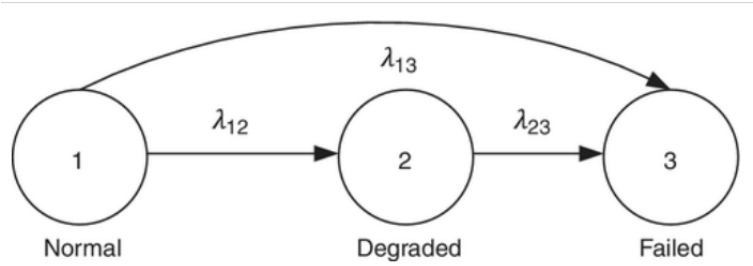

Figure 3.2: Three state Markov chain state diagram (Adumene and Okoro, 2020)

Its 3X3 transition rate matrix is then:

$$Q = \begin{bmatrix} -(\lambda_{12} + \lambda_{13}) & \lambda_{12} & \lambda_{13} \\ 0 & -\lambda_{23} & \lambda_{23} \\ 0 & 0 & 0 \end{bmatrix} \tag{3.20}$$

where Q represents the transition rate/generator matrix. The matrix is built by first filling in the non-diagonal elements using the transition rates from Figure 3.2. Transitions for state 1 to state 2, state 2 to state 3 and state 1 to state 3 are set at their respective positions in cell 1-2, cell 2-3 and cell 1-3. The lower-triangular cell values can be set to 0 with no transitions occurring from higher states to lower states. Finally, the diagonal values are calculated using Equation 3.17, such that the sum of the rows equals zero.

Based on Equation 3.19, the transition probabilities for this Markov chain are:

$$P = \begin{bmatrix} 0 & \frac{\lambda_{12}}{\lambda_{12} + \lambda_{13}} & \frac{\lambda_{13}}{\lambda_{12} + \lambda_{13}} \\ 0 & 0 & \frac{\lambda_{23}}{\lambda_{23}} \\ 0 & 0 & 0 \end{bmatrix} \tag{3.21}$$

Here state 3 is said to be an 'absorbing' state because once the system enters state 3, it cannot transition to any other state and will always remain in that state.

3.2. Markov Chain Monte Carlo Simulations

A Monte Carlo simulation is a mathematical technique for considering the effects of uncertainty in any model. They allow users to model a wide range of possible outcomes and offer a clearer picture of the results than a deterministic forecast (Lutkevich, 2023). When built on top of a Markov Chain, a Markov Chain Monte Carlo (MCMC) is obtained and this is a powerful sampling methodology. Since Markov Chains are stochastic models, they are inherently random processes with values that vary each time the simulations are run. For example, the time it takes for a component to fail, given by the sum of

sojourn times in all states, is a random number obtained from the sum of multiple random exponential variables. Each time a Markov chain is simulated, the value of this time-to-failure parameter can be different.

In order to extract useful data from the Markov chain simulation, a Monte Carlo process is run on top of the chain. In a Monte Carlo process, many representative random values are sampled from the given distribution (Columbia, 2016). Using these samples, multiple Markov chains are simulated and a large sample of outputs is obtained. Subsequently, MCMC simulations allow for parameter estimation from this sample, such as means, variances and standard deviations. In the case of the time-to-failure parameter, this means that if n Monte Carlo simulations are run, n values of the time-to-failure will be obtained. The distribution of these values can then be used to estimate the mean time-to-failure (MTTF).

The choice of the number of Monte Carlo simulations to run is quite important as it greatly affects both the mean and the uncertainty associated with it. With MCMCs, it is seen that with an increasing number of simulations, the process converges to produce a distribution that is a mirror image of the actual distribution (Columbia, 2016). This is known as the 'weak law of large numbers'. Ibe (2014) explains this law as follows. "The weak law of large numbers essentially states that for any nonzero specified margin, no matter how small, there is a high probability that the average of a sufficiently large number of observations will be close to the expected value within the margin." Once an MCMC reaches a stable number of samples, the process is said to have converged. This number can be estimated by quantifying the uncertainty of the results as follows.

Since the model is stochastic, there is a degree of uncertainty associated with its outputs. This is quantified by using standard deviations or standard errors. For any sample, the standard deviation is defined as the dispersion or variability of the sample values from the mean. Further, the sample's mean value is calculated as a single value. However, Altman and Bland (2005) explain that this mean is not representative of the entire population. Here, a population is defined as a collection of samples. If 'k' simulations are run for a model, one sample with 'k' values is obtained with a deterministic mean and standard deviation. However, the next time the model is run for 'k' simulations, different values of the mean and standard deviation might be obtained. Thus, the sample mean varies for each sample. Hence, for a stochastic simulation, one should be interested in the mean of the population from which all the samples are derived. The population mean is estimated to lie within a range defined by the standard error. The standard error can be understood as a measure of the precision of the sample mean and is defined as:

$$Se = \frac{\sigma}{\sqrt{n}} \tag{3.22}$$

where Se represents the standard error, σ represents the standard deviation and n represents the number of samples or the sample size of a sample. With larger sample sizes, the standard error decreases due to the reduced dispersion and the sample mean getting closer to the population mean (Herman et al., 2022). On the other hand, the standard deviation does not depend on the sample size of a simulation.

A common way to use standard errors is to calculate Confidence Intervals (CIs) of the mean values. A CI is a range of values within which the population mean is expected to lie and is calculated as:

$$CI = \mu \pm Z \times Se \tag{3.23}$$

where μ is the mean and Z is a reliability factor obtained from the sample size and the confidence percentage. The confidence percentage is defined as follows. A 95% CI (95% and 99% are typical values) means that for 95% of the samples, the CI range contains the true population mean (AnalystPrep, 2021, Herman et al., 2022). For any non-normal distribution with a sufficiently large sample size, the area under the curve from -1.96 σ to +1.96 σ covers 95% of the total area (Meyer, 2022). Thus, 1.96 is the reliability factor for a 95% CI. AnalystPrep (2021) further adds that for Z to be 1.96, a sample size greater than a thousand values must be used. Since, all the simulations in this study use more than

a thousand samples, Z equal to 1.96 is used to obtain the 95% CI range. Using Equation 3.22 and Equation 3.23, the 95% CI is calculated as:

$$95\%\ CI = \mu\ \pm\ \frac{1.96\ \sigma}{\sqrt{n}} \tag{3.24}$$

Besnard and Bertling (2010) introduce another uncertainty parameter called Coefficient of Variation (CV). It is defined as (Hayes, 2024):

$$CV = \frac{\sigma}{\mu} \tag{3.25}$$

The CV measures the variability of the sample around the mean. It is useful for comparing different samples with varying means. Finally, the sample size is selected based on the values of the 95% CI and the CV.

A general outline of the steps included in a Monte Carlo simulation is given as follows (Lutkevich, 2023):

1. Build the model: construct the mathematical model, further discussed in Chapter 4.
2. Selection of simulation variables: choose variables of the model which exhibit uncertainty. Subsequently, select suitable probability distributions for each random variable.
3. Run multiple simulations: generate random samples for the random variables and run the mathematical model for multiple iterations.
4. Aggregate and analyze results: with a large data set as output from the multiple simulations, calculate statistical measures such as mean and standard deviation.

3.3. Copula Models

As discussed earlier in Section 2.5, a number of models exist to simulate dependency in degradation. Of all these models, copula models are very popular due to their ease of modelling dependency based on only the marginal distributions. Furthermore, the complex mathematics involved can be easily dealt with by readily available copula packages in Python. Thus, copula modes will be used in this project to represent dependencies. To provide a basic explanation of copulas, Y. Li et al. (2021) cite Sklar's theorem who first introduced the concept of copulas. The theorem states that any multivariate joint distribution can be written in terms of univariate marginal distribution functions and a copula which describes the dependence structure between the variables.

Healy (2020) provides a concise and clear explanation of copulas. Consider a distribution X from which random variables $(x_1, x_2 ... x_n)$ are simulated. Since the x_n variables are drawn from this distribution independently, X can be referred to as a marginal distribution $f_X(x)$. In case there exist d distributions, each marginal distribution will be referred to as $f_{X_1}(x_1), f_{X_2}(x_2) ... f_{X_d}(x_d)$. The correlation between each of these marginal distributions is a fundamental property of the copula and it is defined as:

$$\theta = \begin{pmatrix} \theta_{X_1X_1} & \theta_{X_1X_2} & .. & \theta_{X_1X_d} \\ \theta_{X_2X_1} & \theta_{X_2X_2} & .. & \theta_{X_2X_d} \\ : & : & : & : \\ : & : & : & : \\ \theta_{X_dX_1} & \theta_{X_dX_2} & .. & \theta_{X_dX_d} \end{pmatrix} \tag{3.26}$$

where each term of the matrix $\theta_{X_iX_j}$ is the correlation between two independent distributions. Sklar's theorem can then be written as:

$$f_{X_1,X_2 ... X_d}(x_1, x_2 ... x_d) = C(f_{X_1}(x_1) \cdot f_{X_2}(x_2) \cdots f_{X_d}(x_d)) \tag{3.27}$$

where the function on the left is the joint distribution and C is the copula.

For two independent marginal distributions X_1, X_2, their correlation ($\theta_{X_1X_2}$) will be equal to zero. Due to independence, changes in one process do not affect the other. Subsequently, their joint distribution is simply the product of their marginal distributions:

$$f_{X_1,X_2}(x_1, x_2) = f_{X_1}(x_1) \cdot f_{X_2}(x_2) \tag{3.28}$$

There exist several families of copula functions such as the Elliptical copula family and the Archimedean copulas family (De Nie, 2016). Most common Elliptical copulas are Gaussian copula and Student-t copula. Prominent Archimedean copulas are Ali–Mikhail–Haq copula, Frank copula, Clayton copula and Gumbel copula. Archimedean copulas have an explicit formula i.e. a known mathematical expression, which is not the case for Gaussian copulas (Nelsen, 2006). Furthermore, they only require a single parameter to define the strength of the dependency compared to Gaussian copulas (De Nie, 2016). The selection of the most apt copula function and its parameters to represent the multivariate joint distribution is an important task. The entire process is not dealt with in detail, however, a concise explanation is provided in this section. The selection of the copula model is based on previous research studies on the topic. The equations of the cumulative distributions for a few of the popular and well-known bivariate copula functions are (Wikipedia, 2024):

Clayton Copula,

$$C_\theta(u, v) = [max\{u^{-\theta} + v^{-\theta} - 1; 0\}]^{-1/\theta} \tag{3.29}$$

$$\theta \in [-1, \infty) \setminus \{0\} \tag{3.30}$$

where u and v represent variables from the marginal distributions and θ represents the correlation between the two distributions (as per Equation 3.26) for all copula equations.

Gumbel Copula

$$C_\theta(u, v) = \exp[-((-\log(u))^\theta + (-\log(v))^\theta)^{1/\theta}] \tag{3.31}$$

$$\theta \in (1, \infty) \tag{3.32}$$

Frank Copula

$$C_\theta(u, v) = -\frac{1}{\theta} \log\left[1 + \frac{(\exp(-\theta u) - 1)(\exp(-\theta v) - 1)}{\exp -\theta - 1}\right] \tag{3.33}$$

$$\theta \in \mathbb{R} \setminus \{0\} \tag{3.34}$$

AMH Copula

$$C_\theta(u, v) = \frac{uv}{1 - \theta(1 - u)(1 - v)} \tag{3.35}$$

$$\theta \in [-1, 1] \tag{3.36}$$

Student-t Copula,

$$C_{\theta\nu}(u, v) = t_{\theta\nu}(t_\nu^{-1}(u), t_\nu^{-1}(v)) \tag{3.37}$$

$$t_\nu(x) = \int_{-\infty}^{x} \frac{\Gamma((\nu + 1)/2)}{\sqrt{\pi\nu}\Gamma(\nu/2)} \left(1 + \frac{s^2}{\nu}\right)^{-\frac{\nu+1}{2}} ds \tag{3.38}$$

$$t_\nu(x, y) = \int_{-\infty}^{x} \int_{-\infty}^{y} \frac{1}{2\pi\sqrt{1 - \theta^2}} \left(1 + \frac{s^2 + t^2 - 2\theta st}{\nu(1 - \theta^2)}\right)^{-\frac{\nu+2}{2}} ds\, dt \tag{3.39}$$

$$\theta \in (-1, 1) \tag{3.40}$$

with ν degrees of freedom and Γ representing the Gamma function.

The plots of the PDFs for the copulas functions (C_θ) discussed above are shown in Figure 3.3

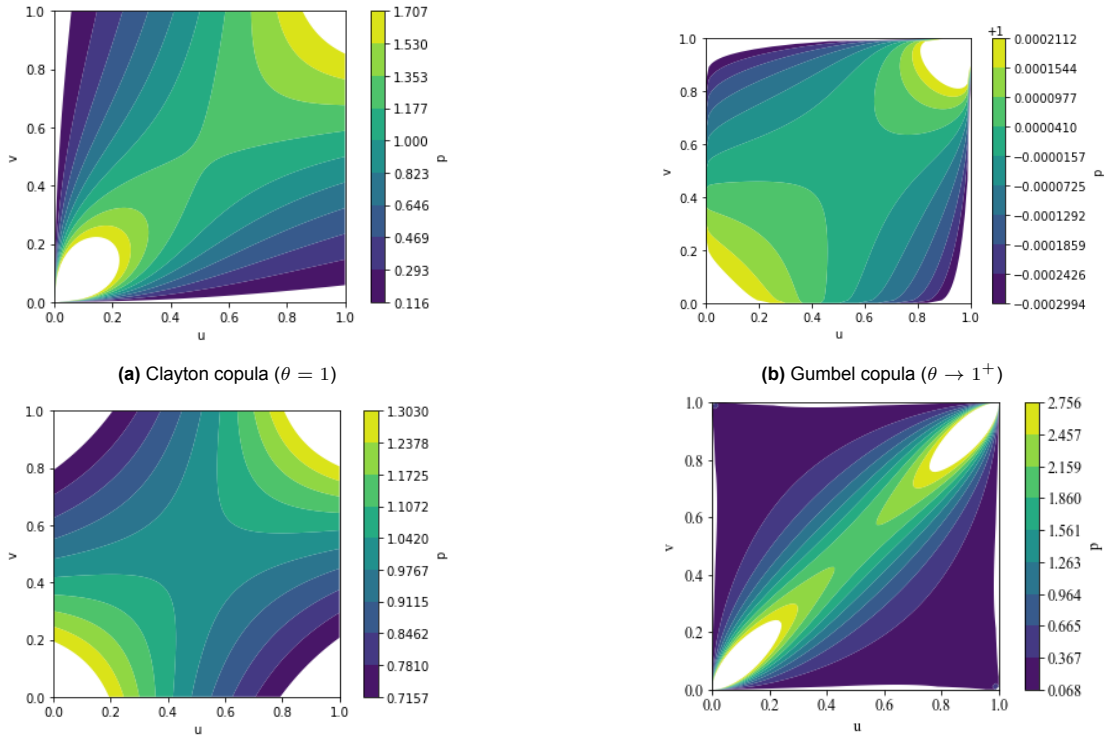

(a) Clayton copula ($\theta = 1$)

(b) Gumbel copula ($\theta \to 1^+$)

(c) Frank copula ($\theta = 1$)

(d) Student-t copula (θ = 0.8, ν = 2)

Figure 3.3: PDFs of a) Clayton, b) Gumbel, c) Frank and d) Student-t copulas

An important property of the copulas is the tail dependence which measures the distribution dependence in the upper-right and lower-left quadrants. Thus, it represents the tendency for extreme values of the two variables to occur together. According to De Nie (2016), "tail dependence in a bivariate distribution can be represented by the probability that the first variable exceeds its q-quantile, given that the other exceeds its own q-quantile. The limiting probability, as q goes to infinity, is called the upper-tail dependence coefficient, and a copula is said to be upper-tail dependent if this limit is not zero". Specifically, according to FinRGB (2023), "tail dependence refers to the conditional probability of an extreme move in one variable given an extreme move in another variable"

Tail dependencies are particularly important for non-normal multivariate distributions. For example, interactions between extreme wind and wave events are perfectly captured by an upper tail-dependent copula (De Nie, 2016). Similarly, a multivariate distribution with exponential marginals and high values for lower indices might benefit from a lower tail-dependent copula. Tail dependency is also observed in the plots of the probability density functions for the different copulas in Figure 3.3. Orcel et al. (2021) quantifies this tail-dependence using tail-dependence coefficients for a variety of copulas. The AMH copula is seen to have neither lower nor upper tail dependence. Healy (2020) states that the Gaussian copula is the standard normal copula without any particular weighting towards the different parts of the distribution. The Student t-Copula (Figure 3.3d) on the other hand assigns more weight to both tails of the distribution. The Clayton copula (Figure 3.3a) is only lower-tail dependent while the Gumbel copula (Figure 3.3b) is upper-tail dependent. Similar to the Gaussian and AMH copula, the Frank Copula (Figure 3.3c) is neither lower nor upper tail dependent (De Nie, 2016). Since tail-dependence is important for exponential distributions, only one of the three (Frank copula) is shown for the comparison.

For dependant degradation modelling, Equation 3.27 is used to create a joint distribution. The independent exponential distributions of the sojourn times (Figure 3.1) for each failure mode are used as marginal distributions (f_{X1} and f_{X2}). These marginal distributions are combined with a copula (C_θ) to obtain a bivariate sojourn time distribution. This bivariate distribution can further be used to draw random samples of the sojourn time values instead of the previously used independent exponential distributions. Since the marginal distributions for this study are exponential distributions following the

Markov chain properties, the copula functions are applied to sample marginal exponential distributions which represent sojourn time PDFs. The bivariate sojourn time PDFs are plotted in Figure 3.4. The X and Y axis values correspond to sojourn times of individual FMs and the color of PDF corresponds to the value of probability. Here, the spread of the PDF plot and the variation of the values can be linked back to the individual functions. Compared to the others, the Student-t copula (Figure 3.4d) shows a narrower spread with higher values towards the upper tail. This is due to its both upper and lower tail dependency properties. Gumbel (Figure 3.4b) and Frank copulas (Figure 3.4c) show a wider spread of high probability values but the peak value is smaller than the Clayton copula (Figure 3.4a). Finally, the Clayton copula shows a balanced spread and high peak values because of its lower tail dependence property. Due to the exponential distribution, a larger probability of occurrence is seen for the smaller values. As a result, more focus must be applied to the lower-left region of the copula which is equivalent to a copula with a lower-tail dependency. Thus, the Clayton copula is chosen and applied to the dependent degradation modelling case for this study. To understand the impact of other copulas, the Gumbel copula is also applied to the final proposed dependent model. This is presented in section A.1.

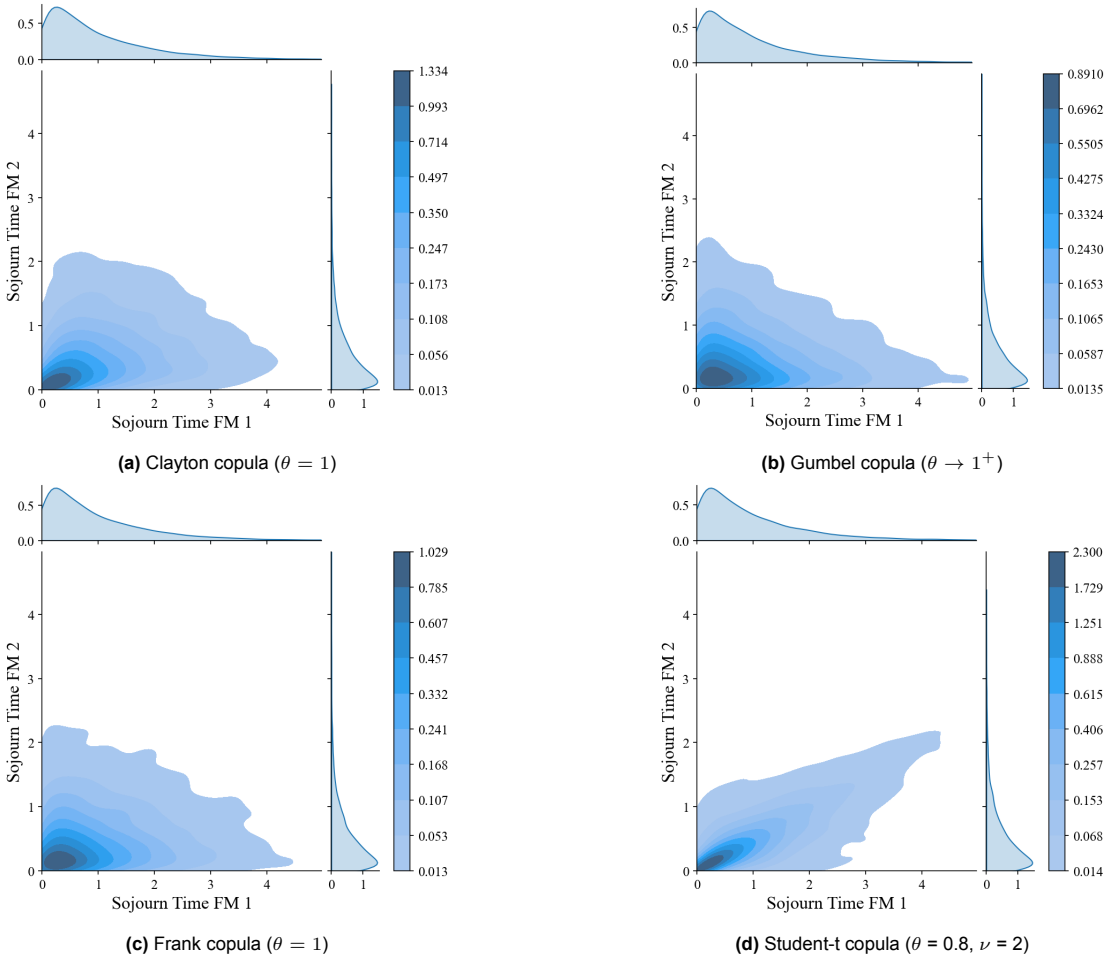

(a) Clayton copula ($\theta = 1$)

(b) Gumbel copula ($\theta \to 1^{+}$)

(c) Frank copula ($\theta = 1$)

(d) Student-t copula (θ = 0.8, ν = 2)

Figure 3.4: Bivariate sojourn time PDFs of a) Clayton, b) Gumbel, c) Frank and d) Student-t copulas applied to marginal exponential distributions

In Figure 3.3 and Figure 3.4 the correlation coefficient, θ, is assumed to be equal to 1 for the Clayton copulas. Bolbolian (2020) explains the significance of this coefficient for extreme limiting/boundary values. As θ tends to infinity, the degree of dependency increases and the copula approaches the monotonic copula, which corresponds to a very strong correlation. Vice versa, as θ tends to zero, the independence copula is obtained, which corresponds to no correlation. Figure 3.5 shows the dependency of the PDF of the Clayton copula applied to exponential marginal distributions on θ. As θ increases, the curve peaks become higher and sharper with steeper declines on both sides (seen with

increasing upper limit values on the colour bar). The spread of the peaks is also seen to reduce with increasing θ as the distribution becomes narrower and more concentrated towards the diagonal. Financial Wisdom Forum (2010) calculated the Pearson correlation coefficient for Clayton copula with varying copula correlation coefficient d as shown in Figure 3.6. Although d is used instead of θ in the study, both parameters correspond to the copula correlation coefficient. The figure shows a steep increase in the correlation for small values of θ with the curve reaching an asymptote for larger θs. For θ equal to 5, a Pearson correlation of 87% is observed. For most applications and from most studies in literature (Y. Li et al., 2021), Sari, 2008, Bielecki et al., 2008), it is gleaned that θ is estimated from data. Usually, multivariate data already exists, such as wind and wave parameters over a defined time duration, and a copula is fit to this data. One of the outputs of this fitting is the value of θ which will most closely correspond to physical data. For this study, a similar bivariate distribution representing the dependent sojourn times does not exist. Subsequently, a particular value of θ has to be assumed. Both independence copula (very small θs) and monotonic copula (very large θs) show different disadvantages. The independence copula does not capture dependency at all and allows both process to occur independently. On the other hand, a monotonic copula will strongly align the sojourn times of both processes due to peaks of the PDF along the diagonal. This disregards any independent behaviour from the FMs. Hence, a value of $\theta = 1$ is assumed and used for the case study. This corresponds to a Pearson correlation of about 45%. Since this is a strong assumption, a sensitivity study over the correlation coefficient will be carried out in Chapter 6.

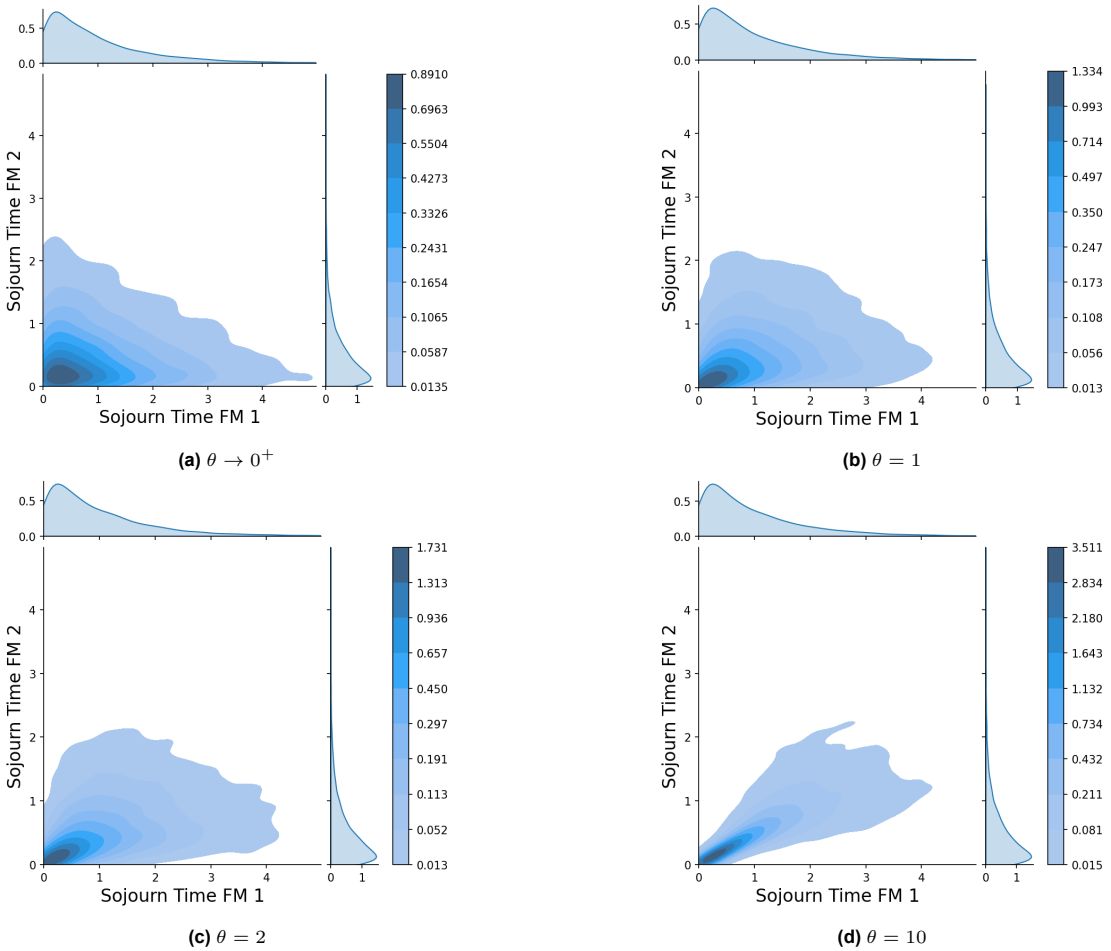

(a) $\theta \to 0^+$ **(b)** $\theta = 1$

(c) $\theta = 2$ **(d)** $\theta = 10$

Figure 3.5: Effect of θ on the PDFs of Clayton copula for a) $\theta \to 0^+$, b) $\theta = 1$, c) $\theta = 2$ and d) $\theta = 10$

Thus, the marginal data and the multivariate dependency can be separated by using the copula function. For degradation modelling, the independent exponential distributions of the sojourn times for each failure mode can be used as the marginal distributions. Combined with the copula function, a multivariate joint distribution can be formed.

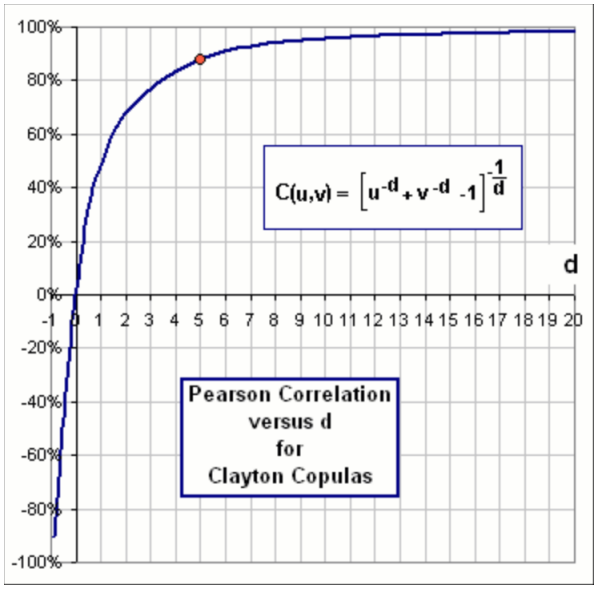

Figure 3.6: Pearson correlation vs. $\theta(d)$ for Clayton copula (Financial Wisdom Forum, 2010)

3.4. Failure & Transition Rates

The Bathtub curve shown in Figure 3.7 is used to represent the failure rate of a component across its entire life cycle (Zheng et al., 2020). The overall curve of failure rate is seen to be the sum of early failures, wear-out failures and random failures which remain constant with age. The curve can be divided into three separate regions. The infant mortality region with high but decreasing failure rates with increasing age. The useful life region, where the failure rates are low and steady for a long period. Occasional or random failures dominate this phase. Finally, in the wear-out region, the failure rate increases rapidly with the increasing age of the component.

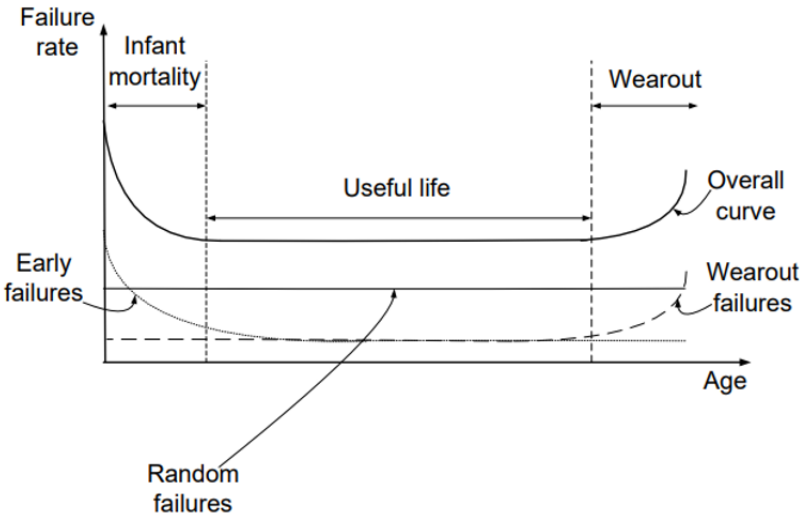

Figure 3.7: Bathtub curve (Abeygunwardane, 2012)

For this study, it is assumed that only random failures will occur in the component to be analysed. The other two regions of infant mortality and wear-out are not included. While this assumption of a constant failure rate represents the useful life region quite well, it underestimates the failure rates in the other two regions. However, one of the main reasons for this consideration is the lack of detailed failure or degradation data available in the literature. Most of the literature on failure rates provides constant values as output, which correspond to the useful life region (De Nie, 2016). Subsequently, exponential

distributions, which can be described with just one variable of failure rate and which represent a constant rate, are applicable.

3.4.1. Transition Rate Estimation

As seen in Section 3.1.5, individual transition rates between states are essential inputs to solve the Markov Chain. However, as discussed earlier in Section 2.4.1.1, most of the existing literature only relies on one constant value of failure rate for each component. Thus, it is necessary to convert the failure rate values to transition rates for each transition. Consider a five-state Markov Chain ($S \in 1, 2, 3, 4, 5$) with State 1 representing the normal condition and State 5 representing the failed condition. Figure 3.8 represents this deterioration along with the sojourn times, i.e. the time spent in each state T_{S1}, T_{S2}, T_{S3} and T_{S4}. This chain is characterised by four transitions and four transition rates, namely $\lambda_{12} : 1 \rightarrow 2, \lambda_{23} : 2 \rightarrow 3, \lambda_{34} : 3 \rightarrow 4$ and $\lambda_{45} : 4 \rightarrow 5$. Assuming that the overall failure rate, λ_f, is known, the transition rates are calculated as per Equations 3.41 to 3.43. For an exponential distribution defined with a failure rate λ_f, sojourn times correspond to time to failure. Hence, the Mean Time to Failure (MTTF) is equal to the expectation (mean) of the distribution. Thus, Equation 3.41 follows Equation 3.12 where the expectation for an exponential distribution was calculated. This MTTF is also equal to the sum of the sojourn times of each state (Equation 3.42). Further assuming each sojourn time T_{Si} to be the mean of their sojourn time probability distributions, Equation 3.42 can be written in terms of the individual transition rates as Equation 3.43 (as per Equation 3.12).

$$MTTF = \frac{1}{\lambda_f} \tag{3.41}$$

$$MTTF = T_{S1} + T_{S2} + T_{S3} + T_{S4} \tag{3.42}$$

$$MTTF = \frac{1}{\lambda_{12}} + \frac{1}{\lambda_{23}} + \frac{1}{\lambda_{34}} + \frac{1}{\lambda_{45}} \tag{3.43}$$

As shown in Figure 3.8 and as normally observed in real-life examples, deterioration processes often accelerate towards the end of life (Welte et al., 2006). This corresponds to smaller sojourn times for the higher degraded states, which in turn corresponds to higher transition rates. Large amounts of degradation data are required to estimate these reductions, which is often unavailable. Previous works (Besnard and Bertling, 2010, Welte et al., 2006) show that this reduction is often quantified by assuming a constant value. For example, Besnard and Bertling (2010) assumed that the reduction in sojourn times can be incorporated by multiplying a constant factor of 2 with the failure rate. This is a strong assumption and hence, a short sensitivity study is carried out over this parameter in Section 6.2.4. Following this assumption, Equation 3.43 can be re-written as:

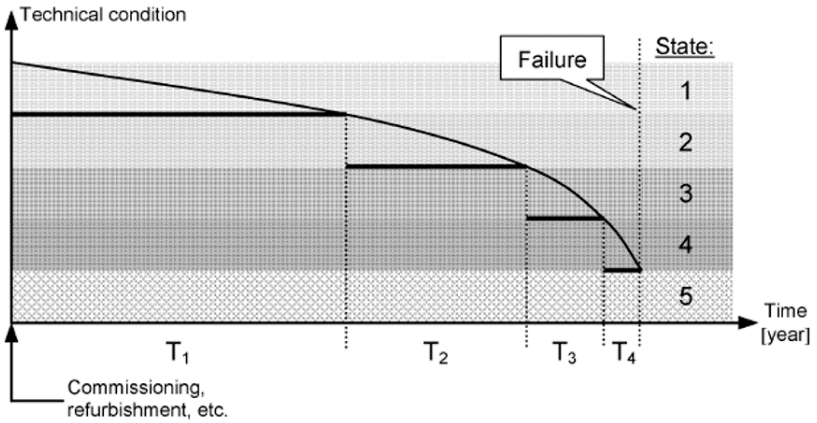

Figure 3.8: System degradation with time (Welte et al., 2006)

$$\frac{1}{\lambda_f} = \frac{1}{\lambda_{12}} + \frac{1}{2\lambda_{12}} + \frac{1}{4\lambda_{12}} + \frac{1}{8\lambda_{12}} \tag{3.44}$$

$$\frac{1}{\lambda_f} = \frac{15}{8\lambda_{12}} \tag{3.45}$$

$$\lambda_{12} = \frac{15\lambda_f}{8} \tag{3.46}$$

Thus, the transition rate λ_{12} can be calculated from the failure rate. Subsequently, the remaining transition rates can be obtained as follows:

$$\lambda_{23} = 2\lambda_{12} \tag{3.47}$$

$$\lambda_{34} = 4\lambda_{12} \tag{3.48}$$

$$\lambda_{45} = 8\lambda_{12} \tag{3.49}$$

It is important to note here that these transition or deterioration rates only represent the component degradation which follows the path from the initial state through all the mid-states and to the final state. Direct transitions from initial states to the failed state, which represent shock failures, have to be accounted for separately while drawing up the transition state diagram.

4
Modelling

This chapter covers the modelling step undertaken in the study. The final objective is to develop a model to account for the impact of degradation dependencies between multiple Failure Modes (FMs) on O&M costs. For all developed models in this study, the modelling procedure starts with developing a degradation model first. This is then integrated with inspection and maintenance functions to simulate maintenance actions and estimate corresponding O&M costs.

The model proposed in this study originates from and extends a baseline model developed at TNO. This model is discussed in Section 4.1. Based on the theory discussed in Chapter 3 and the features introduced in Section 4.2, the baseline model is extended upon. First, a single FM model is created, which is further expanded into a multiple FM model discussed in Sections 4.2.1 and 4.2.2, respectively. A detailed breakdown of the individual functions used in the model is given in Section 4.3. Finally, before concluding the modelling chapter, the fundamental assumptions and limitations of the proposed model are reflected upon briefly in Section 4.4.

4.1. Baseline TNO model

The baseline model is an in-house model developed at TNO which aimed to create a simplified version of a Markov chain-based degradation and maintenance model in Python. The model is developed for a single FM and uses Time-based Maintenance (TM) strategies. A variety of TM strategies are simulated for the maintenance strategy optimization as discussed in Section 2.6.1.

The first step in the modelling process is to build a state transition diagram. As seen in Section 3.1.5, state transition diagrams are graphical methods used to encompass the entire degradation process in a single diagram. They are extremely useful in understanding the process and building on top of the Markov chain model.

First, the degradation model is visualized in Figure 4.1.

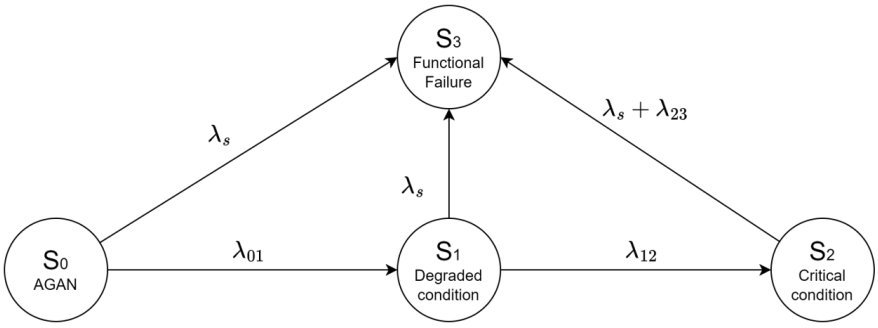

Figure 4.1: Baseline model state transition diagram- degradation model

In this case, the degradation process is divided into 4 states $S \in (0, 1, 2, 3)$. State 0 (S_0) is equivalent to the 'As Good As New' (AGAN) condition. S_1 corresponds to the degraded condition and S_2 to the critical condition which is the final stage before the functional failure represented by S_3. The transitions between these states are represented in the diagram with arrows, linked to their corresponding

transition rates (λ_{01}, λ_{12} and λ_{23}). Shocks to the component directly leading to failure are also included in the model with a shock transition or arrival rate, λ_s. For this study, shocks are assumed to be independent of the degradation process. This is also true for some shocks occurring in reality (Besnard and Bertling, 2010). For example, lightning hitting the blades of a Wind Turbine (WT) occurs independently of component health. Due to this independence, the rate for the transition S_2 to S_3 is the sum of the transition rate between the states and the arrival rate of shocks. This summation represents a higher magnitude of the transition rate which translates to shorter sojourn times and quicker occurrences of failure compared to each individual rate.

Next, maintenance actions are integrated with the degradation model in Figure 4.2. This model includes maintenance actions, both Preventive Maintenance (PM) and Corrective Maintenance (CM) based on the detected state. If a failure occurs, CM is performed at the next inspection interval. This essentially replaces the failed component and brings the system back to the AGAN state. All preventive maintenance actions are also assumed to return the system to the AGAN state.

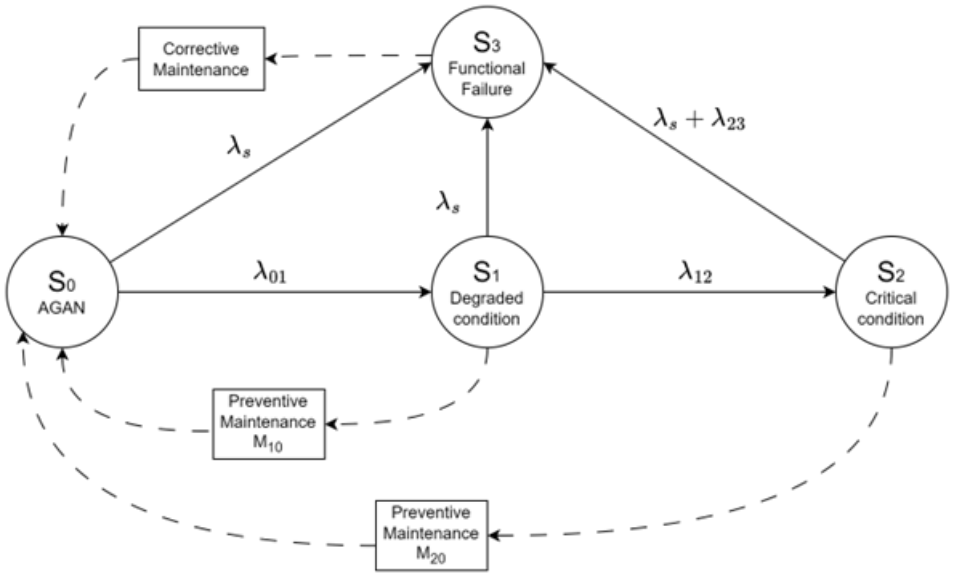

Figure 4.2: Baseline model state transition diagram - degradation & maintenance models

Direct commands are run in the main code function to simulate maintenance activities and failure checks. If WT failure occurs, the operation is halted until the next scheduled inspection and no energy is produced. This Downtime (DT) incurs operation costs as discussed in Section 2.6.1. As discussed in Section 2.6, TM strategies may lead to very large DT and operation costs if failure is encountered between long inspection intervals. Inspections are assumed to be instantaneous with no inspection duration being accounted for in the total repair duration. Inspection costs are modelled as constant values for each inspection.

All maintenance actions are assumed to have a constant repair time of one month, irrespective of the state of the component. Each maintenance action also has some fixed costs associated with it based on the type of repair. One-step repairs from S_1 to S_0 are classified as minor preventive maintenance and two-step repairs from S_2 to S_0 are classified as major preventive maintenance, with both categories having different fixed maintenance costs. All cost parameters are assumed to be constant throughout the WT lifetime with no discount rate discounting future costs.

Each simulation runs over an entire WT lifetime and costs are accrued together to finally output the lifetime O&M costs. Further, multiple such simulations are run based on the input number of Monte Carlo (MC) simulations.

4.2. Developed models

With the simplified baseline model established, it is further extended to a single FM model and a multiple FM model. Both the developed models use the baseline model state transition diagram for the degradation model as shown in Figure 4.1. While the degradation state transition diagram is the same, the mechanisms within the Markov chain for both models are different from the baseline model. This will be further explained in the next sections. An important point of difference is the maintenance strategy being simulated. A TM-CM strategy is used for both the developed models.

With the degradation state transition diagram established, inspection and maintenance functions are integrated into the diagram. Figure 4.3 represents the combined degradation and maintenance model to complete the state transition diagram.

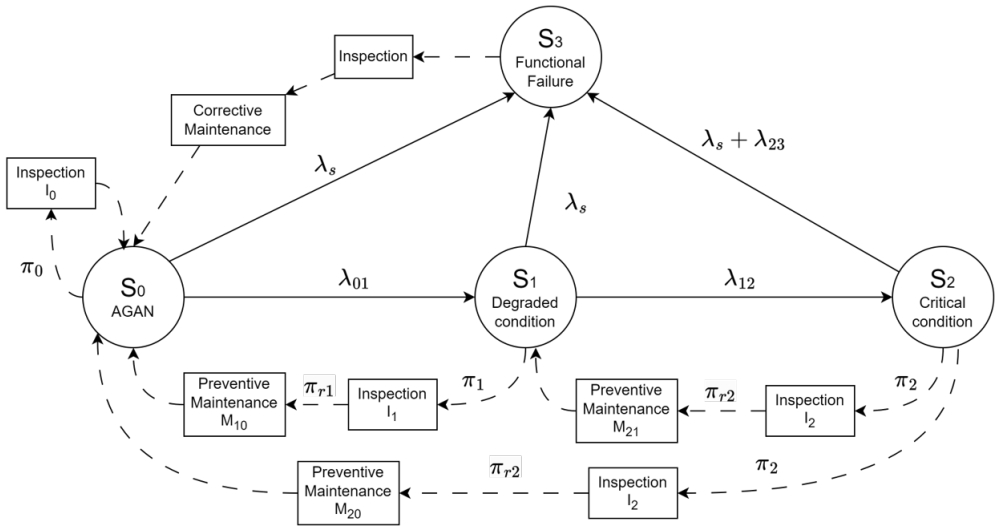

Figure 4.3: State transition diagram - degradation & maintenance models

An addition to Figure 4.3 from the baseline model is the inclusion of the Inspection function. These actions are now modelled with finite inspection durations which contribute to the total repair duration. An inspection with the system in S_0, I_0 does not require maintenance actions and the system continues to remain in the original state. Further, to allow for more flexibility in the model and reflect reality, imperfect inspections are included. Each inspection action is accompanied by probabilities of incorrect detection, namely π_0, π_1 and π_2. Based on these probabilities, the detected state is chosen at each inspection using weighted random choices. Thus, imperfect detection allows the component state to be classified as S_2 when in reality it is only at S_1.

Similar to the baseline model, maintenance actions, both PM and CM are carried out based on the detected state. If a failure occurs, an inspection accompanied by CM is performed. This essentially replaces the failed component and brings the system back to the AGAN state. When the inspection I_1 or I_2 detects either S_1 or S_2, PM actions are carried out to improve system health. In classical state diagrams, maintenance actions are always shown to improve the system state by only one state (Abeygunwardane, 2012). Alternatively, Besnard and Bertling (2010) always assumes that all maintenance actions return the system to the AGAN state. To introduce uncertainty, imperfect maintenance actions or irreparable degradations are accounted for using probabilities of incorrect repair, namely π_{r1} and π_{r2}. Maintenance actions in this model can thus improve system health from the current state to any one of the healthier states, except for failures. So, transitions from $S_1 \rightarrow S_0$, $S_2 \rightarrow S_0$, $S_2 \rightarrow S_1$ and $S_3 \rightarrow S_0$ are allowed. The selection of the repaired state is accomplished with weighted random choices using probabilities of incorrect repair.

Similar to degradation being controlled by transition rates, inspection and maintenance actions can

also be represented by inspection or maintenance rates. These rates would then determine the sojourn time for that particular inspection or maintenance state, i.e. the time required to undertake inspection and maintenance actions. If the rate is a constant value, the sojourn times would be chosen using weighted random choice from an exponential probability distribution. For this model, instead of using one exponential distribution for each inspection and maintenance action, the system is modelled in a way that allows for more detailed considerations. This is achieved by splitting the duration of time required to conduct inspection and maintenance into its individual components as shown in Figure 4.4, similar to the method proposed by Le and Andrews (2016).

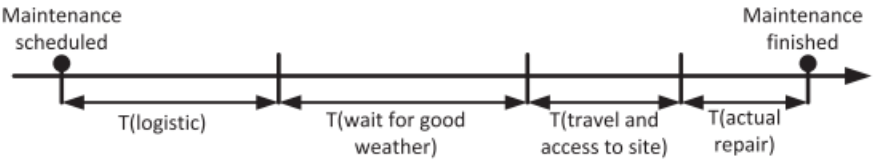

Figure 4.4: Breakdown of maintenance duration (Le and Andrews, 2016)

The individual components are the duration for logistics, the waiting duration for good weather, the travel duration and the repair duration. The logistics duration covers the lead time for a new component or vessel availability. The duration of waiting for good weather is the time spent waiting for a suitable weather window when the vessel and the crew can venture offshore to perform inspection or maintenance operations on the WTs. The weather window depends on metocean conditions such as wave heights H_s, wave periods T_p and wind speeds and the capability of the vessel to withstand those conditions. The weather window is estimated by weighted random choice using probabilities and a Weibull distribution. First, it is decided whether harsh weather is encountered based on the probability of harsh weather experienced in a year. This is modelled as a weighted random binary selection between 0 or 1, where 0 corresponds to harsh weather encountered and 1 corresponds to acceptable weather conditions. Then, if harsh weather is encountered at the time of conducting maintenance, the length of the weather window is calculated by a random Weibull variable as defined in Le and Andrews (2016). The travel duration represents the time taken to reach and come back from the offshore wind farm to the operations port. This depends on the vessel type and speed. Finally, the repair duration is the time spent on the turbine to carry out the actual inspection and repair work which varies for each state.

Each inspection and maintenance action in the proposed model has inspection, maintenance and operation costs associated with it. These costs take into account the cost of labour, vessel, electricity and material repair. A discount rate is considered to calculate the present value of all future costs. The detailed calculations for each category are shown in Section 4.3.2. Each simulation runs over a WT lifetime and costs are accrued together to finally output the lifetime O&M costs. To illustrate the flow of the system through the different states in the state transition diagram, an example is provided. Considering a WT component with a 25-year lifetime, the degradation process starts at S_0, the AGAN state. The component health deteriorates over time and the system moves to S_1. If an inspection is carried out at this point in time, inspection and operation costs are incurred and the system state is detected to be S_1. Based on this inspection, maintenance is carried out, maintenance and operation costs are incurred and the system state is repaired and brought back to AGAN, S_0. This cycle repeats itself for the entire WT lifetime of 25 years. Similar to the baseline model, multiple number of simulations are run based on the input number of Monte Carlo (MC) simulations.

With the completed state transition diagram, the next step of converting it into a Markov model in Python is carried out.

4.2.1. Single Failure Mode Model

The aim of this model is to represent the component degradation considering only one single FM along with the required inspection and maintenance actions. The single FM model framework is shown in Figure 4.5. First, variables of the inspection range, number of MC simulations, WT power rating and WT lifetime are initialized. The inspection range is defined to vary between 0.2 years to 5 years with

varying intervals. The range corresponds to a wide inspection interval which can entirely capture the varying behaviour of O&M costs. A similar range is used in existing literature (Besnard and Bertling, 2010). The minimum interval is selected to be 0.05 years. This corresponds to approximately 18 days which is sufficiently small for maintenance planning.

Next, degradation parameters are input into the model. These parameters include the failure rate and the shock arrival rates. Based on the rates, a transition rate/generator matrix is defined. Next, the first for loop for the inspection interval is encountered where the values are sequentially picked from the inspection range. The total count for the number of MC simulations is also defined and a counter to keep track of the number is initialized. This number is based on the values of the uncertainty parameters discussed in Section 3.2. Both of these parameters are varied using a for loop. Time is initialized as 0 years and the model is set to run for the defined horizon of 25 years, which reflects current WT lifetimes.

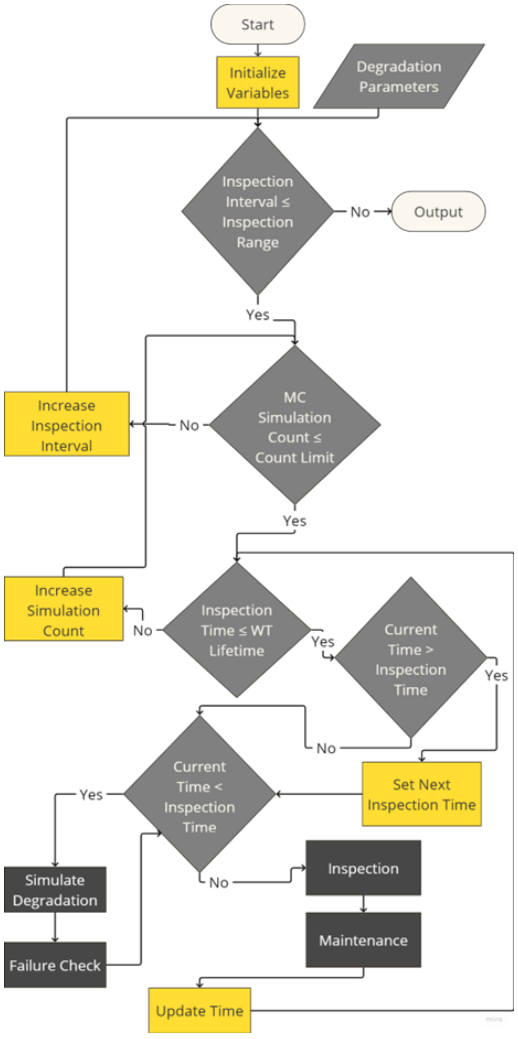

Figure 4.5: Single failure mode model framework

Once the inspection interval and the count for the number of MC simulations have been defined as per the for loop, the inspection time is compared to the WT lifetime value of 25 years using a while loop. For example, if the inspection interval is defined as 0.2 years, then, the first inspection time will be 0.2 years, followed by the second inspection at 0.4 years, the third inspection at 0.6 years and so on until 25 years. The inspection time variable is initialized with a value of 0 years. If the inspection time is less than the WT lifetime and the current time is larger than the inspection time, the next inspection time is set. The current time is similar to a clock for the overall process which monotonically increases

from 0 to 25 years (WT lifetime). It represents the current component age and keeps count of all time instances, i.e. sojourn time between degradation, inspection duration, maintenance duration, WT DT, etc. It is important to note that component age is independent of component health. While health can be improved to AGAN, age can only increase.

If the current time is smaller than the inspection time or if a new inspection time has been set, the model enters a while loop over the current time being smaller than the inspection time. If this condition is met, the Simulate Degradation function is called. This function simulates the next degradation transition and outputs a new state and a new sojourn time. Next, a failure check is performed using the Failure Check function. If failure has occurred or if the loop condition is no longer met, the model breaks out of the while loop. Subsequently, first, the Inspection function and then the Maintenance function are called. These functions carry out the inspection and maintenance actions, accounting for WT health and cost for each action. Finally, the updated current time is obtained. The updated time is the sum of the last scheduled inspection time and the duration of all inspection and maintenance actions that have occurred since then. This is fed back into the while loop comparing WT lifetime with inspection times.

This process repeats until the simulation runs for the set horizon of 25 years. This is repeated for the total number of MC simulations. The entire set of MC simulations represents the model output for the chosen inspection interval. The same procedure is repeated for each inspection interval value within the selected range. Finally, the outputs of mean costs, DTs, state paths and sojourn times can be obtained from the entire dataset.

This model introduced four function blocks, namely the Simulate Degradation, Failure Check, Inspection and Maintenance, all represented by dark grey rectangles in the flow charts. The working of each block will be explained further in Section 4.3.

To illustrate how this model works, two example cases are presented in Figure 4.6 and Figure 4.7. In Figure 4.6, inspections are scheduled to happen at intervals of T_i and the first inspection time is T_i. The simulation starts from S_0 (shown as a circle with the number 0) and the component degrades to S_1 in the sojourn time for state 0, T_{S0} years. Another degradation transition occurs from S_1 to S_2 in T_{S1} years, the sojourn time for state 1. At this instant, the current time ($T_{S0} + T_{S1}$) is less than the inspection time (T_i). Hence, the next degradation is simulated. From this degradation, S_2 would be seen to degrade to S_3 after T_{S2} years. The current time now has been updated to $T_{S0} + T_{S1} + T_{S2}$. However, since the T_i is smaller than the current time, the model moves on to the Inspection function at T_i. At T_i, the state is seen to be S_2, which requires maintenance. Subsequently, the Maintenance function will be called. Maintenance starts at T_i and is carried out for the duration of T_{M2} years. T_{M2} includes all sub-processes discussed in Figure 4.4. As a result of this maintenance action, the process is brought back to S_0 and the cycle continues.

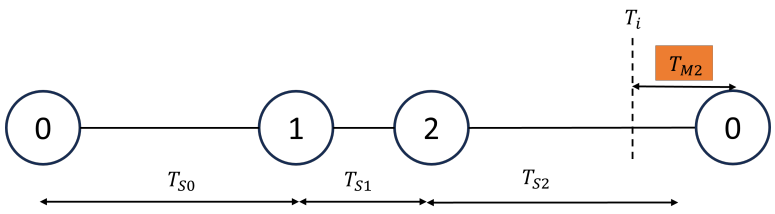

Figure 4.6: Example 1 - Single failure mode model flow

The second example in Figure 4.7 focuses on CM actions included in the model. In this case, there is a direct transition from S_1 to S_3 corresponding to a failure due to shock. The current time, $T_{S0} + T_{S1}$, is still less than T_i. However, since failure has occurred, immediate repair actions need to be carried out. Waiting until the next scheduled inspection time would lead to extremely high operation costs. So, from the time instant of failure, the maintenance process is initiated and completed in T_{M3} years. As per CM, the component is repaired back to S_0. The simulation cycle will continue from here.

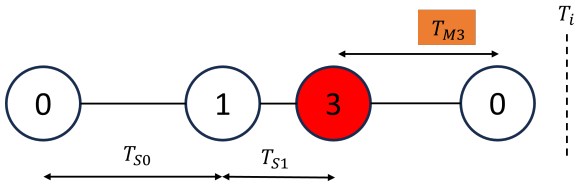

Figure 4.7: Example 2 - Single failure mode model flow

4.2.2. Multiple Failure Mode Model

For modelling dependency in degradation, the single FM model has been extended to handle the concomitant occurrence of two FMs. Hence, there are now two degradation processes to be accounted for. The framework of the multiple FM model is presented in Figure 4.8. This model builds upon the single FM model presented in the previous section and shares many features with it. A difference in the degradation parameters fed into the model is the inclusion of transition rates for both degradation processes. Based on the rates, two different transition rate matrices or generator matrices are defined. The variable initialization process, the layout of the for loops for the inspection interval and the count for the number of MC simulations remain the same as the single FM model. The process then enters the first while loop comparing the current time with the WT lifetime. Similar to the single FM model, further actions take place based on the values of the current time and the scheduled inspection time.

If the current time is smaller than the inspection time or if a new inspection time has been set, the model enters the next while loops over the process-specific current time (current time 1 and current time 2) being smaller than the inspection time. Since two processes are being modelled, two while loops are entered sequentially, first for FM 1 and then for FM 2. If the condition is met, the Simulate Degradation function is called. For this model, the key differences lie in the following steps. Since two unique degradation processes exist, each process has its own Simulate Degradation function. This function simulates degradation and outputs a new state and a new sojourn time. Since the model is stochastic, the sojourn times output for each process are random. Thus, the two sojourn times could be different. For example, say process 1 degrades from S_0 to S_1 in T^1_{S0} years and process 2 degrades from S_0 to S_1 in T^2_{S0} years. These durations could be different and hence the current time associated with each process would be different. This is the reason for introducing process-specific current times in the code.

First, process 1 is simulated up to the scheduled inspection time followed by process 2. Failure checks are run after each degradation step. If failure has occurred or if the loop condition is no longer met, the model breaks out of the while loop and enters the Inspection function. Following this, the Maintenance function is called. The output of the Maintenance function aligns both the process-specific current times with the overall current time for the entire model as explained for the single FM model. The updated process-specific times are the sum of the last scheduled inspection time and the duration of all inspection and maintenance actions that have occurred since then. The updated current time is obtained, which is fed back into the while loop comparing WT lifetime with inspection times.

For the single FM model with just one FM per component, the state represents system health. However, for the multiple FM model, there are now two FM per component state values. A method to obtain the overall system state from both the individual degradation processes was suggested by W. Li and Pham (2005) where a System State Matrix (SSM) was used to define the state of the system. This SSM was obtained based on the states of the individual degradation processes. Considering two processes i and j with their states S_i and S_j, weight factors w_i and w_j can be used to assign importance to each FM over the other and the overall system state can be calculated as:

$$S_{ij} = S_i * w_i + S_j * w_j \tag{4.1}$$

where $w_i + w_j$ = 1. Assuming equal weight factors, $w_i = w_j$ = 0.5, the final SSM, is given by:

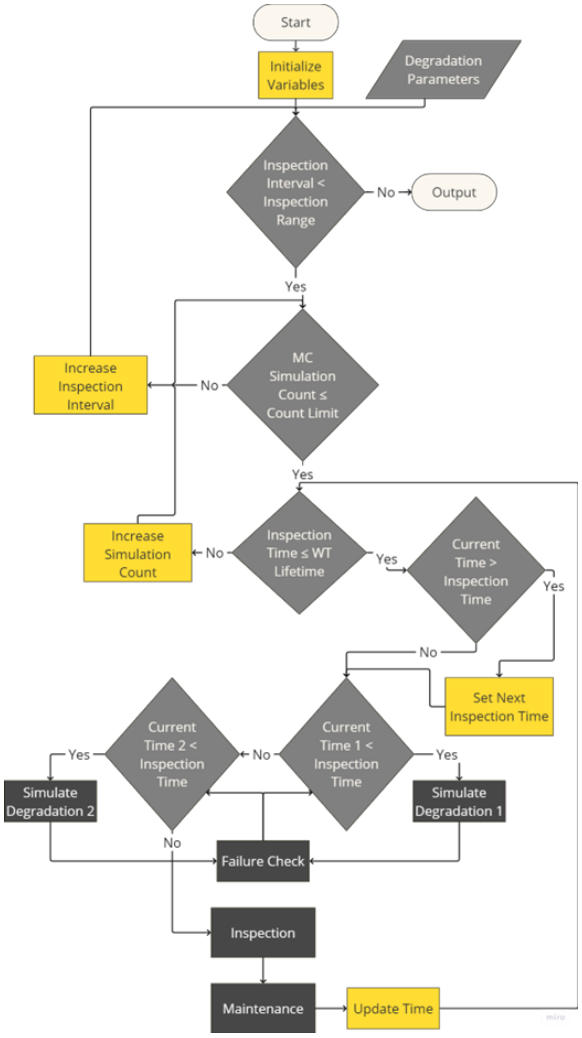

Figure 4.8: Multiple failure mode model framework

$$SSM = \begin{array}{c} \\ S_0 \\ S_1 \\ S_2 \\ S_3 \end{array} \begin{array}{c} \begin{array}{cccc} S_0 & S_1 & S_2 & S_3 \end{array} \\ \begin{bmatrix} 0 & 0 & 1 & 3 \\ 0 & 1 & 2 & 3 \\ 1 & 2 & 2 & 3 \\ 3 & 3 & 3 & 3 \end{bmatrix} \end{array} \tag{4.2}$$

Since states can only be integer numbers, decimal numbers are rounded off. For example, if S_1 = 1 and S_2 = 2, using Equation 4.1, the system state is obtained to 1.5. This is rounded up to 2. Hence the value of the SSM in the cell 1st row and 2nd column is 2. If a failure occurs for any of the individual FMs, the entire system is declared to have failed. This is why the states in the last column and the last row of the SSM are always in state 3 S_3. This process repeats up to the horizon time of 25 years and for the set number of MC simulations. Finally, similar to the single FM model, the outputs of mean costs, DT, state paths and sojourn times are obtained from the model.

Figure 4.9 shows the model operation for multiple FMs. Consider two FMs, process 1 P_1, and process 2 P_2. Inspections are scheduled to occur at T_i intervals.

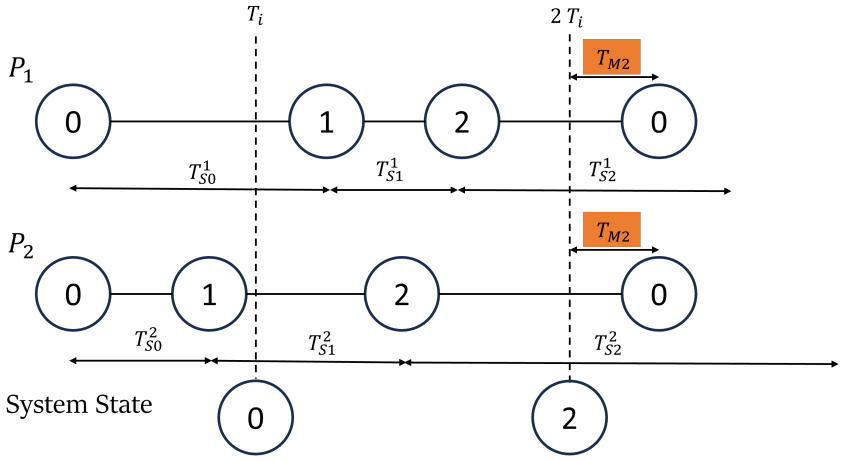

Figure 4.9: Example- Multiple failure mode model flow

Both processes, P_1 and P_2, start at S_0. First, the degradation forP_1 is simulated followed by P_2 until process-specific current times for both are greater than T_i. P_1 degrades from S_0 to S_1 in T^1_{S0} years. P_2 degrades from S_0 to S_1 in T^2_{S0} years and from S_1 to S_2 in T^2_{S1} years. In the example shown in the figure, at T_i, P_1 is in S_0 and P_2 in S_1. As per the SSM, the overall system state would be S_0. In this case, no maintenance would be required and the simulation would continue. Both degradation processes would now be simulated at least up to $2T_i$. In this case, both processes would degrade to S_3, with a failure at T^1_{S2} and T^2_{S2}, respectively. However, since an inspection is scheduled at $2T_i$, component states will never reach S_3. At $2T_i$, the individual states and the system state is seen to be S_2. Here, maintenance would be conducted. Both the process-specific current times $T^1_{S0}+T^1_{S1}+T^1_{S2}$ and $T^1_{S0}+T^1_{S1}+T^2_{S2}$ would be updated to the time at which maintenance is carried out - the inspection time plus the maintenance duration - $2T_i + T_{M2}$. The maintenance duration contains shared durations of lead time, wait time for good weather and travel time to the site. However, the repair times for each component are individual and based on its state of degradation. Both repair times are summed up while calculating the entire maintenance duration. Then, $2T_i + T_{M2}$ would become the overall current time of the entire process and the simulation would continue.

It is important to note here that the two degradation processes in the multiple FM model can be either independent or dependent. The same methodology applies to both. The key difference between these two cases is taken into account and implemented within the Simulate Degradation function block as will be explained in Section 4.3.1.

4.3. Model Functions

Once the overall framework has been established, this section looks at the model function blocks. Each block is broken down into its input and outputs, shown by white elements in the flow diagrams and the processes occurring inside the function. The main functions are - 'Simulate Degradation', 'Calculate Costs', 'Failure Check', 'Inspection' and 'Maintenance'.

4.3.1. Simulate Degradation Function

The Simulate Degradation function, shown in Figure 4.10a, is created to simulate a single step of the degradation process. Apart from the current state and current time, the generator/transition rate matrix is a key input to the function. In the case of multiple FMs, unique transition matrices exist for each FM. Then, FM is also an input to select the correct transition matrix. The function outputs the next deterioration state and the time at which this transition will occur. The next state is obtained via the 'Get Next State' function and the time is obtained via the 'Get Sojourn Time' function, shown in (Figure 4.10b and Figure 4.10c), respectively.

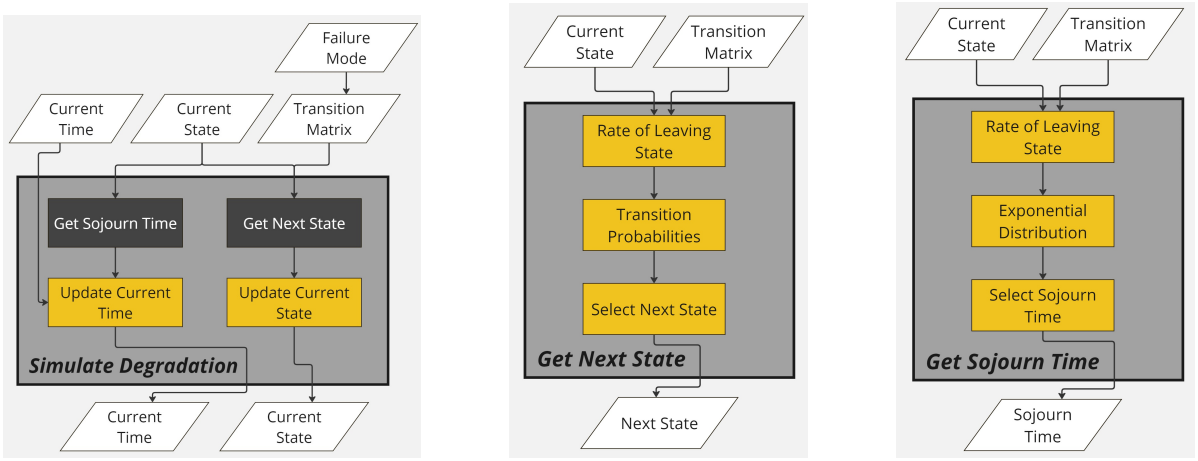

(a) Simulate Degradation function **(b)** Get Next State function **(c)** Get Sojourn Time function

Figure 4.10: Breakdown of Simulate Degradation function into a) Simulate Degradation function, b) Get Next State function and c) Get Sojourn Time function

Both these functions are based on the theory introduced in Section 3.1.4. The Get Next State function calculates the rate of leaving the current state based on the current state and the transition matrix using Equation 3.14. Next, the transition probabilities are calculated for each state using Equation 3.19. Finally, based on the transition probabilities, the next state is chosen using a weighted random choice function in Python. The current state is updated with the value of the next state.

The Get Sojourn Time function allows users to differentiate between the independent and dependent degradation cases, within the multiple FM model, as explained in the next Section.

4.3.1.1. Independent Degradation

For both the single FM model and the independent degradation multiple FM model, the Get Sojourn Time function works as shown in Figure 4.10c. In a similar method to the Get Next State function, the Get Sojourn Time function calculates the rate of leaving the current state (Equation 3.14). Based on this rate, an exponential distribution can be created using Equation 3.8. Next, an exponential random variable is selected from this distribution to be the sojourn time which is the output. The current time is then updated using the value of the sojourn time.

4.3.1.2. Dependent Degradation

For the dependent degradation model, there are a few extra inputs required as shown in Figure 4.11. Every time the Simulate Degradation function is called, it is specifically to simulate one of the FMs. Thus, the multiple FMs can be segregated into active and inactive FMs. For example, the Simulate Degradation function is called for process 2. In that case, process 1 will become the inactive FM. Apart from the current state and the transition matrix of the active FM, the state, the transition matrix and the current time of the inactive FM are also input to the function.

Next, similar to the independent case, the rate of leaving the current state is calculated for both processes using the respective process' transition rate matrix. Using each rate, two different exponential distributions are created. Next, a multivariate distribution is created using the two exponential distributions and the copula function as discussed in Section 3.3. For this study, this will be a 2-dimensional distribution. The current time of the inactive FM is used to identify the array in the 2-dimensional distribution whose index corresponds to the current time value. Finally, based on the values of this array corresponding to the probability of sojourn time, the sojourn time is selected using weighted random choice.

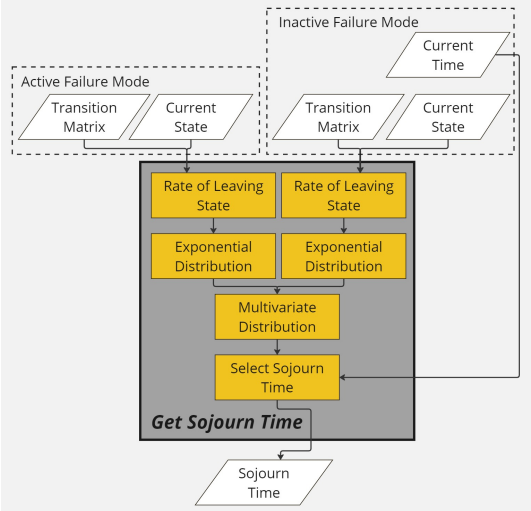

Figure 4.11: Get Sojourn Time function - dependent case

4.3.2. Calculate Costs Function

This function, shown in Figure 4.12 is called to estimate the costs incurred based on the action undertaken. The input 'type' is a string ('maintenance', 'inspection' or 'operation') which determines which costs to calculate. Finally, the costs corresponding to the input string are updated by the Update 'Type' Costs block. It is assumed that long-term contracts exist between the WT operator and the maintenance company. This allows the costs to be assumed constant across the lifetime of the turbine. The costs are always expressed in terms of their present value. The present value is calculated for all future costs as (Besnard and Bertling, 2010):

$$C_{PV} = C * (1 + \delta)^{-n} \tag{4.3}$$

where C_{PV} is the present value, C is the value of the costs in the year they were incurred, δ is the discount rate and n is the year at which the costs were incurred.

Depending on the string input for the 'type' of cost calculation, either maintenance (C_M), inspection (C_I) or operation (C_O) costs can be calculated as follows.

1. Inspection Costs C_I are calculated as

$$C_I = T_I * (n_l * C_l + C_v) \tag{4.4}$$

where C_l (€/hr/person) is the technician/labour cost, n_l is the number of technicians, C_v (€/hr) is the vessel cost and T_I (hr) is the duration of time spent for inspecting the turbine.

2. Operation Costs C_O are calculated as

$$C_O = T_d * P * cf * C_e \tag{4.5}$$

where T_d (hr) is the turbine DT, P (MW) is the turbine's power capacity, cf is the capacity factor and C_e (€/MWh) is the cost of electricity.

3. Maintenance Costs C_M are calculated as

$$C_M = C_r + T_M * (n_l * C_l + C_v) \tag{4.6}$$

where C_r (€) are the repair costs and T_M (hr) is the duration of the maintenance action. A large contributor to the maintenance costs is the cost of repairing or replacing a component. C_r can be estimated based on the improvement from the current state to the repaired state. These costs can take different values for each FM based on the type of maintenance. Similar to inspection cost calculation, labour costs for the technicians C_l (€/hr/person), the number of technicians n_l, vessel costs C_v (€/hr) and the duration of maintenance time T_M (hr) are also input. This maintenance duration includes all sub-processes shown in Figure 4.4.

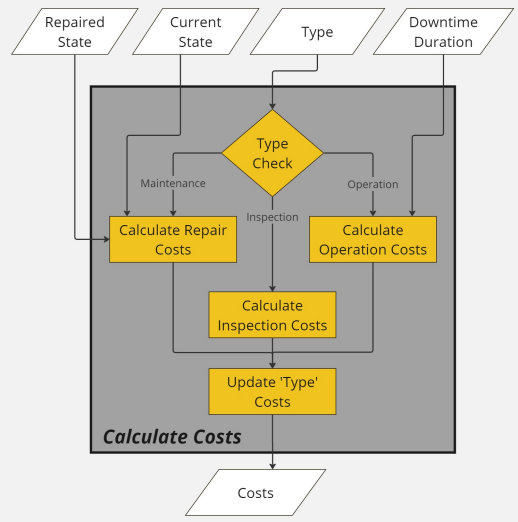

Figure 4.12: Cost function

4.3.3. Failure Check Function

In this function, shown in Figure 4.13, the inputs are the current state, the current time, the next scheduled inspection time and the lead time duration for replacing a component. It outputs the updated value of the current time, the turbine DT and the costs incurred.

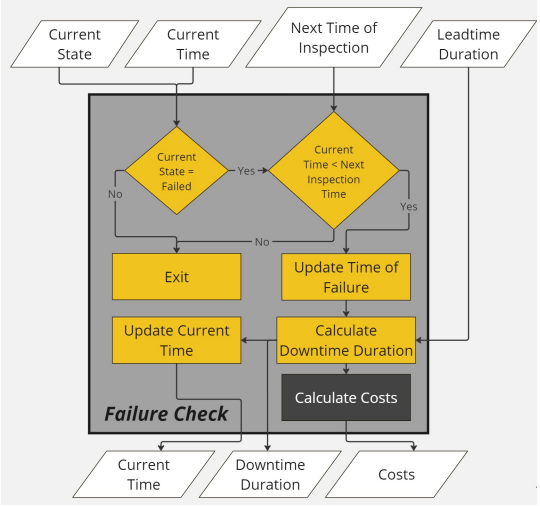

Figure 4.13: Failure Check function

This function checks if a failure has occurred before the next scheduled inspection time. If failure hasn't occurred or will occur after the next scheduled inspection time, it will exit the function and break out of the loop. If the conditions are met, the time instant of failure is noted. S_3 is an absorbing state which means the system can no longer jump to another state. The turbine is also not producing any energy and operation costs are incurred as long as the turbine is non-operational. Maintenance action is initialised immediately. The current time is updated by including the lead time. The lead time also contributes to the DT duration and operation costs.

For the multiple FM model, the function operates similarly. One of the key differences is in the initial step of determining which FM has suffered a failure. Based on this, the process-specific current time of the FM without failure is updated to match the current time of the FM with a failure which becomes the current time of the entire process.

4.3.4. Inspection Function

In this function, shown in Figure 4.14, component inspection is carried out. The current state of the component and the inspection duration are input. The inspection duration is the actual time spent on the turbine inspecting the component. Based on the current state, the probability of incorrect detection is set. Next, the detected state is selected by weighted random choices using these probabilities of incorrect detection. The current state is updated with this detected state value. The inspection duration also contributes to the WT DT and the operation costs. The calculate costs function also calculates the inspection costs accounting for the inspection duration, labour costs and vessel costs. The Inspection function also calculates the duration of the weather window that must be considered before an inspection can be carried out. This value is further fed to the Maintenance function.

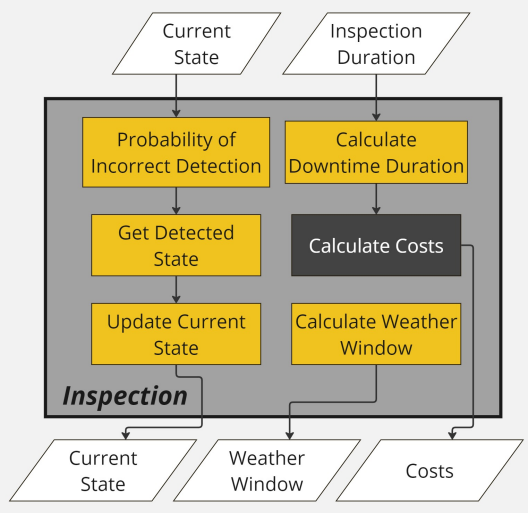

Figure 4.14: Inspection function

4.3.5. Maintenance Function

This function, shown in Figure 4.15, is responsible for all maintenance actions performed on the component. The current state of the component and the current time are input to the function. Along with these, the inspection duration, the travel duration and weather window are input.

Maintenance is only carried out if the process or system state is greater than S_0. Based on the current state, the probability of incorrect repair is set. Next, the repaired state is selected by weighted random choice using the probabilities set before. The repair duration (time spent on the turbine to repair/replace the component) is also obtained based on the repaired state and the initial state. The repair duration, travel duration and the weather window are summed together to obtain the maintenance duration. The DT duration of the turbine is further calculated from this total maintenance duration. The current state is updated with the value of the repaired state. Based on the repaired state, the initial state and the maintenance time, maintenance costs are calculated. Operation costs are also obtained using the DT duration.

Towards the end of the function, the current time for the entire process is updated by summing the duration of all the actions undertaken. The final outputs are the updated current state and current time, the DT duration and the total costs. For the multiple FM model, an additional output of the system state using the SSM method described in Section 4.2.2 is present.

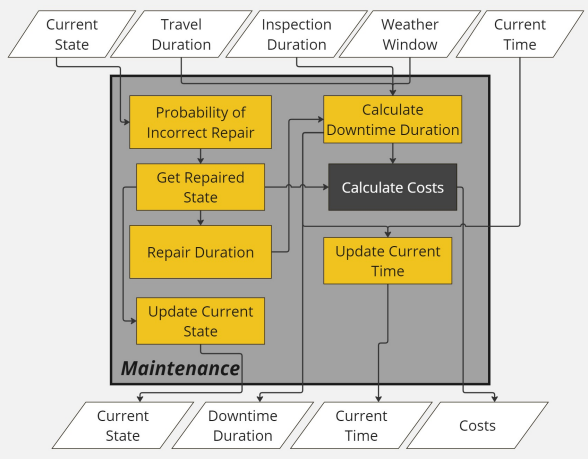

Figure 4.15: Maintenance function

4.4. Model Assumptions & Limitations

Before moving on to the application of the developed model, the fundamental assumptions and limitations of the model are reflected upon briefly.

Assumptions:

1. Using constant failure rate for each FM
2. Value of the constant reduction factor used to convert failure rates to transition rates
3. Value of the copula correlation coefficient
4. Simulating only time-based maintenance strategies
5. Input values of costs, failure rates, probabilities, etc.

Limitations:

1. Validity of the Bathtub curve for the component being modelled: The assumption of considering a constant failure rate is derived from the shape of the bathtub curve with a flat middle section. This further leads to choosing exponential distributions to represent the sojourn time for each state.
2. Conversion of failure rates to transition rates: This conversion is dependent on the assumption of multiplying consecutive transition rates by a constant reduction factor. The methodology is physically valid as it allows for a reduction in sojourn time in degraded states. However, the value of the reduction factor is assumed to be a constant to simplify the process.
3. Representing dependency with the copula correlation coefficient: the physical dependency between different FMs is reduced to a single coefficient to work with copulas. Due to a lack of field data, the correlation coefficient is assumed for this study. Whether this assumption accurately corresponds to the physical dependence between the FMs is unknown.
4. State Space Explosion problem: With a large number of components or processes, an even larger number of states have to be dealt with within the Markov process. This directly scales up the associated computation costs in solving the model.
5. Constant Inspection Intervals - While the model calculates the cost over a range of inspection intervals, the interval is not allowed to vary within the turbine lifetime. Different maintenance strategies based on the system state are not implemented.
6. Input Data: Any model is as good as the data it is fed. Any variation in the input values directly affects the results. For example, uncertainties in costs associated with inspection and maintenance actions or uncertainties associated with failure rates would greatly change the optimum results.

5
Model Validation & Case Studies

In this chapter, first, a validation process is carried out to verify the proposed model in Section 5.1. The setup is presented here while the results are presented in Chapter 6. Next, an application of the model is presented in Section 5.2. The case studies refer to Offshore Wind Turbine (OWT) hydraulic pitch systems. The Failure Modes (FMs) that are selected for the application are detailed in Section 5.2.1. Then the setup for the case studies is explained in Section 5.2.2, detailing all inputs and their values. Finally, each case is shortly reiterated in Section 5.2.3.

5.1. Model Validation

In order to validate the model and its performance, a verification process is undertaken. The verification is conducted by replicating the results of a study from the literature. This study is based on Markov Chain degradation-based maintenance modelling of Wind Turbine (WT) blades (Besnard and Bertling, 2010). In order to replicate the setup followed in this work, a simplified version of the developed single FM model without many additional features is used. Specifically, the following features are changed:

1. Preventive Maintenance (PM) is assumed to be instantaneous with no Downtime (DT) and hence, no operation costs.
2. Operation costs for inspections and Corrective Maintenance (CM) are not calculated separately but are provided as constant values combined with maintenance costs and inspection costs. The DTs associated with all inspection and maintenance actions are assumed to be constant leading to constant operation costs.
3. Imperfect maintenance or irreparable degradation are neglected. However, incorrect detection is implemented.
4. Wait time from bad weather delays and travel time to OWT is neglected.

These generalizations of the developed model both limit its applications and simplify the model. They further divert from reality by ignoring real-life conditions such as bad weather or travel durations. However, a simplified model allows for quick simulations with less computational costs.

5.1.1. Setup

Besnard and Bertling (2010) considered a power capacity P of a 5 MW WT with a 25-year lifetime. A capacity factor (cf) of 0.4 was assumed. A single degradation process (transition rate λ_{det}) for the blades was combined with shocks from lightning (arrival rate λ_l) that could lead to direct failure. The degradation process considered was blade cracking. The process was specified with 5 states - X_1, X_2, X_3, X_4, F with each state corresponding to an increasing length of the crack and F corresponding to failure. The state transition diagram is visualized in Figure 5.1.

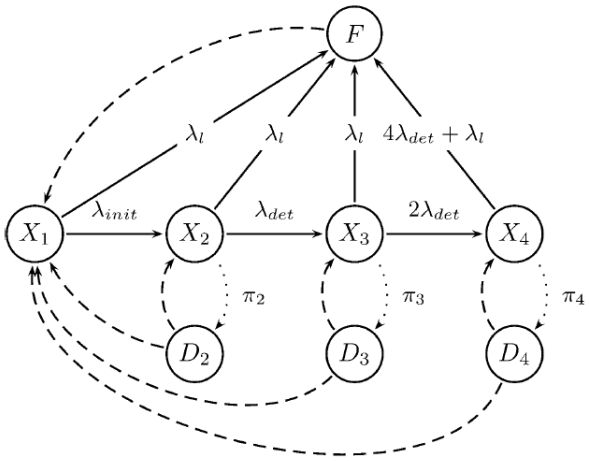

Figure 5.1: State transition diagram for the case study studied by Besnard and Bertling, 2010

For this study, the deterioration rate λ_{det} was taken to be different from the crack initiation rate λ_{init}. Subsequently, λ_{det} was calculated without counting the time spent in state 1. Using the theory explained in Section 3.4.1, λ_{det} was calculated as shown in Equation 5.4. The mean crack time to failure T_{crack} was taken to be 1 year.

$$T_{crack} = T_2 + T_3 + T_4 \tag{5.1}$$

$$T_{crack} = \frac{1}{\lambda_2} + \frac{1}{\lambda_3} + \frac{1}{\lambda_4} \tag{5.2}$$

$$T_{crack} = \frac{1}{\lambda_{det}} + \frac{1}{2\lambda_{det}} + \frac{1}{4\lambda_{det}} \tag{5.3}$$

$$\lambda_{det} = \frac{7}{4\,T_{crack}} \tag{5.4}$$

Uncertainty in the inspection procedure was included by introducing probabilities of defect detection π_2, π_3 and π_4. These represent the probability that a defect is detected in their respective states. This is similar to the probability of incorrect inspection as discussed in Section 4.2. Costs for inspection C_I, CM C_{CM}, minor PM $C_{PM,m}$, major PM $C_{PM,M}$ and electricity C_e were specified in the study and are listed in Table 5.1. For CM, the associated lead time for the blade and the vessel T_{lead} were provided. A discount rate δ was also considered to convert all costs to present value.

A total of 100,000 simulations were carried out as part of the Monte Carlo process. To optimize Time-based maintenance (TM) strategies, the inspection interval T_i was varied in the range of 0.1 - 0.5 years. The results for the model verification process are presented and discussed in Section 6.1.

Table 5.1: Summary of model parameters for the case study studied by Besnard and Bertling (2010)

Parameter	Unit	Value
T_i	Years	0.1-0.5
λ_l	1/Years	0.01
λ_{init}	1/Years	0.01
T_{crack}	Years	1
λ_{det}	1/Years	$7/4 \cdot T_{crack}$
π_2, π_3, π_4	-	0, 0.8, 1
P	MW	5
cf	-	0.4
T_{lead}	Days	21
(δ)	%	7
C_e	€/MWh	50
C_I	€	200
C_{CM}	€	440,000
$C_{PM,2}$	€	3,500
$C_{PM,3}$	€	35,000
$C_{PM,4}$	€	390,000

Correlation coefficients are calculated to quantify the convergence of the model results to the reference results. Since the general nature of the reference curve in the study is non-linear, the commonly used Pearson or Spearman correlation coefficient cannot be used. Alternatively, distance correlation, which measures the nonlinear association or dependence between two random vectors, is used in this analysis (Goldinlocks, 2016).

For two random vectors X, Y, the distance correlation coefficient, $dCorr(X, Y)$, is calculated as:

$$dCorr(X,Y) = \frac{dCOV(X,Y)}{\sqrt{dVar(X)\, dVar(Y)}} \tag{5.5}$$

where $dCOV$ is the distance covariance and $dVar$ is the distance variance. For easy computation, a package in Python is used. $dCorr(X, Y)$ varies from 0 - 2, with 0 being perfect correlation, 1 being no correlation and 2 being perfect negative correlation. The closer the coefficient is to 0, the higher the correlation between the two curves.

5.2. Pitch System Case Studies

Apart from the verification process, the proposed model was applied to 3 pitch system case studies. The first case study simulates the single FM model. The second and third case studies simulate the multiple FM model, for the independent degradation and the dependent degradation cases respectively.

5.2.1. Failure Modes Selection

The reason for focusing on pitch systems specifically was discussed in Section 1.3. Often, the highest failure rates are seen within hydraulic pitch systems among all WT components. The hydraulic pitch system layout and functioning have been explained in detail in Section 2.3. The FMs associated with pitch systems have also been discussed in Section 2.3.1.

In order to apply the multiple FM model, two dependent hydraulic pitch FMs were identified and simulated for both the independent degradation case and the dependent degradation case. While the selected FMs are dependent, the independent degradation case is still simulated to compare results

between both. Comparison of these two case studies takes place on relative terms with two FMs, both of their costs and DTs. However, comparing results between the single FM and the multiple FM models can be relatively difficult to comprehend as a considerable jump will be visible in cost and DT. To understand the layout of the components within the hydraulic pitch system, a detailed schematic is shown in Figure 5.2. The layout shows the connections between the various components of the pump, accumulator, valves, pistons and bearings. 3 independent hydraulic pistons, one for each blade, are provided. According to the discussion in Section 2.3.1, key FMs for the hydraulic system are valve wear, fluid leaks and fluid contamination.

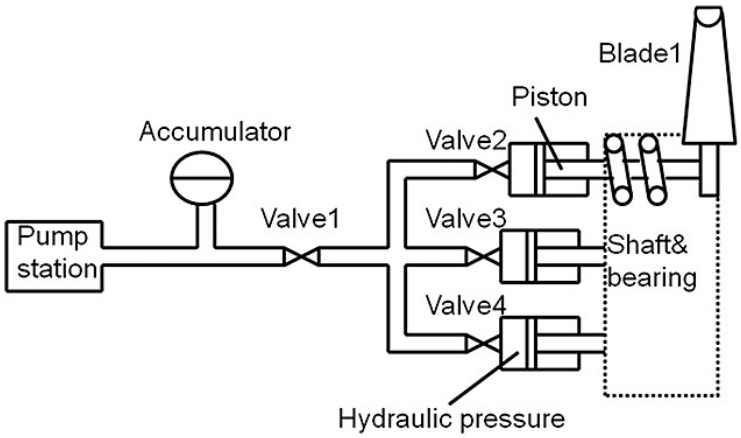

Figure 5.2: Detailed schematic of an hydraulic pitch system (Jiang et al., 2014)

From the schematic, it is clear that issues with the hydraulic fluid will affect the entire system as it circulates throughout the system and is in contact with almost all components. Z. Wang et al. (2022) further confirmed this dependence for pitch gearboxes with oil spills from the gearbox affecting gear and gearbox bearing failures. Thus, fluid leakage was selected to be one of the FMs of this study. Apart from oil issues, the second highest failure rates were seen to occur in hydraulic valves as valve wear, as shown in Figure 2.9. Furthermore, valve wear and hydraulic fluid leaks were found to be dependent on each other. With increasing leaks from a hydraulic system, the fluid circulating in the system reduces. The fluid while responsible for the transfer of force, also ensures adequate lubrication of all mechanical components. A reduction of the fluid will lead to insufficient lubrication which directly leads to an increase in the wear of components like valves and seals (Baker, 2022). Valve wear further links back to fluid leakages as increasing seal wear, causing cracks and crevices, exacerbates leaks from the system (HPS, 2023). Thus, valve wear is selected to be the second FM.

To conclude, the selected FMs are:

1. Failure Mode 1 (FM 1) – Hydraulic fluid Leakage
2. Failure Mode 2 (FM 2)– Valve Wear

5.2.2. Model Setup

With WT sizes growing at a rapid pace, the largest WTs manufactured at the time of the modelling procedure were considered. Thus, the modelled WT is considered to have a power rating P of 15 MW. For deployed OWTs, the capacity factor cf is seen to have high variability with values from 0.3 to 0.57 based on the location (Smith, 2022, Havtil, 2024). With the WT being deployed far offshore, a cf of 0.4 is assumed similar to what was proposed by C. Dao et al. (2019) and Haring (2018). With average lifespans varying between 20 to 30 years (Thomas, 2024), the modelled WT lifetime T_{hor} is assumed to be 25 years. This is fed as the time horizon to the model. All WT parameters used in this case study are listed in Table 5.2.

The state transition diagram for this case study is shown in Figure 4.3. For each FM, 4 states are chosen to describe the degradation process. These states are, as discussed earlier, S_0 As Good

As New (AGAN), S_1 Degraded, S_2 Critical and S_3 Failure. The states can also be defined in a way that gives them some physical significance. For FM1, hydraulic fluid level or pressure indicators can be used to estimate how severe the leakage is. For FM2, with an increase in valve wear, flow rate inconsistencies across the valve increase. This indicator can be used to estimate the amount of valve wear. For example, S_0 can stand for 0-30% pressure loss or flow rate variations from the reference value, S_1 for 30-50% pressure loss or flow rate variation, S_2 for 50-70% and S_3 for greater than 70%. Alternatively, the study by Carroll et al. (2016) segregated the states based on the material repair costs incurred. S_1 was set as minor repair with material costs being less than € 1,000. S_2 stood for major repair where material costs were greater than € 1,000 but less than € 10,000. Finally, S_3 represented a major replacement with material costs greater than € 10,000.

Table 5.2: Wind Turbine Parameters

Parameter	Unit	Value	Reference
P	MW	15	Schwarzkopf et al. (2021)
cf	-	0.4	C. Dao et al. (2019), Haring (2018)
T_{hor}	Years	25	Thomas (2024)

Since this study is primarily focused on analysing lifetime costs, the segregation as proposed by Carroll et al. (2016) is used. Based on the individual states for each FM, the System State Matrix (SSM) is created as discussed in Section 4.2.2. Equal weight factors w_1 & w_2 of value 0.5 are assigned to both FMs considering the lack of detailed data on cause and effect or propagation matrix between the selected FMs.

With limited data available for OWT pitch system failure rates, the data from C. Dao et al. (2019) and Carroll et al. (2016) is compared. The failure rates from both studies match closely with each other. Thus, the failure rate value of 1.076 failures per turbine per year from Carroll et al. (2016) is finalised for the simulation. From Figure 2.9, the failure rates for the individual FMs of fluid leakages and valve wear are calculated. As per Carroll et al. (2016), FM 1 has a failure rate of 17% of the total failure rate, which comes out to 0.183 failures per year. This calculation is further supported by a study from H. Li et al. (2020) focusing on pitch systems where the failure rate for fluid leakages was obtained to be 0.42 failures per year. Using the same logic, the failure rate for FM2 of valve wear is calculated. 14% of the total failure rate (Carroll et al., 2016) is calculated to be 0.150 failures per year. From these failure rates, the transition rates λ^1_{det} and λ^2_{det} between the states can be calculated as per Equation 5.8, where transition rates are equal to 7/4 times the failure rate. The methodology followed is the same as discussed earlier in Section 3.4.1. The failure rate is written in terms of the transition rates. Using a constant reduction factor, the transition rate is calculated.

For the shock rates λ^1_s and λ^2_s, the same value as used by Besnard and Bertling (2010) to represent lightning strikes is assumed. For this study, defined shock rates for the pitch system are not encountered in the literature. However, possible shocks can include large impulses to the piston via the blades or accumulator bursts. Due to a lack of data, the rates which represent lightning are also applied to this study. The correlation coefficient θ for the Clayton copula implemented in the dependent model is assumed to be 1 as discussed in Section 3.3. All degradation parameters are compiled in Table 5.3.

$$\frac{1}{\lambda_f} = \frac{1}{\lambda_{01}} + \frac{1}{\lambda_{12}} + \frac{1}{\lambda_{23}} \tag{5.6}$$

$$\frac{1}{\lambda_f} = \frac{1}{\lambda_{det}} + \frac{1}{2\lambda_{det}} + \frac{1}{4\lambda_{det}} \tag{5.7}$$

$$\lambda_{det} = \frac{7\,\lambda_f}{4} \tag{5.8}$$

As in the study by Welte et al. (2006), a discount rate δ of 7% is assumed to calculate the present

value of money. Long-term contracts are assumed between the operator and the maintenance provider which allows for constant costs for different activities. Using the rates from Carroll et al. (2016) and Schwarzkopf et al. (2021) conducted a comprehensive O&M cost model analysis for future floating offshore wind farms. A large farm consisting of 80 15-MW units with a lifetime of 25 years was considered. Accordingly, all values obtained from the literature were scaled up to represent 15 MW turbines, which aligns well with this study. The values include cost parameters (Table 5.4) and duration parameters (Table 5.5).

Table 5.3: Degradation Parameters

Parameter	Unit	Value	Reference
λ_{det}^1	1/Years	(7/4) · 0.183	Carroll et al. (2016)
λ_s^1	1/Years	0.01	Besnard and Bertling (2010)
λ_{det}^2	1/Years	(7/4) · 0.149	Carroll et al. (2016)
λ_s^2	1/Years	0.01	Besnard and Bertling (2010)
w_1	-	0.5	-
w_2	-	0.5	-
θ	-	1	-

Schwarzkopf et al. (2021) and Haring (2018) state that all pitch repair actions can be handled with a Crew Transfer Vessel (CTV) which costs € 3500 per day (C_v). CM actions require the lifting service of the internal crane of the WT, as the parts cannot be carried manually. However, a CTV is adequate for the transport of pitch system components. The CTV is considered to be owned by the maintenance provider with no extra lead time required to be considered. The labour costs C_l was estimated from J. A. Andrawus et al. (2007) and Carvalho et al. (2013) to be around € 50-60 per hour. Subsequently, a labour cost of € 55 per hour is applied to the model. The labour rates are the same for both inspection and maintenance actions. However, the duration of each action is different and hence, the total labour costs incurred for each action are different. The number of technicians n_l for repair actions to the pitch system was given to be 2 for S_1, 3 for S_2 and 4 for replacement in S_3 as per Schwarzkopf et al. (2021) and Carroll et al. (2016). The cost of electricity C_e is considered to be 100 €/MWh (Zhou et al., 2023). All inspection durations are considered to be constant and equal to 3 hours. The subsequent inspection cost C_I is obtained by considering the labour and vessel costs for the inspection duration.

During the literature review stage, no cost data was found for individual FMs within the pitch system. All available studies with cost data covered the entire pitch system. According to Schwarzkopf et al. (2021), pitch minor preventive repair $C_{PM,m}$, major preventive repair $C_{PM,M}$ repairs and complete replacements C_{CM}, cost € 500, € 1900 and € 14000, respectively. These costs only included the cost of materials required in the maintenance procedure. Due to the lack of detailed data available in the literature, the same costs are applied to both FMs. Repair work involving one state transition, $S_1 \rightarrow S_0$ or $S_2 \rightarrow S_1$, are regarded as minor preventive repairs. Two state transitions, $S_2 \rightarrow S_0$, are regarded as major preventive repairs and transitions from S_3 to S_0 as complete replacements of the system. All cost parameters are listed in Table 5.4.

Table 5.4: Cost Parameters

Parameter	Unit	Value	Reference
δ	%	7	Besnard and Bertling (2010)
C_v	€/day	3500	Schwarzkopf et al. (2021), Haring (2018)
C_l	€/hr	55	J. A. Andrawus et al. (2007), Carvalho et al. (2013)
C_e	€/MWh	100	Zhou et al. (2023)
C_I	€	767.5	-
C_{CM}	€	14,000	Schwarzkopf et al. (2021)
$C_{PM,m}$	€	500	Schwarzkopf et al. (2021)
$C_{PM,M}$	€	1,900	Schwarzkopf et al. (2021)
n_l	-	S_1-2, S_2-3, S_3-4	Schwarzkopf et al. (2021), Carroll et al. (2016)

The inspection interval T_i is varied in the range from 0.1 years to 5 years with steps of 0.2 years as discussed in Section 4.2.1. The inspection duration T_I is considered to be a constant value of 3 hrs as per Haring (2018). No lead time is required for minor repairs and major repairs. However, for system replacement, a constant lead time T_{lead} duration of 7 days is applied as proposed by Schwarzkopf et al. (2021). The travel duration T_{travel} to and from the WT is calculated assuming the WTs are deployed offshore at a distance of 60 kilometres off the coast. This is a conservative estimate with the current average distance to shore of 20 km (Díaz and Guedes Soares, 2020). Using a CTV speed of 22 knots (Haring, 2018), a time of 1.6 hours for the one-way journey is estimated. Schwarzkopf et al. (2021) provides repair durations for the entire OWT pitch systems: for minor preventive repairs, $S_1 \rightarrow S_0$ and $S_2 \rightarrow S_1$, $T_{PM,m}$ is assumed equal to 18 hours, for major preventive repairs, $S_2 \rightarrow S_0$, $T_{PM,M}$ is 38 hours and for major replacements T_{CM} is 75 hours. With data available only for entire pitch systems, assumptions need to be made for each FM. Both the FMs are considered to contribute equally to the repair durations and hence, the durations for minor and major repairs are broken down into 9 hours and 19 hours, respectively, for each FM. This equal split of the repair durations between the two FMs is made due to the lack of detailed maintenance data, however, they can be tuned as per the system requirements if more information is available.

The duration of the weather window, $T_{weather}$, which refers to the waiting time for accessing the turbine under safe and operable wind speeds and wave heights, is estimated by weighted random choice using probabilities and a Weibull distribution in the model as discussed in Section 4.2. Haring (2018) estimated the probability of harsh weather $\pi_{weather}$ to be 0.2 in the summer and 0.7 in winter with a waiting time $T_{weather}$ of 2 and 10 days, respectively. Byon and Ding (2010) provided much lower harsh weather probabilities of 0.4 in winter to 0.1 in summer. Schwarzkopf et al., 2021 took into account wind and wave metocean conditions for CTVs and estimated that on average a WT is accessible approximately 240 days in a year off the coast of Ireland. This translates to a harsh weather probability of 0.35 in an entire year. Since in this study, all maintenance actions are undertaken by CTVs and wave conditions in the North Sea are similar to off the coast of Ireland, the value of harsh weather probability is selected to be 0.35 (Schwarzkopf et al., 2021). Then, if harsh weather is encountered at the time of conducting maintenance, the length of the weather window is calculated. Instead of using constant values the weather window is represented by a random Weibull variable as defined in Le and Andrews (2016), with shape parameter α = 3.3 and scale parameter β = 1. The mean value of the distribution is approximately 6.2 days. The value is also in line with the averaged weather window length proposed by Haring (2018).

Due to the lack of available data, incorrect detection and incorrect repair probability inputs are as-

sumed. The probabilities of incorrect detection, $\pi_0, \pi_1 and \pi_2$, for both FMs are assumed equal to 0.07, 0.08 and 0.09, respectively. These values are assumed to be small as inspections are carried out physically by technicians with only human error to account for. Further, a sensitivity analysis is not carried out on these values as they are secondary features causing minor variations in the costs. Incorrect detection when the system is in S_0 can lead to the detected system state S_1. For S_1, the detected states can be S_0, S_1 and S_2 and for S_2, the detected states can be S_1 and S_2. S_3 is always assumed to be correctly detected. The probabilities of incorrect repair or irrepairable degradation π_{r0}, π_{r1} and π_{r2} is assumed to be 0.005. Both of these probability values are assumptions owing to a lack of literature on the topic. The possible repaired states for S_1 are S_0 and S_1, for S_2 are S_0, S_1 and S_2 and for S_3 is always S_0. This is also reflected in the state transition diagram shown in Section 4.2 Figure 4.3. All duration parameters discussed here are compiled in Table 5.5.

Table 5.5: Duration Parameters

Parameter	Unit	Value	Reference
T_i	Years	0.2 - 5	Besnard and Bertling (2010)
T_I	Hours	3	Haring (2018)
T_{lead}	Days	7	Schwarzkopf et al. (2021)
T_{travel}	Hours	1.6	Haring (2018)
T_{CM}	Hours	75	Schwarzkopf et al. (2021)
$T_{PM,m}$	Hours	9	Schwarzkopf et al. (2021)
$T_{PM,M}$	Hours	19	Schwarzkopf et al. (2021)
$\pi_{weather}$	-	0.65	Schwarzkopf et al. (2021)
$T_{weather}$: α, β	Weeks	3.3, 1	Le and Andrews (2016)
π_0, π_1, π_2	-	0.07, 0.08, 0.09	-
$\pi_{r0}, \pi_{r1}, \pi_{r2}$	-	0.005	-

The total number of Monte Carlo simulations conducted varies from 100 to 100k for each model based on the values of the uncertainty parameters obtained as explained in Section 3.2.

An earlier version of the model accounted for seasonality effects within a year. Varying seasons affected WT cf and waiting time due to harsh weather. For example, higher cfs in winter lead to higher energy production. At the same time, maintenance in winter is often difficult due to harsh weather conditions, such as high wind speeds and wave heights. The result of a simulation incorporating this effect is visualized in section A.2. However, no difference was seen in lifetime cost if seasonality was incorporated or averaged values of cf and weather window were used across the entire year. Furthermore, accounting for seasonality had the drawback of introducing dependency of the results on the season at the start of the simulation. To get rid of this dependency, multiple simulations with different starting seasons had to be run and an average was taken. This unnecessarily increased the computational cost and the time taken to solve the model. Since using averaged values of the parameters from the beginning provided the same results, the feature of seasonality was removed from the model.

5.2.3. Model Cases

Using the setup discussed in Section 5.2.2, first the Single Failure-Mode model, shown in Figure 4.5, is run. Each FM along with all of its parameters is fed as input to the model individually. The results are discussed in Section 6.2.1. All the other parameters of WT, Cost and Duration are set as per the values discussed in Section 5.2.2.

Next, the multiple failure-mode model described in Figure 4.8 is run. Both the independent and the dependent cases are simulated. All the parameters of Degradation, WT, Cost and Duration are set as

per the values discussed in Section 5.2.2.

For the independent degradation processes, each process runs independently. Each transition in a process including the sojourn time and the new state is independent of the other process. The two processes are linked using only a System State Matrix. The results are discussed in Section 6.2.2.1.

For the dependent degradation processes, the Clayton copula is used as discussed in Section 3.3. The copula links the two individual exponential distributions and is used to calculate the sojourn time for each state. The results are discussed in Section 6.2.2.2.

6
Results and Discussion

This Chapter presents the results for the various cases laid out in Chapter 5, summarized as follows. First, the model proposed in this thesis is verified in Section 6.1 by comparing its results with reference results from Besnard and Bertling (2010). Using the results from the validation, a sensitivity analysis to estimate the appropriate number of Monte Carlo simulations is carried out in Section 6.1.1. Next, in Section 6.2 the model is applied to the pitch system case studies. The results for individual Failure Modes (FMs) are presented and discussed in Section 6.2.1. The results from the multiple FM model, for both independent and dependent cases, are covered in Section 6.2.2. Finally, Section 6.2.4 carries out a sensitivity study for the key assumptions made throughout the simulations.

6.1. Model Validation Results

The primary objective of the reference study (Besnard and Bertling, 2010) was to analyze how Operations & Maintenance (O&M) costs vary between inspection intervals to optimize Wind Turbine (WT) blade Time-based Maintenance (TM) strategies. The black dashed plot in Figure 6.1 shows the results of the reference study, while the dark blue curve is the output of the model developed in this study, under similar assumptions. The red dot displays the optimum point on the curve which corresponds to the minimum costs and the optimum inspection interval, shown by the vertical red dashed line. The light blue shaded area around the dark blue curve corresponds to the 95% Confidence Interval (CI) after running multiple Monte Carlo (MC) Simulations as discussed in Section 3.2.

The output of the reference paper was an optimal inspection interval of 3 months with expected lifetime O&M costs of € 80,200 per blade. Figure 6.1 shows that the proposed model closely replicates the results of the reference study over the entire inspection interval range. The model optimum inspection interval is 0.26 years, corresponding to 3 months and 3 days. with an expected lifetime cost of € 79,600. The optimum inspection intervals, corresponding to the lowest lifetime costs, lie very close to each other for both curves. Further, a difference of 0.75% is seen in the minimum lifetime O&M costs between both curves. Thus, it is clear that the proposed model works as expected.

For Figure 6.1, a total of 100,000 MC simulations are carried out. Each point on the dark blue curve represents the mean value of a sample consisting of 100,000 simulations. The selection of this sample size is further discussed in Section 6.1.1.

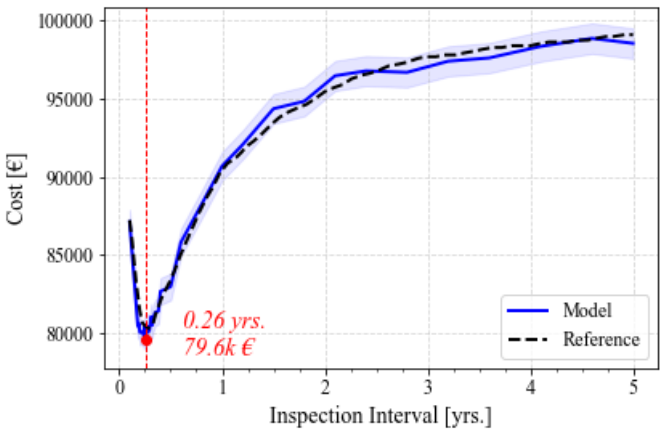

Figure 6.1: Lifetime costs vs. inspection interval

In order to understand the variations in the cost with inspection intervals, lifetime costs are broken down into their individual components and plotted in Figure 6.2. Only inspection and maintenance cost curves are seen with the values of operation costs included as explained in Section 5.1.

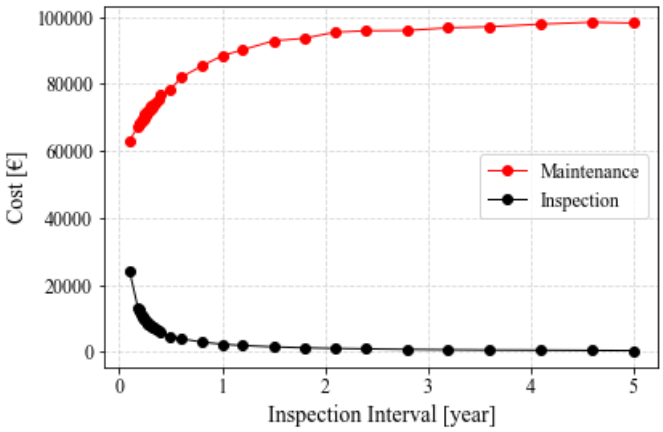

Figure 6.2: Costs breakdown vs. inspection interval

It is seen that the high costs for short inspection intervals are mainly due to the high inspection costs as short inspection intervals lead to frequent inspection actions. At the same time, due to frequent inspections, the system is often found in healthier states and thus it requires very little maintenance. As a result, maintenance costs are the lowest with very little maintenance required. With increasing inspection intervals, the inspection cost curve falls rapidly due to fewer inspections scheduled. However, now with longer durations between each inspection, the system state will degrade to a greater extent. Subsequently, maintenance costs will increase as now the system has to be repaired to S_0 from higher states. For extremely long inspection intervals, both the inspection and maintenance cost curves seem to reach an asymptotic trend. This happens because changing the inspection interval does not have a significant impact on those costs. Waiting for 5 years instead of 4 years reduces the inspection costs and increases the maintenance costs only by a small amount. Further, longer inspection intervals lead to very small inspection costs compared to maintenance costs. For example, an inspection interval of 5 years with € 200 for every inspection (from Table 5.1) barely leads to € 1,000 for the total inspection costs. This is a very small contributor to the total costs compared to the maintenance cost of almost € 100,000 (from Figure 6.2) at the same inspection interval.

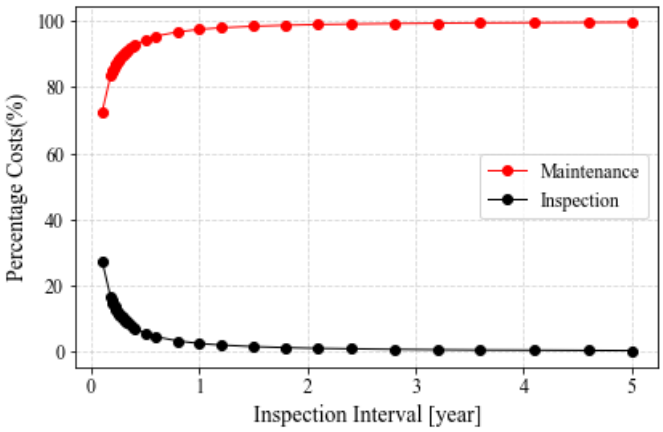

Figure 6.3: Percentage costs breakdown vs. inspection interval

Figure 6.3 shows the same costs in terms of percentages of the total lifetime costs. It is seen that maintenance cost is the major contributor to the total lifetime cost in this validation study. Similar to Figure 6.2, maintenance costs increase rapidly, starting from approximately 70%, for short inspection

intervals and almost flatten out close to 100 % for very long intervals. The rapid increase in maintenance costs is matched by a rapid decline in inspection costs for short inspection intervals. For long inspection intervals, the inspection cost barely contributes 1% to the total lifetime costs. It is important to note that operation costs are combined in this study and thus, the nature of the operation cost curve is unknown.

6.1.1. Sample Size Sensitivity

Besnard and Bertling (2010) chose to run 100,000 Monte Carlo simulations. This is done to ensure that the Coefficient of Variation (CV) between the results is less than 1. For a sample size of 100,000, a distribution of 100,000 points exists for each data point of the dark blue cost curve. Thus, the CV can be calculated for each point. Finally, the mean value of all CV is presented for the results. For the case of 100,000 simulations, a mean CV of 1.6 was obtained.

To better understand the significance of the sample size and to visualize the effects of varying it, a model sensitivity analysis is conducted. The sample size or the number of MC simulations is varied while keeping all other parameters the same. Figure 6.4 shows the model output, lifetime costs vs. inspection intervals, for a few selected sample sizes. The uncertainty parameters discussed in Section 3.2 are also compared. This analysis further helps in deciding the sample size for the pitch system case studies discussed in Section 5.2.

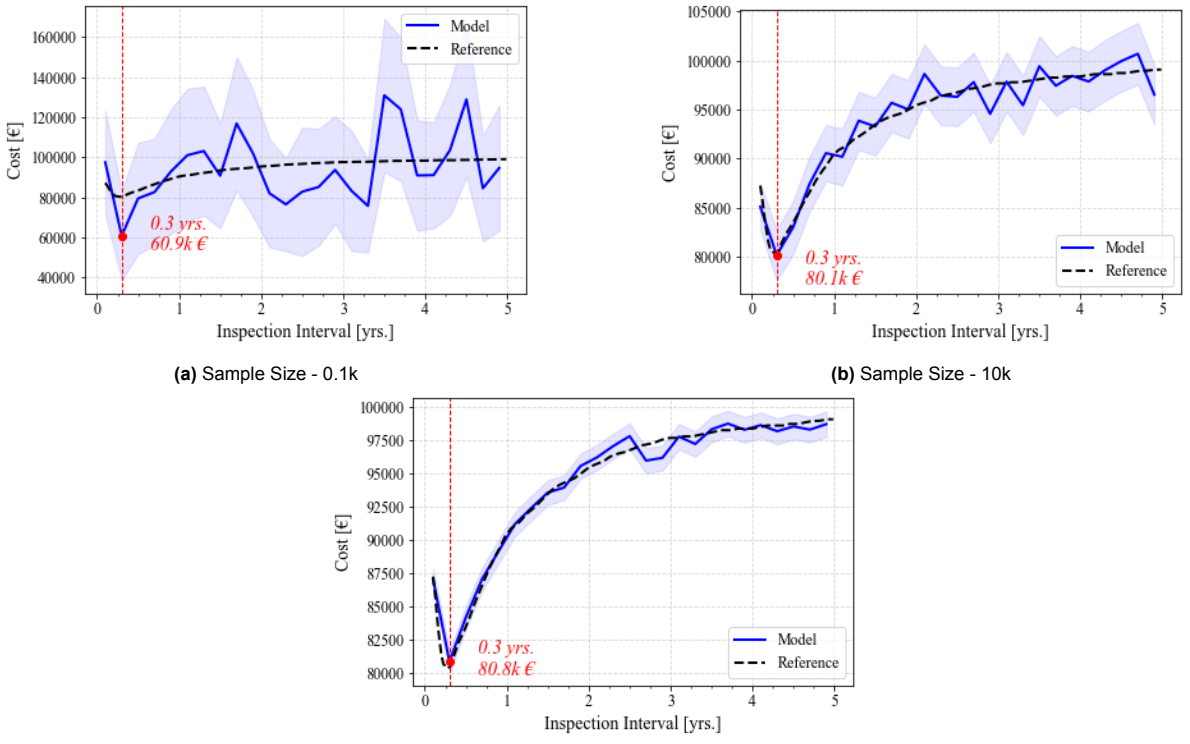

(a) Sample Size - 0.1k

(b) Sample Size - 10k

(c) Sample Size - 100k

Figure 6.4: Lifetime costs vs. inspection interval plots with 95% confidence interval for sample sizes of a) 0.1k, b) 10k and c) 100k

The dependence of the cost curve and its CI on the sample size is clearly visible from the comparison of the three plots. For small sample sizes (Figure 6.4a), large deviations from the reference curve are visible. They can be attributed to the randomness of the stochastic process. The convergence to the reference values with increasing sample sizes (Figure 6.4c) is due to the convergence property for the weak law of large numbers. Correlation coefficients are calculated to quantify this effect as discussed in Section 5.1. Increasing convergence is seen for increasing sample sizes. The results of the correlation coefficients are shown in Table 6.1. Further, the 95% CI band is seen to narrow with

increasing sample sizes depicting higher confidence in the mean cost values. To quantify the convergence of the CIs with increasing sample sizes, the mean standard error is also included in Table 6.1

In Figure 6.5, standard deviations σ are depicted in the light blue area instead of the 95% CI. The figure confirms the independence of standard deviations to varying sample sizes. While increasing sample size reduces the deviations of the mean values from the reference curve, the range of σ does not change significantly. The same is reflected in the values of the mean CV in Table 6.1 which remain almost constant across different sample sizes.

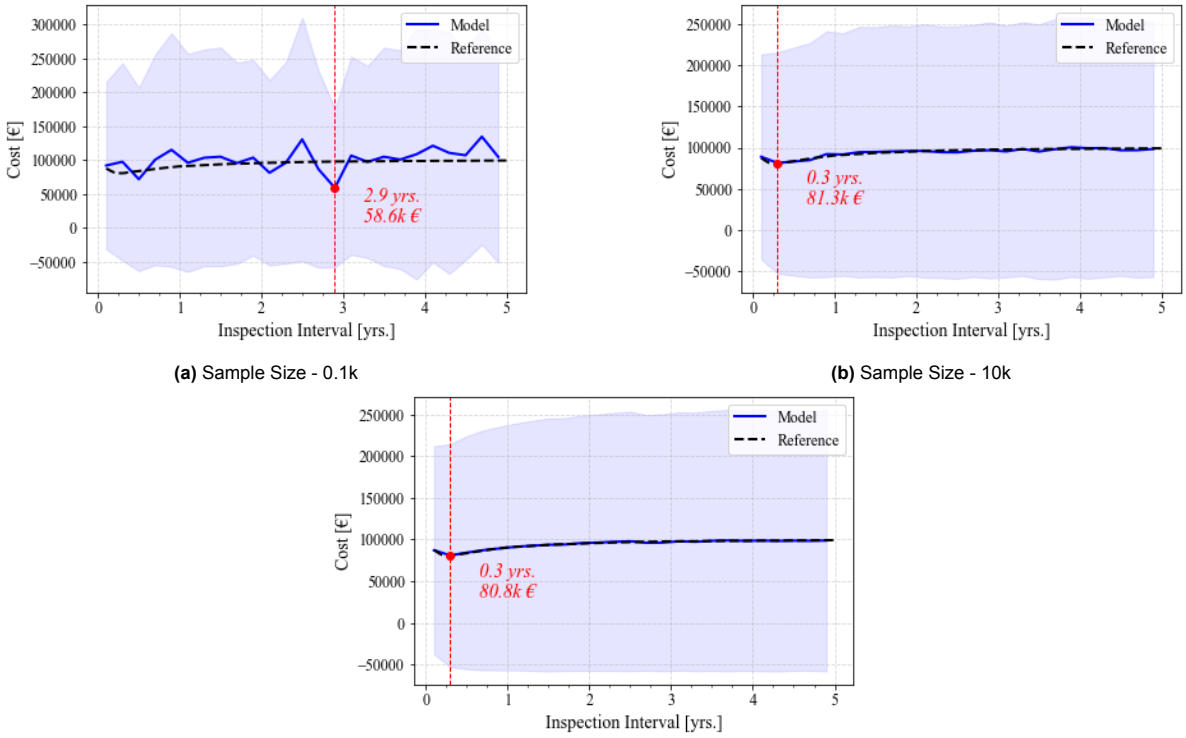

(a) Sample Size - 0.1k

(b) Sample Size - 10k

(c) Sample Size - 100k

Figure 6.5: Lifetime costs vs. inspection interval plots with standard deviations for sample sizes of a) 0.1k, b) 10k and c) 100k

Another important parameter varying with the sample size is the computational cost. This cost is quantified in terms of elapsed time from the start of the code to the printing of the output and is included in Table 6.1.

Table 6.1: Sample Size Sensitivity

Sample Size	Elapsed Time [hr:min:sec:ms]	Distance Correlation	Mean Coefficient of Variation	Mean Standard Error [€]
100	0:00:01.204328	0.298	1.590	14,747.9330
1,000	0:00:03.979313	0.254	1.592	4760.2719
10,000	0:00:34.480015	0.047	1.602	1,505.6274
50,000	0:02:47.638364	0.008	1.598	675.4993
100,000	0:09:01.230913	0.005	1.599	477.4916

The results in Table 6.1 show an increase in the elapsed time with the increase in sample sizes, as expected. The model takes approximately 9 minutes to run 100k simulations. The distance correlation coefficient between the model mean curve and the reference curve decreases with the sample sizes,

corresponding to an improving correlation. Since the mean CV is a measure of σ of the samples, it is not dependent on the sample size as visible in Figure 6.5. Accordingly, the mean CV value in Table 6.1 does not change with the sample sizes. Finally, the mean standard error which is a measure of both the standard deviation and the sample size is seen to decrease for the sample sizes as expected. A decrease of approximately 96% in the mean standard error is seen between the sample sizes of 100 and 100k.

Based on this study, an estimate of the required sample size for the pitch system case studies is generated. It is seen that plots with sample sizes lower than 10,000 have a large amount of variations with respect to the reference curve. These sample sizes take the least time to solve the model. However, the results cannot be assumed to be accurate due to the large variations as well as uncertainties in the mean values. Thus, sample sizes of 10,000 and above will be used for the pitch system case studies.

6.2. Pitch System Case Study Results

6.2.1. Single Failure Mode Model

First, the individual FMs are simulated using the single FM model presented in Section 4.2.1.

6.2.1.1. FM 1: Hydraulic Fluid Leakage

Table 6.2 shows the model key outputs: the optimum inspection interval in years, the corresponding minimum lifetime costs and the Downtime (DT). Figure 6.6 and Figure 6.7 show the lifetime costs and DT, and the cost breakdown across the inspection interval range, respectively.

Table 6.2: Single Failure Mode Model FM 1 Results

Optimum Inspection Interval [yrs.]	Lifetime Costs [€]	Downtime [hrs.]
0.7	242,696	542.882

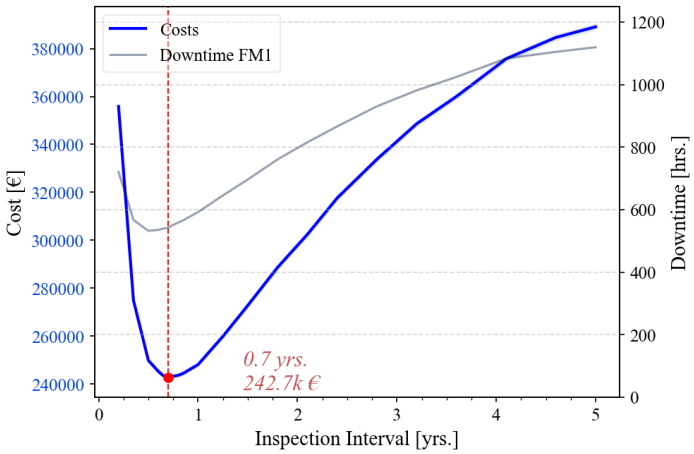

Figure 6.6: FM 1 - Lifetime costs and downtime vs. inspection interval

The optimum inspection interval is seen to occur at 0.7 years with lifetime costs of € 242,696. The corresponding DT is 542.882 hours at the intersection of the grey curve with the vertical red line, which is approximately equal to 22.6 days. On the other hand, a minimum DT of 532.028 hours is seen to occur at inspection intervals of 0.5 years. Thus, the minimum DT is not seen to occur at the inspection interval of the minimum lifetime costs. The behaviour of the DT curve corresponds to the behaviour

of the operation cost curve in Figure 6.7 with the minima for both occurring at the same inspection interval. The operation costs are calculated as the monetary loss due to no power production from the WT DT. Thus, the effect of DT is taken into account when calculating the total lifetime costs. Hence, the most economical solution for a WT operator will be the optimum inspection interval of 0.7 years with minimum lifetime costs of € 242,696. In case a WT operator wants to achieve the highest availability at the expense of higher costs, the minimum of the DT curve with an optimum inspection interval of 0.5 years can be utilised. The corresponding lifetime costs at this inspection interval are € 249,882.

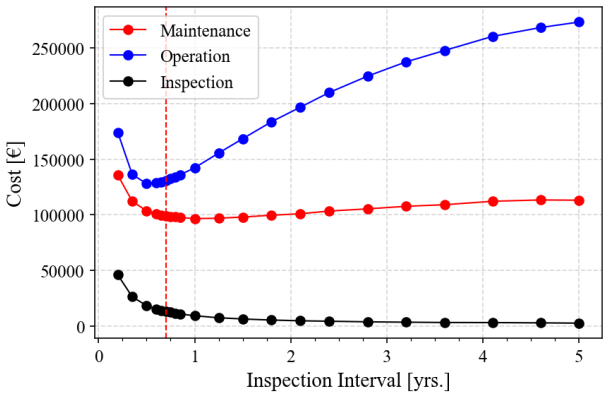

Figure 6.7: FM 1 - Cost breakdown vs. inspection interval

Figure 6.7 shows the individual costs making up the total lifetime costs. The behaviour of each of the cost curves is explained in detail in Section 6.1. For inspection costs, the behaviour of the curve is similar to Figure 6.2. Shorter inspection intervals cause frequent inspections and thus higher costs. With increasing inspection intervals, the number of inspections carried out will reduce and subsequently, the cost will decrease. Next, the behaviour of the operation costs, not seen in the validation case, can be analysed. As explained earlier, operation costs occur because of the WT DT. DT can be segregated into DT from inspection actions, preventive maintenance actions and corrective maintenance actions due to WT failures. Based on these individual contributors, the operation cost curve can be broken down into regions with different primary contributors. For shorter inspection intervals, inspection actions contribute the most to the DT. Frequent inspections lead to a higher count of hours when the turbine has to be switched off. Consequently, high operation costs are observed in this region. For longer inspection intervals, DT from failures and maintenance actions is the major contributor. DT from WT failures are always considered to be constant with immediate repair scheduled following a lead time of 7 days as explained in Section 5.2.2. However, with increasing inspection intervals, the number of times the system fails increases. As a result, the DT due to failure increases. Similarly, for longer inspection intervals, the system has to be repaired from higher degraded states, requiring longer maintenance durations. This leads to higher DT due to maintenance actions.

The behaviour of the maintenance curve in Figure 6.7 differs from that in Figure 6.2 where the maintenance cost monotonically increases with the inspection interval. In Figure 6.7, the maintenance cost curve has higher initial values for shorter inspection intervals. These reduce up to a minimum for a particular inspection interval and then start increasing again with a very small slope for longer inspection intervals. There are two reasons for this behaviour:

1. In Figure 6.2, the operation costs were not considered separately from the others. Instead, both inspection and maintenance costs collectively covered the total operation costs incurred. In Figure 6.7, with operation costs separated, the large increase in maintenance costs for longer inspection intervals reduces. However, still some increase is seen which corresponds to the higher repair costs of the system in higher degraded states.
2. Compared to the reference model Besnard and Bertling (2010), the proposed model contains a few additional parameters such as the inclusion of weather windows in the maintenance steps. For each maintenance action, a weather window is calculated based on probabilities of encountering harsh weather. The costs incurred during this weather window are added to the maintenance

costs which causes the behaviour change. These costs are the costs of the rented vessel and the labour for the unused bad weather duration. This is very similar to the inspection costs which also comprise the labour and the vessel costs. As a result, the maintenance cost curve resembles the inspection cost curve for shorter inspection intervals.

Two simulations, with sample sizes of 10,000 and 100,000 are carried out as part of the Monte Carlo simulations and the key results are summarised in Table 6.3. Figure 6.8 shows the lifetime cost vs inspection interval plot for the 10,000 Monte Carlo simulation case. A few kinks are seen near the minima of the cost curve for the 10,000 sample size case. These are due to a high number of points near the minimum where the cost is calculated. Despite a large sample size, due to the stochastic behaviour of the curve, slight variations in the mean values can occur. To remove these variations, the 100,000 sample size simulation is run. A smooth curve is observed as previously seen in Figure 6.1 and all the results presented here refer to it. The computational cost in terms of the elapsed time along with other uncertainty parameters is specified in Table 6.3. The total time taken to run the simulation is approximately equal to 6 minutes for the 10k sample size and 1 hour and 56 minutes for the 100k sample size. Compared to the model used for the verification process, this is a significant increase of more than 12 times for the same sample size. This is attributed to the multiple new features such as detailed cost calculations, weather windows, probabilities of incorrect repair and detections introduced in the model. The mean CV is approximately 0.5 for both cases. The mean standard error obtained, as described in Equation 3.22, is approximately equal to € 465. The 95% CI calculated using this standard error is plotted as the light blue band in the plots of lifetime costs vs inspection interval. However, since the number of simulations is fairly large, the CI range and the width of this band are quite small and unobservable in Figure 6.1. The CI is larger and visible for lower sample sizes, as seen in Figure 6.8. Focusing on the optimum inspection interval with minimum costs, the corresponding standard error is approximately equal to € 392 for the 100,000 sample size.

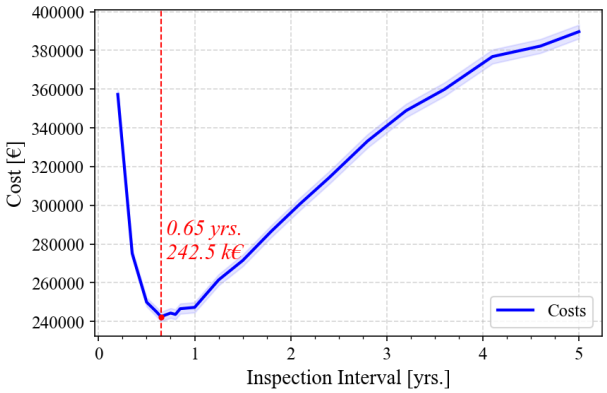

Figure 6.8: FM 1 - Lifetime costs vs. inspection interval for 10k Monte Carlo simulations

Table 6.3: Single Failure Mode Model FM 1 Uncertainty Parameters

Sample Size	Elapsed Time [hr:min:sec:ms]	Mean Coefficient of Variation	Mean Standard Error [€]	Standard Error @ Optimum Inspection Interval [€]
10,000	0:06:05.502	0.501	1,473.837	1,221.168
100,000	1:56:32.736	0.500	465.112	391.943

6.2.1.2. FM 2: Hydraulic Valve Wear

An important point to note here is that the value of the failure rate for FM 2 is smaller than that for FM 1. Most of the other parameters stay the same as discussed in Section 5.2.2. Table 6.4 shows the key outputs of the optimum inspection interval with the corresponding minimum lifetime costs and the DT.

The plots of lifetime costs, the DT and the cost breakdown across the range of inspection interval are shown in Figure 6.9 and Figure 6.10.

Table 6.4: Single Failure Mode Model FM 2 Results

Optimum Inspection Interval [yrs.]	Lifetime Costs [€]	Downtime [hrs.]
0.85	201,234	460.287

The optimum inspection interval is seen to occur at 0.85 years with minimum lifetime costs of € 201,234. The corresponding DT at the intersection of the grey curve with the vertical red line is 460.287 hours, which is approximately equal to 19.2 days. On the other hand, a minimum DT of 453.067 hours is seen to occur at inspection intervals of 0.7 years with lifetime costs of € 203,786. Thus, similar to FM 1, the minimum DT is not seen to occur at the same inspection interval as the minimum lifetime costs. Instead, the minimum of the DT curve corresponds to the minimum of the operation cost curve, as shown in Figure 6.10.

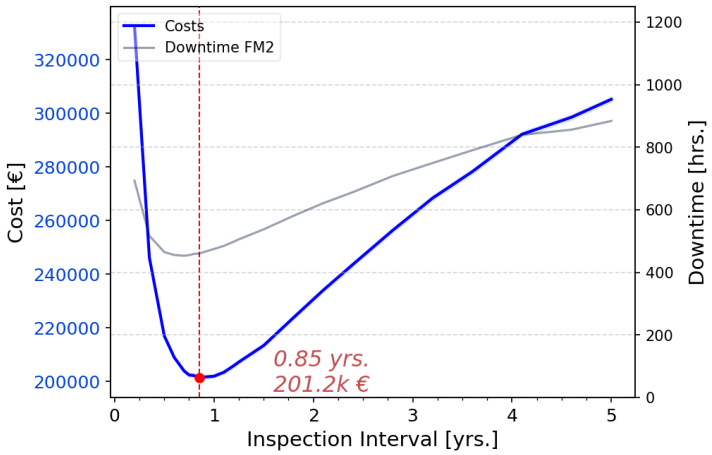

Figure 6.9: FM2 - Lifetime costs and downtime vs. inspection interval

Comparing Figure 6.9 with Figure 6.6, the optimum is seen to shift towards longer inspection intervals with lower lifetime costs. This corresponds to the lower failure rates for FM 2. Due to lower failure rates, the degradation process occurs slower than for FM1. As a result, less maintenance is required and the optimum lifetime costs are lower with higher optimum inspection intervals.

Figure 6.10 shows the individual inspection, maintenance and operation costs. The behaviour of each curve follows the same trend as seen for FM1 in Figure 6.7. Thus, the same explanation is valid for the behaviour of these plots. Similar to FM1, two simulations of sample sizes 10,000 and 100,000 are carried out. The computational cost in terms of the elapsed time along with other uncertainty parameters is specified in Table 6.5. The total time taken to run the simulation is approximately equal to 2 hours and 15 minutes for the 100k sample size. This is of the same order as the time taken for FM 1. The mean CV is obtained to be approximately equal to 0.55. The mean standard error obtained is approximately equal to € 412. The standard error at the optimum inspection interval is approximately equal to € 361.

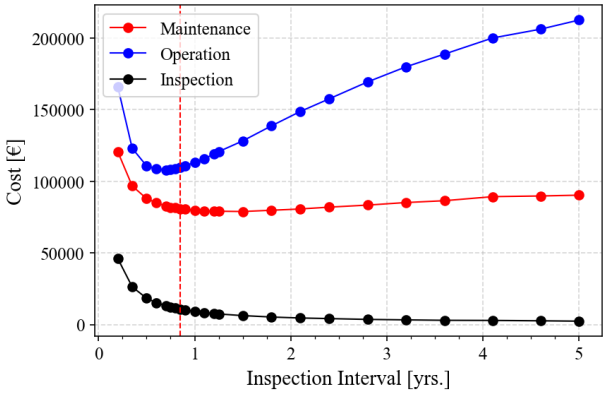

Figure 6.10: FM2 - Cost breakdown vs. inspection interval

Table 6.5: Single Failure Mode Model FM 2 Uncertainty Parameters

Sample Size	Elapsed Time [hr:min:sec:ms]	Mean Coefficient of Variation	Mean Standard Error [€]	Standard Error @ Optimum Inspection Interval [€]
10,000	0:07:14.981	0.556	1,303.950	1,169.671
100,000	2:15:56.988	0.555	411.723	360.806

6.2.1.3. Combined Failure Mode 1 & Failure Mode 2

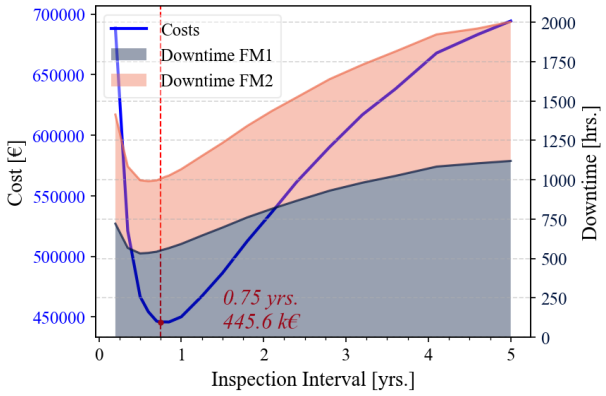

Figure 6.11: FM1 & FM2 - Summation of lifetime costs and downtime vs. inspection interval

Before simulating the multiple FM model, an attempt is made to combine the results of the two FMs directly. The lifetime costs and the DT for individual FMs are summed up for their respective inspection intervals. Figure 6.11 represents the results of this summation. The optimum inspection interval is now 0.75 years with minimum total lifetime costs of € 445,618. This is higher than the sum of the two individual optima by € 1,688 and corresponds to 0.75 years not being the optimum inspection interval for either of the individual FMs. The lifetime costs for each FM at 0.75 years are slightly higher than the minimum. The total DT at this inspection interval is 1006.263 hours, with 551.171 hours from FM 1 and 455.092 hours from FM 2, which is approximately equivalent to 42 days. It is important to note here that this results from the direct summation of the two FMs, without considering any relation between them.

6.2.2. Multiple Failure Mode Model

With the results for the individual FMs established, now the multiple FM model is simulated. For the first case study, both the degradation processes are considered to be independent. The only link between the two FMs is the system state matrix, which defines the state of the system based on the state of each FM. The next case study dives into dependent degradation processes. Here the processes are intricately related via a multivariate distribution. The distribution is created by linking the independent sojourn time distributions.

For both the independent and the dependent degradation cases, first, a 10,000 sample size simulation is carried out. This choice is due to the large computational costs (elapsed time) associated with a larger sample size. However, due to this limitation, a few kinks were seen near the minima of the cost curve. Hence, to obtain detailed results, the 100,000 sample size simulation is run and presented.

6.2.2.1. Independent Degradation Processes

Table 6.6 presents the key outputs for the multiple FM model simulating the two independent degradation processes. The graphs of lifetime costs, the DT and the cost breakdown across the range of inspection interval are shown in Figure 6.12 and Figure 6.13.

Table 6.6: Multiple independent FM model results

Optimum Inspection Interval [yrs.]	Lifetime Costs [€]	Downtime [hrs.]
0.35	478,192	1055.923

The optimum inspection interval is 0.35 years, with minimum lifetime costs of € 478,192. The DT at this inspection interval is 1055.923 hours or 44 days. This is split between the two FMs with FM 1 having a DT of 551.054 hours and FM 2 having a DT of 504.869 hours. Similar to the previous case studies, this minimum does not correspond to the inspection interval with the minimum DT. A minimum DT of 1054.11 hours, 547.872 hours from FM 1 and 506.238 hours from FM 2 is observed at an inspection interval of 0.3 years. The corresponding lifetime costs are € 484,132.

The comparison with the results in Figure 6.11 shows that the optimum inspection interval has reduced from 0.75 years for the combined case to 0.35 years for the independent case. The minimum lifetime costs at the optimum inspection interval have increased slightly from € 445,618 in the combined case to € 478,192, with an increase of € 32,574 or 7.3%. The DT at the optimum inspection interval has also increased from 1006.263 hours in the combined case to 1055.923 hours in the independent case, with an increase of 49.66 hours or 4.9%.

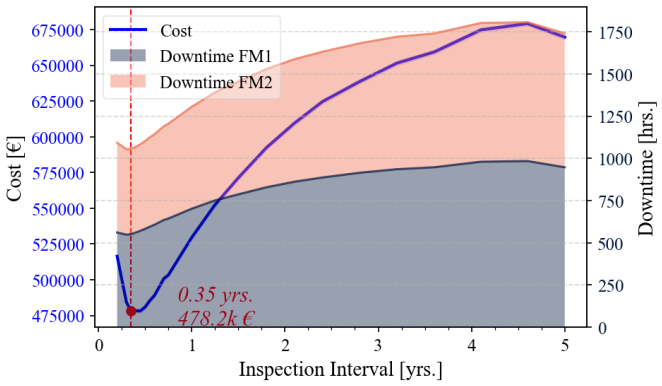

Figure 6.12: Multiple Independent FMs - Lifetime costs and downtime vs. inspection interval

The different inspection interval regions of each curve are analysed in detail. First, the short inspection interval range, 0.2-0.5 years is analysed. The steep decrease in the costs associated with this range observed in the combined case has now reduced significantly, where the drop in the lifetime costs is much smaller. This behaviour is also reflected in Figure 6.13, where for short inspection intervals the operation and the maintenance costs have reduced greatly compared to both Figure 6.7 and Figure 6.10. The same trend is also observed in the DT curves for this region. The steep decrease in DT observed for the combined case is now barely decreasing for the independent case. This is primarily due to changes in the inspection costs. While the inspection cost curve retains the same behaviour as before, the costs are now half of the value in the combined case. A similar behaviour is expected because these costs are determined by the costs of labour and the costs of the vessel which remain the same. However, the number of inspections creates the difference. In the independent case, both processes share the same inspection. In contrast, for the combined case, each process has its own inspection and inspection costs which are summed up. Thus, effectively the number of inspections has halved compared to the combined case. This reduction in the number of inspections directly reduces the DT of the turbine. Hence, the previously observed large drop in DT (around 400 hours) for the short inspection interval has now reduced to around 100 hours. The reduction in DT also translates to a reduction in the operation costs for short inspection intervals. From around € 335,000 for the combined case, the operation costs have dropped to € 300,000, a reduction of 10%. A similar decrease seen in the maintenance cost, from approximately € 265,000 to € 160,000, a reduction of 40%, is due to the lower time spent waiting for a working weather window. Since the number of inspections and subsequent maintenance instants has halved, the average weather window will also be halved. Hence the steep drop is not seen in the maintenance curve.

Towards the end of this region, there is already a visible reversal in the curve behaviours. An increase in the DT, and subsequently the operation costs, is observed. This is the reason behind the shift of the minima of optimum cost towards shorter inspection intervals. The reason for this reversal is as follows. From the end of the short inspection interval range and for moderate inspection intervals of 0.5 - 3 years, both DT and operation costs are higher than for the combined case. The operation costs have increased from approximately € 350,000 to € 430,000 at the inspection interval of 2 years, an increase of 22%. This is because of the implementation of the system state matrix. As per the matrix, the failure of a single FM declares the entire system to have failed, regardless of the other FM's state. Thus, a higher number of system failures occur for the independent case. Once the entire system is declared to have failed, maintenance is required. Subsequently, the DT and the operation costs have increased for the independent case study.

For the longer inspection intervals (3-5 years), the slope of the curves is seen to decrease with the curves reaching constant values. In this region, the costs are lower compared to Figure 6.11. While the maximum costs are around € 700,000 for the combined case, the maximum costs are approximately € 675,000 for the independent case. A similar trend is seen for the DT curve. Most of the curve in this region has shifted down from 2000 hours to 1750 hours and the DT has reduced. The maintenance costs have been reduced in the long term, from € 200,000 in the combined case to around € 170,000 for the independent case, a reduction of 15%. On the other hand, the operation costs for the independent case are just slightly higher than for the combined case. Despite this, the lower maintenance and inspection costs lead to lower total lifetime costs for the independent case.

The computational cost in terms of the elapsed time along with other uncertainty parameters for two MC sample sizes is specified in Table 6.7. The total time taken to run the simulation is approximately equal to 1 hour and 53 minutes for a sample size of 10,000 and 17 hours and 2 minutes for a sample size of 100,000. The mean CV is equal to 0.38 for both cases. The mean standard error obtained is approximately equal to € 2,133 and € 673 for the 10,000 and 100,000 sample sizes, respectively. The standard error at the optimum inspection interval is approximately equal to € 1,947 and € 585 for the two cases, respectively.

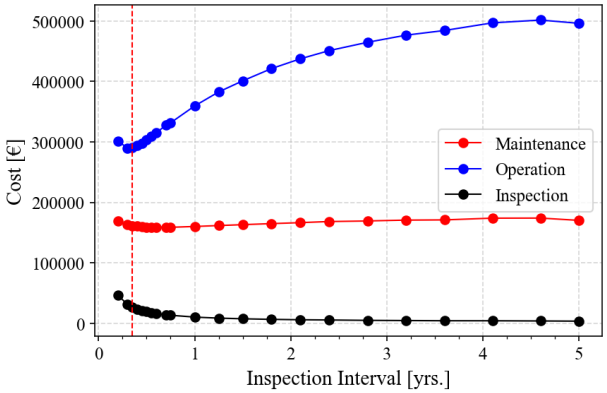

Figure 6.13: Multiple independent FMs - Cost breakdown vs. inspection interval

Compared to the individual FM simulations, the model running time is approximately 16 and 7.5 times higher for sample sizes of 10,000 and 100,000, respectively. The primary reason is that the model now needs to account for both degradation processes simultaneously. While each transition is independent, the states of both processes must be obtained at each time of inspection. Then, based on the System State Matrix (SSM), further maintenance can be scheduled. Keeping track of the entire timeline and properties of each process at each inspection increases computational complexity and the associated time.

Table 6.7: Multiple independent FM model uncertainty parameters

Sample Size	Elapsed Time [hr:min:sec:ms]	Mean Coefficient of Variation	Mean Standard Error [€]	Standard Error @ Optimum Inspection Interval [€]
10,000	1:53:28.899	0.382	2,132.973	1,947.452
100,000	17:02:45.311	0.382	672.770	585.498

6.2.2.2. Dependent Degradation Processes

Table 6.8 presents the key outputs for the multiple FM model simulating the two dependent degradation processes. The graphs of lifetime costs, the DT and the cost breakdown across the range of inspection interval are shown in Figure 6.14 and Figure 6.16.

Table 6.8: Multiple dependent FM model results

Optimum Inspection Interval [yrs.]	Lifetime Costs [€]	Downtime [hrs.]
0.6	292,431	581.961

In this case the optimum inspection interval is 0.6 years, corresponding to the minimum lifetime costs of € 292,431. The DT at this inspection interval is 581.961 hours or 24.2 days. This is split between the two FMs with FM 1 having a DT of 311.889 hours and FM 2 having a DT of 270.072 hours. Similar to the previous case studies, this minimum does not correspond to the inspection interval with the minimum DT. A minimum DT of 576.701 hours (FM 1 - 306.359 hours, FM 2 - 270.342 hours) is observed at an inspection interval of 0.5 years. The corresponding lifetime costs are € 293,792.

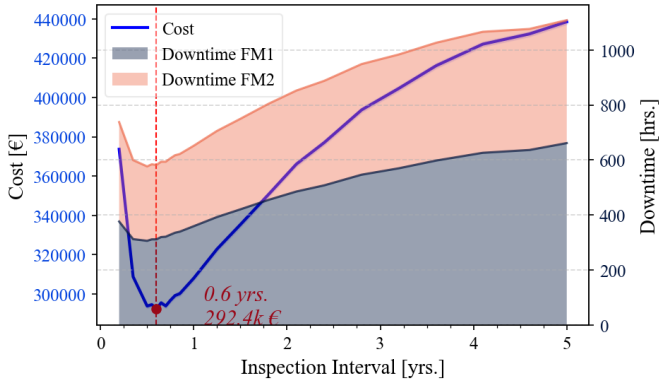

Figure 6.14: Multiple Dependent FMs - Lifetime costs and downtime vs. inspection interval

Compared to the independent case seen in Figure 6.12, the optimum inspection interval has increased. This translates to a lower frequency of inspections of the WTs. Larger inspection intervals are accompanied by a decrease in the optimum lifetime costs of € 186,285, or approximately 39%, from € 478,716 to € 292,431. This amounts to considerable cost savings for the dependent case compared to the independent case. To better compare the independent and the dependent simulations, both plots are shown in Figure 6.15 with the same axes scales.

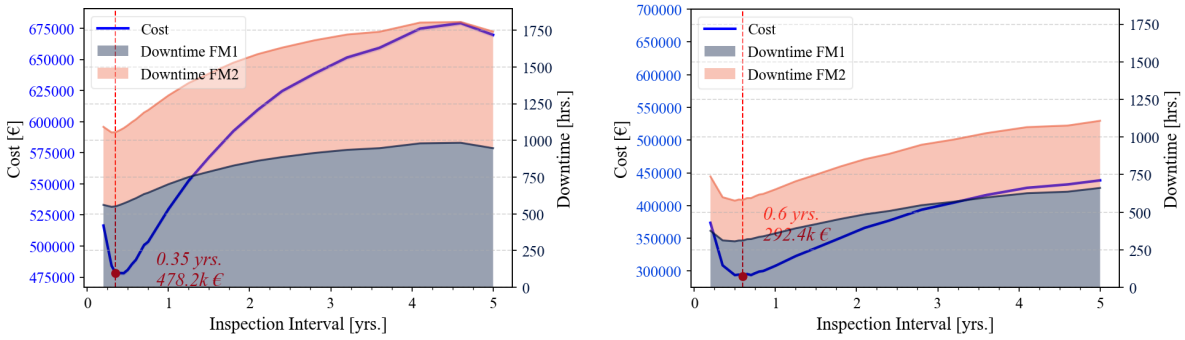

(a) Multiple independent FMs

(b) Multiple dependent FMs

Figure 6.15: Comparison of independent and dependent results - Lifetime costs and downtime vs. inspection interval

This reduction in costs is mainly driven by the decrease in DT which brings down the operation costs. While the inspection costs remain the same as before, maintenance costs show a decrease compared to the independent case. The extremely sharp reversal of the operation costs in Figure 6.13 is now much smoother in Figure 6.16, which shows a smaller increase in these costs for larger inspection intervals compared to the dependent case. This causes the shift in the optimum inspection interval towards longer intervals.

To understand the reason for the reduction in costs, the difference between the independent and the dependent model is analysed. The primary difference lies in the calculation of the sojourn times for each transition as discussed in Section 4.3.1. The independent model uses exponential 1-dimensional distributions while the dependent model uses a bivariate 2-dimensional joint distribution which cannot be directly compared. To carry out a fair comparison, the 1-dimensional exponential distribution is replaced with a 2-dimensional joint distribution. However, instead of using a Clayton copula as was originally done for the dependent case, an Independence copula is implemented. This copula maintains independence between the two processes. Figure 6.17 shows the joint distribution with the Independence copula in Figure 6.17a and with the Clayton copula in Figure 6.17b. The dashed red line represents the expectation/mean of the sojourn times for both processes and is further explained ahead. To verify the validity of this comparison, the results for the multiple independent FM model are compared with the multiple dependent FM model utilising the Independence copula. The results for both the simulations

are shown in section A.3. It is seen from the results that the independence copula can successfully replicate the multiple FM independent case results with less than a 1% difference between both.

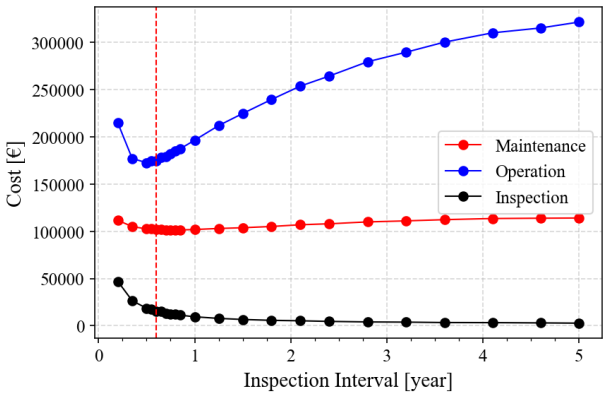

Figure 6.16: Multiple Dependent FMs - Cost breakdown vs. inspection interval

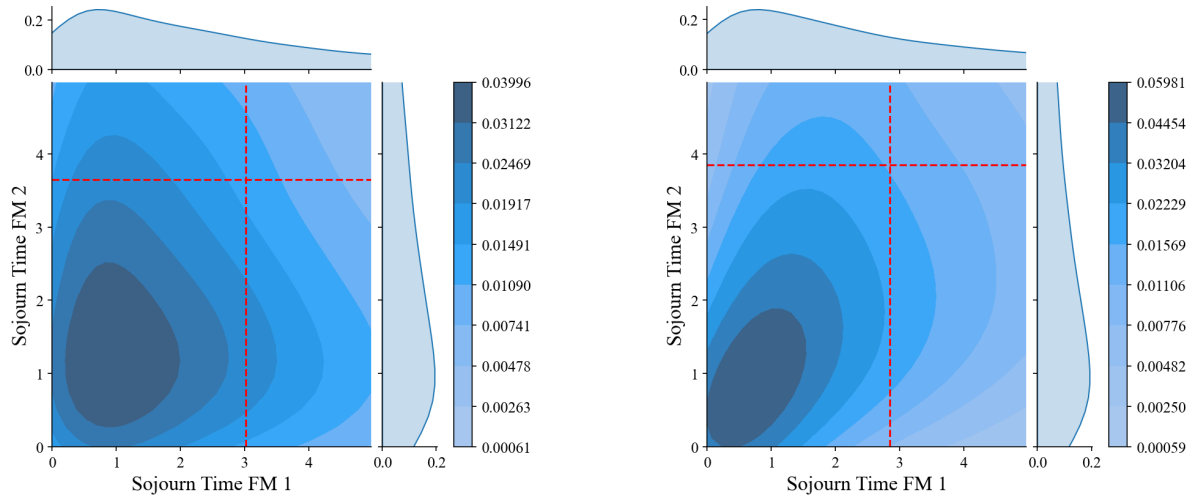

(a) Independence copula

(b) Clayton copula

Figure 6.17: Sojourn time bivariate PDFs for a) Independence copula and b) Clayton copula

Equation 3.12 displays the calculation of the expectation for an exponential distribution. The expectation of any function can be calculated using the same formula and is applied to the bivariate distribution. For each value of sojourn time 1, a 1-dimensional distribution corresponding to the shape of sojourn time 2 is obtained. The expectation is calculated for each of these distributions. The expectation of these multiple expectation values is calculated and shown by the dashed red line in Figure 6.17. This is done for both sojourn times to obtain two means, one for each FM. Similar to the exponential distribution, the mean sojourn time directly corresponds to the transition rate between states. Comparing Figure 6.17a with Figure 6.17b, the mean sojourn times are not seen to vary greatly between the plots. Thus, the transition rates remain the same for both cases and the degradation processes for both models proceed with the same rate.

Comparing Figure 6.17a with Figure 6.17b, a significant variation in the behaviour of the joint PDF is observed. For the Independence copula, high probabilities are seen to occur at sojourn times corresponding to the peaks in the marginal distributions. The shape of the joint PDF strongly corresponds to the marginal distributions. Two lines of peaks (high probability values) are observed, perpendicular to each other. When the two degradation processes occur independently, the input degradation rates define the individual sojourn times. There is no interaction between the two processes.

In the dependent case, the Clayton copula alters this joint PDF and narrows the space between the two peaks, aligning them with the diagonal. The sojourn times for one process are defined after taking into account the sojourn times for the other process as described in Section 4.3.1.2. The high probabilities along the diagonal correspond to high probabilities for equal sojourn times. Consequently, both sojourn times are pulled towards each other causing simultaneous degradation. If process 1 is in a particular state of degradation S_i with sojourn time T_{Si} in that state, this affects process 2 to have a sojourn time that is close to T_{Si}. In terms of the physical degradation process, if FM 1 is healthy and has a long sojourn time, this allows FM 2 to also have a long sojourn time, which corresponds to a healthy state. However, if FM 1 is in the higher degraded state and has a short sojourn time, this pushes FM 2 to also have a short sojourn time. This way the independent behaviour is altered and a correlation between both the FMs is introduced. The strength of this correlation, specified by the copula correlation coefficient, determines the proximity between the two sojourn times.

This occurrence of similar sojourn times saves cost if both FMs fail together instead of at separate sojourn times. Similar times of failure reduce the number of operations required and the DT from subsequent inspection and maintenance actions. Thus costs are lesser for CM actions. However, the same cannot always be said for PM actions. For example, PM of both FMs from $S1$ is more expensive than maintenance of FM 1 from $S1$ along with FM 2 from $S0$. Thus, aligning the peaks with the diagonal reduces costs for CM while PM can be either cheaper or more expensive. To better understand the contribution of CM and PM to lifetime costs, a breakdown of lifetime costs of the dependent model into corrective costs and preventive costs is provided in Figure 6.18. All O&M actions are segregated into corrective actions or preventive actions, if the action is taken after or before the failure of the system, respectively.

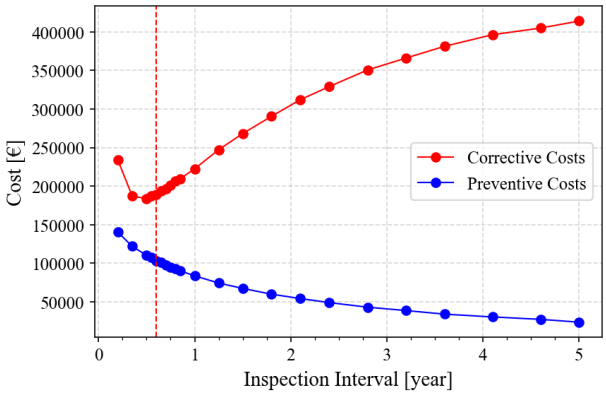

Figure 6.18: Multiple Dependent FMs - Corrective and preventive costs vs. inspection intervals

Figure 6.18 shows that corrective costs are much larger than preventive costs throughout the inspection interval range. At the optimum inspection interval, corrective costs are almost 1.75 times preventive costs. These costs dominate the lifetime costs which justify the reduction in lifetime costs for the dependent case due to the Clayton copula's shape. To further connect this with the degradation process, the process is quantified using visit frequencies. Abeygunwardane (2012) defines these frequencies as the count of the number of times the system is detected in a particular state over a year. Table 6.9 presents the visit frequencies of the 4 states for both the independent model and the dependent model results.

Table 6.9: Multiple independent & dependent FM model degradation process results

State	Visit Frequencies [1/yrs.]	
	Multiple FM independent model	Multiple FM dependent model
0	2.625	1.749
1	0.360	0.246
2	0.053	0.033
3	0.092	0.045

Table 6.9 shows that visit frequencies for $S3$ are larger for the independent model as compared to the dependent model. This further supports the reduction of lifetime costs in the dependent model. Multiplying state visit frequencies with WT lifetime outputs the count of the number of times the system is found in a particular state. Subsequently, the number of failures is 2.3 times in the WT lifetime and 1.125 times in the WT lifetime for the independent and the dependent model respectively. A higher number of failures (almost twice that of the dependent model) occur in the independent model due to the independence between the sojourn times. Each component can fail at any time, regardless of the other component's health. However, in the dependent model, both components degrade simultaneously and fail at similar sojourn times, reducing the total number of system failures. For both cases, higher visit frequencies are observed for $S3$ than for $S2$ corresponding to more time spent by the system in $S3$ than $S2$. This successfully concludes the reasoning for the lower lifetime costs obtained for the dependent model.

Table 6.10: Multiple dependent FM model uncertainty parameters

Sample Size	Elapsed Time [hr:min:sec:ms]	Mean Coefficient of Variation	Mean Standard Error [€]	Standard Error @ Optimum Inspection Interval [€]
10,000	1:58:25.9426	0.498	1,705.855	1,513.790
100,000	15:00:27.692	0.498	539.700	489.864

The computational cost in terms of the elapsed time along with other uncertainty parameters is specified in Table 6.10. The total time taken to run the 10,000 sample size simulation is approximately equal to 1 hour and 58 minutes. The time taken for the 100,000 sample size is approximately 15 hours. For each sample size, the model running time is approximately the same as that associated with the independent FM simulation case. The mean standard error is approximately € 1,706 and € 540 for sample sizes of 10,000 and 100,000, respectively. These values have reduced from € 2,133 and € 673 from the independent case which corresponds to a reduction of 20%. Since the sample sizes are the same for both cases, the reduction is attributed to a reduction in the standard deviation. Thus, a decrease in the spread of the results is observed for the dependent case. The standard error at the optimum inspection interval is approximately equal to € 1,514 and € 490 for the sample sizes of 10,000 and 100,000. These values have also reduced from the dependent case values of € 1,947 and € 585 respectively, corresponding to reductions of 22% and 16%. The mean CV is approximately 0.5 which is higher than the independent case value of 0.38. Based on the formula of CV from Section 3.2, this corresponds to either an increase in the standard deviation or a decrease in the mean cost values for the dependent case. The comparison for standard error shows that the standard deviation decreases for the dependent case. Thus, the increase in CV is from a reduction in the mean cost values.

6.2.3. Summary of Results

Table 6.11 summarizes the results of all the case studies. Large variations are seen across the case studies with the optimum inspection interval and lifetime cost strongly depending on the model. The single FM FM 2 model outputs slightly smaller values of lifetime costs and standard error as compared to the FM 1 model. This is attributed to the smaller failure rate for FM 2. A longer optimum inspection interval corresponding to fewer inspections is obtained for FM 2 with comparable simulation times for both. While the combined FM is not a model and has no results for elapsed time and standard error, its results are also presented for complete comparison. For the combined model, the optimum inspection interval is similar to a weighted average from the single FM results. However, this is far from the best maintenance strategy with high lifetime costs of € 445,618 and is comparable to the sum of minimum lifetime costs from the single FM models. The independent model performs worse than the combined model with a shorter optimum inspection interval and even higher lifetime costs. Further, approximately 17 hours are taken to simulate the independent model as compared to 4 hours (the sum of elapsed time of both single FM models) for the combined model. Compared to the single FM models, the standard error has increased for the independent case. The multiple FM dependent model performs quite well in terms of the lifetime cost output. A much smaller value of € 292,431 is obtained which is almost comparable with the single FM results. The optimum inspection interval is longer than the independent case but shorter than the other three cases. While the simulation time decreases slightly from the independent case, it is still considerably large, approximately 7 times the elapsed time of the single FM models. The standard error for the dependent case improves compared to the independent case, demonstrating lesser variability in the mean lifetime costs.

Table 6.11: Summary of results

Parameter	Single FM FM 1	Single FM FM 2	Combined FM FM 1 & FM 2	Multiple FM Independent	Multiple FM Dependent
Optimum Inspection Interval [yrs.]	0.7	0.85	0.75	0.35	0.6
Lifetime Costs [€]	242,696	201,234	445,618	478,192	292,431
Elapsed Time [hr:min:sec:ms]	1:56:32.736	2:15:56.988	-	17:02:45.311	15:00:27.692
Standard Error @ Optimum Inspection Interval [€]	391.943	360.806	-	585.498	489.864

6.2.4. Sensitivity Studies

In order to understand the sensitivity of the results of the multiple FM dependent model to the assumptions considered in this study, a sensitivity study is carried out. The values of the various parameters used in the proposed model have been selected from the available literature after extensive research. However, there is almost always some uncertainty associated with them. The parameters considered in the sensitivity study are listed here:

1. Failure rates λ^1_{det} and λ^2_{det}, which can vary for the same component across WT manufacturers (Walgern et al., 2023). Further, Walgern et al. (2023) show variations in the failure rates across power ratings, with higher-rated WTs being more prone to failures. Due to this volatility, rates are selected for the sensitivity study. These rates directly affect the degradation process and the results.
2. Discount rate δ, which is used to convert the future value of money to the present value. Since this factor applies to all incurred costs, the value of the optimum cost might be quite sensitive to the discount rate.

3. Cost values, such as maintenance C_M, electricity C_e, labour C_l and vessel costs C_v are assumed as constants in the study. Variations in these costs directly affect the minimum lifetime costs. Further, this would also help in identifying the most critical cost value.
4. Copula correlation coefficient θ, is varied as discussed in Section 3.3. The coefficient defines the shape of the joint sojourn time PDF and is used to obtain sojourn times. Variations in θ might affect these sojourn times and hence the degradation process.
5. Reduction factor, which aims to quicken degradation for the higher degraded states. Currently, this is assumed as a constant value. Varying these factors strongly affects the transitions between the states.

For the sensitivity study, only one parameter is varied at a time and all other parameters are kept constant. The value of this parameter is then set to vary within $\pm$5% and $\pm$10% limits. For all figures, the original parameter value is shown by a green coloured curve, except where specified otherwise. Similarly, 5% variations are shown by orange and red colours and 10% variations by blue and purple. Similar to the case studies, lifetime costs are calculated across inspection intervals and the minimum cost corresponding to the optimum inspection interval can be determined. To prevent extremely high model run times, a few changes are made. The number of Monte Carlo simulations is reduced from 100,000 to 50,000 for faster results at the expense of an increase in uncertainty, or standard error. The inspection interval range which initially varied from 0.2 to 5 years is reduced to vary from 0.3 to 1 year. This range is selected since all the optimum inspection intervals are always seen to lie within it for the previous case studies.

6.2.4.1. Deterioration & Discount Rate Parameters

Figure 6.19 presents the results of the sensitivity study for the FM2 deterioration rate. The initial value was 0.26 failures per year as shown in Table 5.3. This rate is then varied and lifetime costs over the inspection interval range are plotted. The first observation is the unvarying optimum inspection interval. For all values of the deterioration rate, 0.6 years is obtained as the optimum inspection interval. This might be because the $\pm$5% and $\pm$10% perturbations affect the deterioration rate merely slightly. The rate value varies by very small amounts from 0.24 failures per year to 0.29 failures per year. The second observation is the gradual increase in lifetime costs for higher deterioration rates. This is consistent with the theory that components with higher deterioration rates fail more frequently and hence, require more frequent maintenance which incurs higher costs. Figure 6.20 shows the difference in the optimum lifetime cost between the initial value and the $\pm$10% variations.

Along with deterioration rate 2, Figure 6.20 also shows the sensitivity study results for deterioration rate 1 and the discount rate. Among these three parameters, variations in the discount rate cause the largest variations in the optimum lifetime costs. The lifetime costs change by approximately 6% when the discount rate is increased by $\pm$10% from its initial value of 7%. Since it applies to all incurred costs, a large sensitivity of the results to the discount rate is expected. The discount rate is closely followed by deterioration rate 1 with variations of approximately 5.6% for each perturbation. On the other hand, variations in deterioration rate 2 have a much smaller effect of around 2% on the optimum costs. This large difference in the sensitivity study results can be attributed to the initial difference between the values of both rates. The deterioration rate 1, with an initial value of 0.32 failures per year, is larger than the initial value of deterioration rate 2. Subsequently, FM 1 deteriorates more frequently and has a larger impact on the lifetime costs. Further, with the perturbations being percentage-based, a 10% variation in deterioration rate 1 causes a larger increase than a 10% variation in deterioration rate 2.

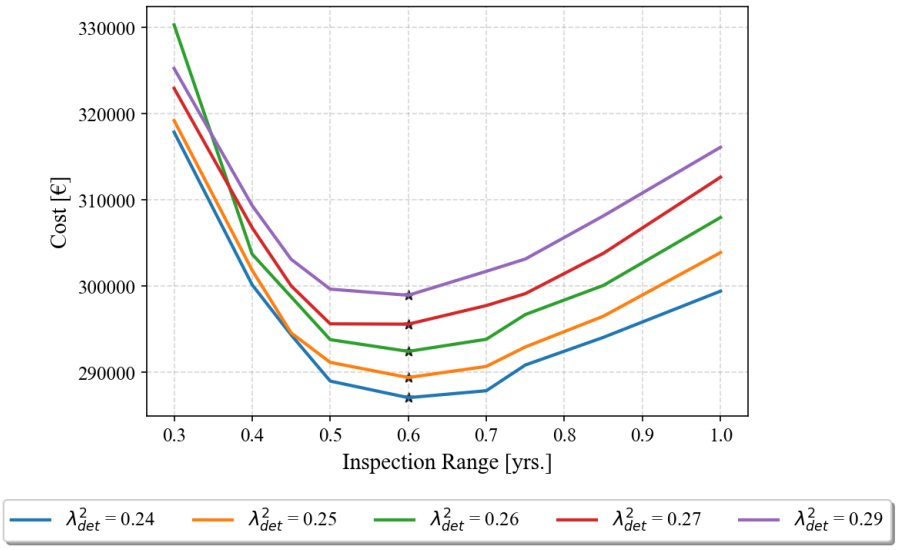

Figure 6.19: Variations in deterioration rates of FM2 - Lifetime costs vs. inspection interval plots

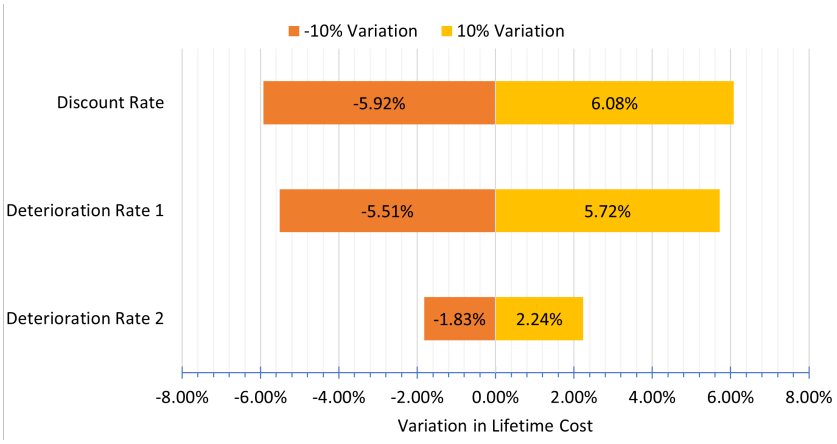

Figure 6.20: Sensitivity of the optimum lifetime cost to deterioration and discount rates

Figure 6.19 shows that the optimum inspection interval does not vary for small perturbations in the FM2 deterioration rate. To check the effect of larger perturbations, the rate was varied from 10% of the initial value, corresponding to 0.03 failures per year, to 400%, corresponding to 1.05 failures per year. Figure 6.21 presents the plot for the total lifetime costs against the inspection interval for these larger variations. Here the original rate is shown by the orange curve. Confirming the theory discussed above, larger variations in the rate cause large variations in the optimum inspection interval. With increasing deterioration rates, the optimum inspection interval shifts towards smaller intervals, apart from one exception, in the case of a deterioration rate of 0.03 failures per year. Further, the lifetime costs also increase significantly with increasing rates. The shift in the optimum inspection interval is due to faster degradation causing higher maintenance and operation costs. The exception for the case of a deterioration rate of 0.03 failures per year can be explained as follows. When the deterioration rate becomes very small, the shock rate λ_s becomes more dominant in the transitions and the costs. The shock rate throughout this study is taken to be 0.01 failures per year. Since the values of these rates are now comparable, a large number of direct transitions to failure S_3 take place. Since corrective maintenance is required after failure, the costs of repair are quite high compared to preventive maintenance from S_2 or S_1. This changes the maintenance cost curve and as a result, the lifetime cost curve for this rate does not follow the trend of decreasing optimum inspection intervals for increasing rates.

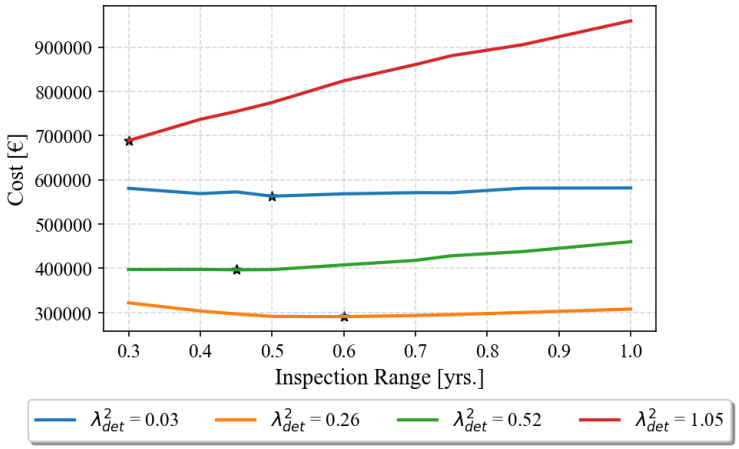

Figure 6.21: Larger variations in deterioration rates of FM2 - Lifetime costs vs. inspection interval plots

6.2.4.2. Cost Parameters

A similar study is conducted for the various cost parameters summarised in Table 5.4. For maintenance costs, all three costs of corrective (C_{CM}), minor preventive ($C_{PM,m}$) and major preventive ($C_{PM,M}$) maintenance are varied together. Figure 6.22, Figure 6.23 and Figure 6.24 present the lifetime costs vs. inspection interval plots for variations in vessel costs, electricity costs and maintenance costs, respectively.

In Figure 6.22, the day rate of the Crew Transfer Vessel (CTV) is varied from the initial assumed value of € 3,500 per day. With an increase in the day rate, the total lifetime costs increase as expected. The increase is quantified in Figure 6.25. An increase of approximately € 3,500 is seen between the initial value and the $\pm$10% variations. This corresponds on average to 1.35% variation from the optimum lifetime costs. Another interesting observation is the shift towards lower optimum inspection intervals for higher day rates. This shift towards shorter inspection intervals translates to carrying out inspections more frequently. While this seems counterintuitive at first, it can be explained by referring to the time taken to carry out maintenance. For shorter inspection intervals, the system will be found more often in lower degraded states, such as S_1 and S_2. For higher inspection intervals, there is a higher chance that the system has degraded further to S_2 and S_3 states. The duration of the maintenance action for minor preventive maintenance is only 9 hours compared to corrective maintenance requiring 75 hours. Thus, the incurred vessel costs increase for longer inspection intervals. Hence, it is more cost-effective to shift towards shorter inspection intervals for higher day rates.

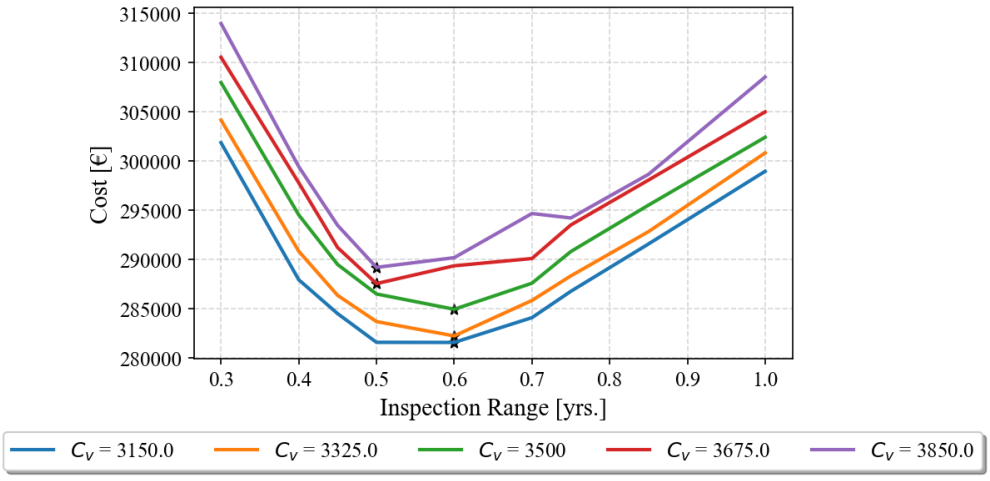

Figure 6.22: Variations in vessel costs - Lifetime costs vs. inspection interval plots

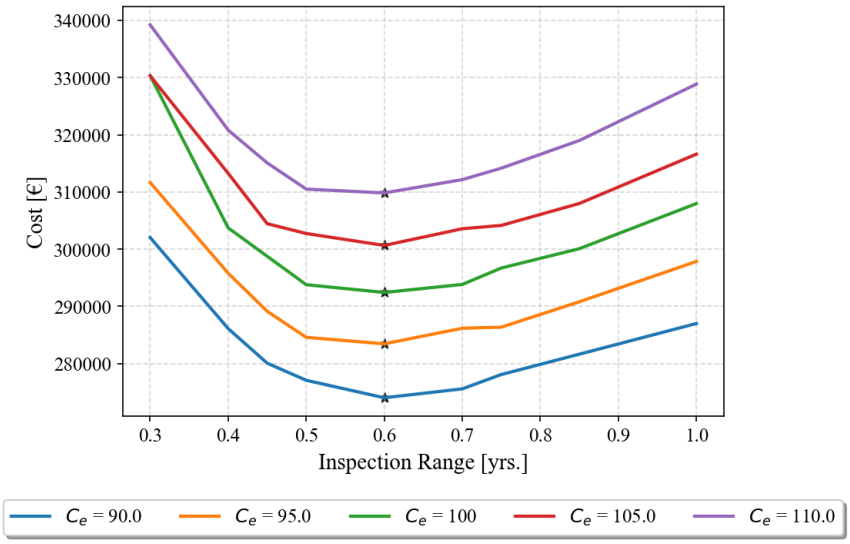

Figure 6.23: Variations in electricity costs - Lifetime costs vs. inspection interval plots

Figure 6.23 shows the sensitivity of the lifetime costs to the variations in the cost of electricity, from the initial assumed value of € 100 per MWh. The optimum inspection interval does not change with the cost of electricity. An almost consistent increase of € 9,000 is observed in the minimum lifetime cost. This is the largest variation in the optimum costs among all the parameters as compared in Figure 6.25. $\pm$10% variations in the electricity cost alter the optimum costs on average by 6%.

Figure 6.24 presents the sensitivity of the total lifetime costs to the variations in the cost of maintenance. The legend shows the percentage variation in maintenance costs compared to the initial assumed value. Compared to the other parameters, the lifetime costs do not vary much with maintenance costs. All the optima lie quite close to each other at the same inspection interval of 0.6 years. The change between the lifetime costs is approximately € 1,000 between the initial value and the $\pm$10% variations. This translates to the smallest variations in lifetime costs of about 0.36%, as reflected in Figure 6.25. These very small variations are attributed to the maintenance costs contributing less to the lifetime costs compared to the operation costs.

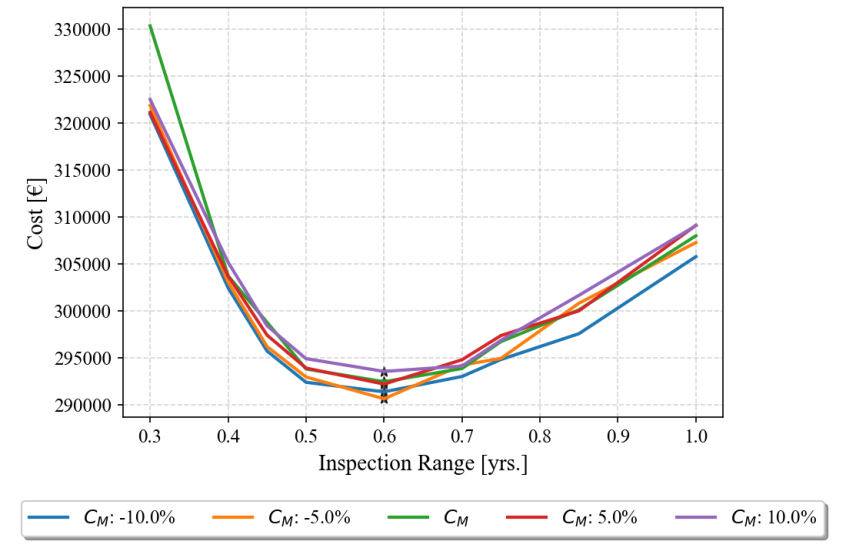

Figure 6.24: Variations in maintenance costs - Lifetime costs vs. inspection interval plots

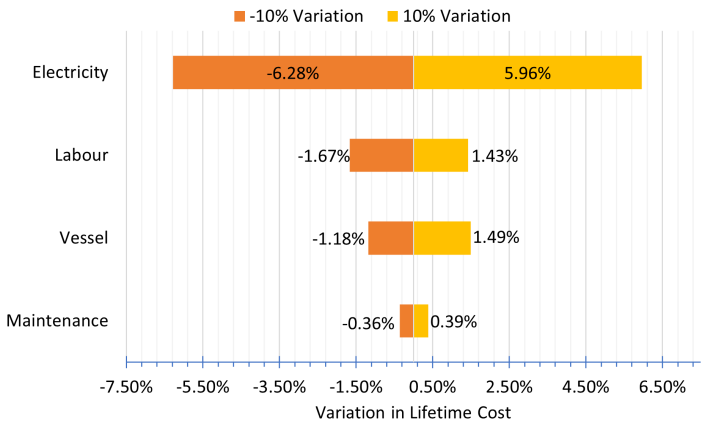

Figure 6.25: Sensitivity of the optimum lifetime cost to cost parameters

Figure 6.25 compares the effect of variation of the various cost parameters on the optimum lifetime costs. Electricity costs are seen to have the highest effect on lifetime costs. Labour costs and vessel costs have similar effects with variations on average of about 1.6% and 1.3%, respectively. The optimum lifetime cost is least sensitive to variations in the maintenance costs with average changes of approximately 0.37%. Since the operation costs from WT DT contribute the most to the lifetime costs, parameters affecting the operation costs or DT are more sensitive than others. Electricity costs affect the operation costs directly and thus, show the highest sensitivity. Labour and vessel costs affect inspection and maintenance costs and thus, show a lower sensitivity compared to the electricity costs. Maintenance costs affect only material costs for repairs and thus, have the least sensitivity.

6.2.4.3. Copula Parameter

The copula correlation coefficient is varied from values of 0.1 to 4 to observe the behaviour of costs for a wide range of coefficients. Figure 6.26 shows this variation where an increasing coefficient is seen to reduce minimum lifetime costs and increase the optimum inspection interval. This relates to the reasoning discussed in Section 6.2.2.2, where increasing correlation brings the individual sojourn times closer to each other. This reduces operation and CM costs. From values of 0.1 to 1, a large reduction of 33% in lifetime cost from approximately € 440,000 to € 290,000 is seen. However, the decrease in costs is seen to slow down for higher values of θ. This is similar to Figure 3.6 where the Pearson correlation coefficient had an asymptotic trend with increasing θ. The variations in the optimum inspection interval are relatively smaller and vary from 0.5 years for θ = 0.1 to 0.75 years for θ = 4.

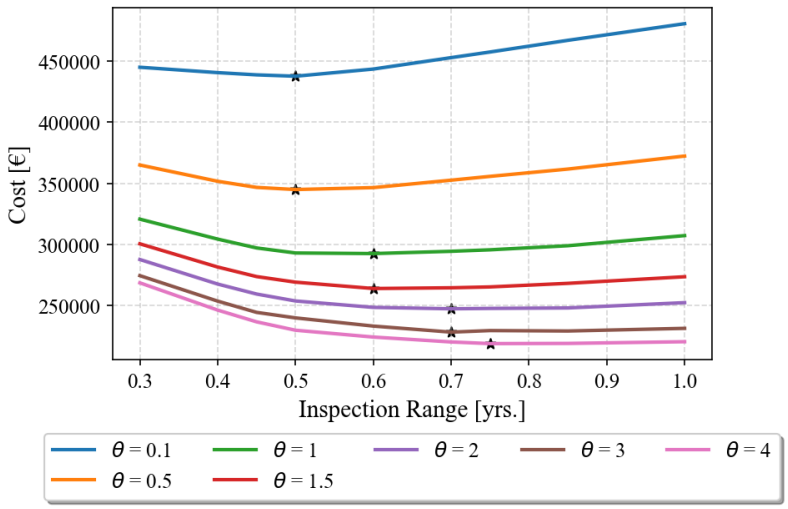

Figure 6.26: Variations in copula correlation coefficient - Lifetime costs vs. inspection interval plots

6.2.4.4. Reduction Factor

For the sensitivity study on the reduction factor, a single simulation is carried out. The initial assumed value of 2 is changed to 3 and the multiple FM dependent model is simulated. Figure 6.27 presents the variation of lifetime cost, downtime and cost breakdown with inspection interval. Compared to the initial assumption results shown in Figure 6.14 and Figure 6.16, a significant difference is observed. The optimum inspection interval reduces from 0.6 years to 0.35 years and corresponding lifetime costs increase by approximately 26% to € 368,800. This assumption is thus seen to be very critical to defining the degradation process and attempts must be made for its accurate estimation.

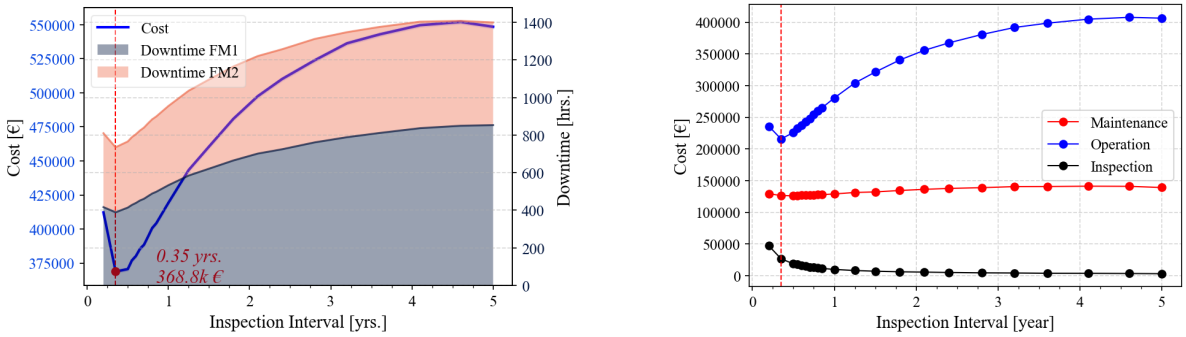

(a) Lifetime costs and downtime vs. inspection interval

(b) Cost breakdown vs. inspection interval

Figure 6.27: Higher reduction factor - Lifetime costs vs. inspection interval results

7
Conclusions

In order to meet the Net Zero scenario by 2050, large strides must be made for the growth of renewable energy in the world. An ambitious target of 1221 GW of new wind power capacity, with the majority being offshore wind, must be met before 2030. An important step towards this goal is the economic optimization across the entire process to reduce the LCOE of offshore wind energy. This study focuses on reducing O&M costs associated with offshore wind energy, which contribute to around a quarter of its total costs. This reduction is driven by the optimization of maintenance strategies in order to obtain the most economical approach. In this work, a degradation-based maintenance model is developed and various maintenance strategies are simulated. While studies implementing such models already exist, degradation dependence between multiple components is often ignored. Thus, for this study, a dependent degradation-based maintenance model is developed. For the application of the developed model, pitch systems are chosen due to high failure rates among Wind Turbine (WT) systems. The key conclusions derived for each of the research questions are presented here.

1. *How does the process of degradation occur in OWT pitch systems? Which are the most commonly occurring failure modes?*

   Extensive literature and studies conducting Failure Mode (FM) analysis and failure rate estimation are studied to answer the first research question. The main components and their layouts for both hydraulic and electric pitch systems are studied. Further, the forces applied to the system are also analysed to understand the cause of deterioration. Subsequently, the primary FMs are identified. They are motor failure, controller failure and power source failure for the electric system and valve joints wear, fluid leaks and fluid contamination, for hydraulic systems. Among the two, this work focuses on hydraulic pitch systems due to the difficulty of detecting deterioration in electric systems. An overall failure rate of 1.076 failures per year is obtained for the hydraulic pitch system. This is further broken down into 0.32 for fluid leakage and 0.26 for valve wear.

2. *How to model the degradation of a system across its entire lifetime?*

   A variety of methods exist to model the degradation of a system. For the application of this study, data-driven models are opted for due to their wide applicability, their ability to include uncertainties in degradation and to avoid detailed physical modelling. This allows the developed methodology to not be bound to WT pitch systems and is applicable even for the balance of system components. Within data-driven models, finite state continuous-time Markov chains are used as the basis for the degradation model. Such a model represents the system's health in terms of a finite number of states. The transition between the states represents degradation and is determined based on the input failure rate data. State transition diagrams are used to represent the entire process graphically. On top of the Markov chain, a Monte Carlo simulation is run multiple times to converge results. Based on the theory for both Markov processes and Monte Carlo simulations and the input failure rate data, a Monte Carlo Markov chain model is built in Python.

3. *How to model inspection and maintenance actions for a subsystem of an Offshore Wind Turbine (OWT)?*

   A maintenance model performs maintenance as per the input maintenance strategy and calculates the costs incurred by the inspection and maintenance actions. For this purpose, function

blocks for each process are created in Python. The Inspection function carries out the inspection process, detects the system state and calculates the Downtime (DT) for the action. With the input of the detected state, the Maintenance function carries out repair work and outputs the repaired state of the system. Along with this, the DT for the action is also accounted for. Both functions also call the Calculate Costs function. The Calculate Costs function calculates inspection costs, maintenance costs and operation costs. A variety of features are included in each of the blocks. For example, features of incorrect detection, incorrect repair or irreparable degradation, time delays from harsh weather conditions and lead time are included in the functions.

4. *How to incorporate a degradation model into an inspection and maintenance model and create a degradation-based maintenance model?*

   In order to analyse various maintenance strategies and find an optimum, an integrated degradation-based maintenance model is required. The two individual models discussed earlier are combined to form a degradation-based maintenance model to simulate both processes simultaneously for the lifetime of the system. Inspection and maintenance actions are modelled to occur at fixed inspection intervals. For each action, the incurred costs are calculated. Finally, the costs are summed up over a WT lifetime and compared for various strategies to determine an optimum.

5. *What is the optimum maintenance schedule for an OWT pitch system in the case of multiple independent FMs?*

   The multiple FM independent model simulates two FMs, fluid leakage and valve wear, independently. The FMs are only linked via the system state matrix which determines the overall health of the system based on the state of both degradation processes. In this case, the optimum inspection interval is 0.45 years which corresponds to the minimum total lifetime costs of € 478,716. A few differences are observed compared to the combined single FM simulations. The minimum cost is higher than the combined FM case by € 33,098. Further, the optimum inspection interval of 0.45 years is more frequent than that of 0.75 years for the combined case. This increase is attributed to the matrix, where the failure of a single FM declares the entire system to have failed, regardless of the other FM's state.

6. *How to introduce and model dependency between multiple failure modes in degradation models?*

   Among the many stochastic approaches available to model dependency, copula models are selected to represent degradation dependencies between FMs of the pitch system. Specifically, a Clayton copula is utilised for the exponential marginal distributions due to its lower-tail dependency. For dependant degradation modelling, the independent exponential distributions of the sojourn times for each FM are used as the marginal distributions. These distributions are combined with the Clayton copula to obtain a bivariate sojourn time distribution. This distribution is further used to draw random samples of the sojourn time values instead of the previously used independent exponential distributions.

7. *What are the impacts of modelling dependent degradation processes on the O&M strategy and costs for OWT pitch systems?*

   There is a significant difference in the model results depending on whether degradation dependency is taken into account, with an increase in the optimum inspection interval from 0.45 to 0.6 years. This translates to a lower frequency of OWT inspections accompanied by a decrease in the optimum lifetime costs. Lifetime costs decrease by € 186,285, or approximately 39%, from € 478,716 to € 292,431. This amounts to huge cost savings for the dependent case compared to the independent case. The large reduction in costs is driven mainly by the decrease in DT which subsequently brings down the operation costs. In terms of the physical degradation process, the reduction in DT and costs is attributed to the interaction between the individual processes which

increases the proximity between sojourn times for both. The increased proximity allows both processes to degrade and fail simultaneously, saving costs compared to failing independently.

8. *Which input parameters of the degradation-based maintenance model have the largest impact on O&M costs and strategy?*

   A sensitivity analysis is conducted for the parameters of deterioration rates, discount rates, costs of maintenance, labour, vessel and electricity and copula correlation coefficient. A variation of 10% in the discount rate and the cost of electricity is observed to have lifetime cost variations of approximately 6%. Comparatively, variations in degradation rate 2 and costs of maintenance do not affect the optimum as much. The copula correlation coefficient is seen to have very large variations from the optimum lifetime costs. Variations up to 50% are seen for the smaller values of the correlation coefficients.

7.1. Future Work

Based on the work carried out for this study, several key points for improvement have been identified.

1. Expansion of the model to an entire wind turbine or wind farm.

   In this study, the developed model is applied solely to two FMs of two different components of the hydraulic pitch system. While the optimum inspection interval is obtained for this system, this is not directly applicable to offshore wind farms as maintenance actions need to account for all WT components. The optimum inspection interval for pitch systems might not be the optimum for other WT systems. A model including all WT systems or even multiple WTs in a wind farm would be much more applicable. This can be achieved by developing an approach to construct a modified reliability block diagram or fault tree that can be combined with the copula model. This will be able to capture both multi-directional dependencies between components and the hierarchy of components within a system.

2. Accurate estimation of reduction factors and copula correlation coefficients for the creation of the multivariate distribution.

   The selection of the reduction factor is seen to strongly affect the degradation process. Further, defining the copula correlation coefficient is a critical step in determining the shape of the multivariate distribution. This shape then directly affects the sojourn times of the simulation and can have a large effect on the optimum inspection interval and lifetime cost. Due to a lack of degradation data and research on degradation dependencies between components, a rough estimate was used for both the parameters for this study. These parameters should be chosen based on the physical interactions of failure modes and establishing a methodology for their quantification would be an important step to making degradation dependency modelling more applicable.

3. Introduce variable inspection intervals to model a wider range of maintenance strategies.

   The model proposed in this thesis has the limitation of assuming a constant inspection interval throughout the WT lifetime. This restricts the user to adopting only one optimum maintenance strategy throughout the WT lifetime. On the other hand, allowing for a wider variety of maintenance strategies could lead to more optimum solutions. For example, within time-based strategies, multiple fixed strategies for each state of the system might output improved results.

4. Implementation of condition-based maintenance modelling techniques and integration with degradation dependency modelling.

   Condition-based monitoring techniques are an important area of current research. A condition-based model takes into account the current health of the system, the current and predicted

weather conditions and other similar uncertain parameters while planning each inspection or maintenance action. Integrating degradation dependencies into such a model would greatly aid in the process of optimising OWT maintenance strategies.

References

Abeygunwardane, S. K. (2012, December 27). *Probabilistic models for reliability assessment of ageing equipment and maintenance optimization* [Thesis] [Accepted: 2013-04-30T18:00:39Z]. Retrieved April 2, 2024, from https://scholarbank.nus.edu.sg/handle/10635/37555

Abid, K., Mouchaweh, M. S., & Cornez, L. (2019). Fault prognostics for the predictive maintenance of wind turbines: State of the art. In A. Monreale, C. Alzate, M. Kamp, Y. Krishnamurthy, D. Paurat, M. Sayed-Mouchaweh, A. Bifet, J. Gama, & R. P. Ribeiro (Eds.), *ECML PKDD 2018 workshops* (pp. 113–125). Springer International Publishing. https://doi.org/10.1007/978-3-030-14880-5_10

Adumene, S., & Okoro, A. (2020). A markovian reliability approach for offshore wind energy system analysis in harsh environments [_eprint: https://onlinelibrary.wiley.com/doi/pdf/10.1002/eng2.12128]. *Engineering Reports*, *2*(3), e12128. https://doi.org/10.1002/eng2.12128

Altman, D. G., & Bland, J. M. (2005). Statistics notes: Standard deviations and standard errors [Publisher: BMJ Publishing Group]. *BMJ : British Medical Journal*, *331*(7521), 903. https://doi.org/10.1136/bmj.331.7521.903

AnalystPrep. (2021, September 22). *Confidence intervals* [AnalystPrep | CFA® exam study notes] [Running Time: 2261]. Retrieved June 19, 2024, from https://analystprep.com/cfa-level-1-exam/quantitative-methods/confidence-intervals-2/

Andrawus, J., Watson, J., Kishk, M., & Adam, A. (2006). The selection of a suitable maintenance strategy for wind turbines. *Wind Engineering*, *30*. https://doi.org/10.1260/030952406779994141

Andrawus, J. A., Watson, J., & Kishk, M. (2007). Wind turbine maintenance optimisation: Principles of quantitative maintenance optimisation [Publisher: SAGE Publications]. *Wind Engineering*, *31*(2), 101–110. https://doi.org/10.1260/030952407781494467

Arzaghi, E., Abaei, M. M., Abbassi, R., O'Reilly, M., Garaniya, V., & Penesis, I. (2020). A markovian approach to power generation capacity assessment of floating wave energy converters. *Renewable Energy*, *146*, 2736–2743. https://doi.org/10.1016/j.renene.2019.08.099

Baker, M. (2022). *Most common causes of hydraulic systems failure* [YorkPMH]. Retrieved June 19, 2024, from https://yorkpmh.com/resources/common-hydraulic-system-problems/

Besnard, F., & Bertling, L. (2010). An approach for condition-based maintenance optimization applied to wind turbine blades [Conference Name: IEEE Transactions on Sustainable Energy]. *IEEE Transactions on Sustainable Energy*, *1*(2), 77–83. https://doi.org/10.1109/TSTE.2010.2049452

Bielecki, T., Vidozzi, A., & Vidozzi, L. (2008). A markov copulae approach to pricing and hedging of credit index derivatives and ratings triggered step-up bonds. *The Journal of Credit Risk*, *4*(1), 47–76. https://doi.org/10.21314/JCR.2008.068

Bolbolian, M. (2020). Relationship between kendall's tau correlation and mutual information. *Revista Colombiana de Estadística*, *43*, 3–20. https://doi.org/10.15446/rce.v43n1.78054

Byon, E., & Ding, Y. (2010). Season-dependent condition-based maintenance for a wind turbine using a partially observed markov decision process [Conference Name: IEEE Transactions on Power Systems]. *IEEE Transactions on Power Systems*, *25*(4), 1823–1834. https://doi.org/10.1109/TPWRS.2010.2043269

Carroll, J., McDonald, A., & McMillan, D. (2016). Failure rate, repair time and unscheduled o&m cost analysis of offshore wind turbines. *Wind Energy*, *19*(6), 1107–1119. https://doi.org/10.1002/we.1887

Carvalho, M., Nunes, E., & Telhada, J. (2013). Maintenance costs of a pitch control device of a wind turbine.

Chang, Y., & Mosleh, A. (2017). Physics-based model of the degradation of cable insulation subject to radiation and heat. *2017 IEEE Conference on Electrical Insulation and Dielectric Phenomenon (CEIDP)*, 145–148. https://doi.org/10.1109/CEIDP.2017.8257450

Climate Brief. (2020). Guest post: A brief history of climate targets and technological promises. https://www.carbonbrief.org/guest-post-a-brief-history-of-climate-targets-and-technological-promises/ Accessed: 22.02.2024.

Columbia. (2016, August 5). *Markov chain monte carlo* [Columbia university mailman school of public health]. Retrieved June 12, 2024, from https://www.publichealth.columbia.edu/research/population-health-methods/markov-chain-monte-carlo

Dao, C., Kazemtabrizi, B., & Crabtree, C. (2019). Wind turbine reliability data review and impacts on levelised cost of energy [_eprint: https://onlinelibrary.wiley.com/doi/pdf/10.1002/we.2404]. *Wind Energy*, *22*(12), 1848–1871. https://doi.org/10.1002/we.2404

Dao, C. D., Kazemtabrizi, B., Crabtree, C. J., & Tavner, P. J. (2021). Integrated condition-based maintenance modelling and optimisation for offshore wind turbines. *Wind Energy*, *24*(11), 1180–1198. https://doi.org/10.1002/we.2625

De Nie, R. C. (2016). Maintenance optimization of tidal energy arrays: Design of a probabilistic decision support tool for optimizing the maintenance policy. Retrieved June 12, 2024, from https://repository.tudelft.nl/islandora/object/uuid%3A1f228e88-c7e7-431d-96af-df1abb195edd

Díaz, H., & Guedes Soares, C. (2020). Review of the current status, technology and future trends of offshore wind farms. *Ocean Engineering*, *209*. https://doi.org/10.1016/j.oceaneng.2020.107381

El-Henaoui, S. (2009). When the wind blows. Retrieved June 15, 2024, from https://www.moog.com/literature/ICD/Moog_WindArticle_ENGLISH_1July09.pdf

European Council. (2024a). *Clean energy*. https://www.consilium.europa.eu/en/policies/clean-energy/ Accessed: 22.02.2024.

European Council. (2024b). *Climate change: What the eu is doing*. https://www.consilium.europa.eu/en/policies/climate-change/ Accessed: 22.02.2024.

Financial Wisdom Forum. (2010). *Copulas*. https://www.financialwisdomforum.org/gummy-stuff/copulas-3.htm Accessed: 28.06.2024.

FinRGB. (2023). *Correlations and copulas*. https://www.finrgb.com/uncategorized/correlations-copulas/ Accessed: 22.06.2024.

Gayo, J. B. (2011). Reliability-focused research on optimizing wind energy system design, operation and maintenance: Tools, proof of concepts, guidelines & methodologies for a new generation. Retrieved March 4, 2024, from https://cordis.europa.eu/docs/results/212/212966/110513-reliawind-final-publishable-summary-to-ec.pdf

Goldinlocks. (2016). *Linear and nonlinear correlations*. Retrieved June 19, 2024, from https://goldinlocks.github.io/Comparing-Linear-and-Nonlinear-Correlations/

Government of the Netherlands. (2020). *Offshore wind energy*. https://www.government.nl/topics/renewable-energy/offshore-wind-energy#:~:text=In%202022%20and%202023%2C%20the,cables%2C%20i.e.%20the%20offshore%20grid. Accessed: 23.02.2024.

GWEC. (2023). *Global wind report 2023*. https://gwec.net/globalwindreport2023/ Accessed: 22.02.2024.

Haring, M. R. (2018, July 11). *Optimal maintenance planning using reliability information for offshore wind turbines* [Doctoral dissertation, Uiniversity of Twente]. Retrieved January 5, 2024, from https://essay.utwente.nl/76863/1/Haring_BA_BMS.pdf

Havtil. (2024, July 2). *Facts: Offshore wind power* [Havtil - norwegian ocean industry authority]. Retrieved June 19, 2024, from https://www.havtil.no/en/about-us/role-and-area-of-responsibility/facts-offshore-wind-power/

Hayes, A. (2024, March 19). *Coefficient of variation: Meaning and how to use it* [Investopedia]. Retrieved June 19, 2024, from https://www.investopedia.com/terms/c/coefficientofvariation.asp

Healy, L. (2020, February 16). *Copulas in python* [Kaggle]. Retrieved June 21, 2024, from https://kaggle.com/code/liamhealy/copulas-in-python

Herman, E., Stewart, A., & Rand, E. (2022, October 26). *Statistical analysis for public health: Statistical thinking (version 0.1.0)* [The carpentries incubator]. Retrieved June 1, 2024, from https://carpentries-incubator.github.io/statistical-thinking-public-health/02-estimation/index.html

HPS. (2023, March 15). *HPS troubleshooting tactics: Common hydraulic valve issues* [Hydraulic parts source]. Retrieved June 19, 2024, from https://hydraulicpartssource.sites.aes2.com/blog_post/hps-troubleshooting-tactics-common-hydraulic-valve-issues

Ibe, O. C. (2014, January 1). Chapter 6 - functions of random variables. In O. C. Ibe (Ed.), *Fundamentals of applied probability and random processes (second edition)* (pp. 185–223). Academic Press. https://doi.org/10.1016/B978-0-12-800852-2.00006-7

IEA. (2023a). *Renewable power on course to shatter more records as countries around the world speed up deployment*. https://www.iea.org/news/renewable-power-on-course-to-shatter-more-records-as-countries-around-the-world-speed-up-deployment Accessed: 22.02.2024.

IEA. (2023b). *Tripling renewable power capacity by 2030 is vital to keep the 1.5°c goal within reach*. https://www.iea.org/commentaries/tripling-renewable-power-capacity-by-2030-is-vital-to-keep-the-150c-goal-within-reach Accessed: 22.02.2024.

Jiang, Z., Karimirad, M., & Moan, T. (2014). Dynamic response analysis of wind turbines under blade pitch system fault, grid loss, and shutdown events. *Wind Energy*, *17*(9), 1385–1409. https://doi.org/10.1002/we.1639

Kececioglu, D., & Jacks, J. A. (1984). The arrhenius, eyring, inverse power law and combination models in accelerated life testing. *Reliability Engineering*, *8*(1), 1–9. https://doi.org/10.1016/0143-8174(84)90032-5

Kerres, B., Fischer, K., & Madlener, R. (2015). Economic evaluation of maintenance strategies for wind turbines: A stochastic analysis [_eprint: https://onlinelibrary.wiley.com/doi/pdf/10.1049/iet-rpg.2014.0260]. *IET Renewable Power Generation*, *9*(7), 766–774. https://doi.org/10.1049/iet-rpg.2014.0260

KPMG. (2019, October). *The socioeconomic impacts of wind energy in the context of the energy transition*. https://assets.kpmg.com/content/dam/kpmg/dk/pdf/DK-2019/11/The-socioeconomic-impacts-of-wind-energy_compressed.pdf

Laggoune, R., Chateauneuf, A., & Aissani, D. (2010). Impact of few failure data on the opportunistic replacement policy for multi-component systems. *Reliability Engineering & System Safety*, *95*(2), 108–119. https://doi.org/10.1016/j.ress.2009.08.007

Le, B., & Andrews, J. (2016). Modelling wind turbine degradation and maintenance. *Wind Energy*, *19*(4), 571–591. https://doi.org/10.1002/we.1851

Lee, Y.-b., Lee, G.-c., Yang, J.-d., Park, J.-w., & Baek, D.-c. (2020). Failure analysis of a hydraulic power system in the wind turbine. *Engineering Failure Analysis*, *107*, 104218. https://doi.org/10.1016/j.engfailanal.2019.104218

Li, H., Guedes Soares, C., & Huang, H.-Z. (2020). Reliability analysis of a floating offshore wind turbine using bayesian networks. *Ocean Engineering*, *217*, 107827. https://doi.org/10.1016/j.oceaneng.2020.107827

Li, J., Zhang, X., Zhou, X., & Lu, L. (2019). Reliability assessment of wind turbine bearing based on the degradation-hidden-markov model. *Renewable Energy*, *132*, 1076–1087. https://doi.org/10.1016/j.renene.2018.08.048

Li, N., Xu, P., Lei, Y., Cai, X., & Kong, D. (2022). A self-data-driven method for remaining useful life prediction of wind turbines considering continuously varying speeds. *Mechanical Systems and Signal Processing*, *165*, 108315. https://doi.org/10.1016/j.ymssp.2021.108315

Li, W., & Pham, H. (2005). Reliability modeling of multi-state degraded systems with multi-competing failures and random shocks [Conference Name: IEEE Transactions on Reliability]. *IEEE Transactions on Reliability*, *54*(2), 297–303. https://doi.org/10.1109/TR.2005.847278

Li, Y., Bai, X., Shi, S., & Wang, S. (2021). Dynamic fatigue reliability analysis of transmission gear considering failure dependence [Publisher: Tech Science Press]. *Computer Modeling in Engineering & Sciences*, *130*(2), 1077–1092. https://doi.org/10.32604/cmes.2022.018181

Lin, Y.-H., & Ding, Z.-Q. (2022). An integrated degradation modeling framework considering model uncertainty and calibration. *Mechanical Systems and Signal Processing*, *166*, 108389. https://doi.org/10.1016/j.ymssp.2021.108389

Lutkevich, B. (2023, March). *Monte carlo simulation* [Cloud computing]. Retrieved June 16, 2024, from https://www.techtarget.com/searchcloudcomputing/definition/Monte-Carlo-simulation

Lyu, H., Qu, H., Xie, H., Zhang, Y., & Pecht, M. (2023). Reliability analysis of the multi-state system with nonlinear degradation model under markov environment. *Reliability Engineering & System Safety*, *238*, 109411. https://doi.org/10.1016/j.ress.2023.109411

Mammadov, I. (2024). *Wind turbine main bearing degradation monitoring using physics-based analysis of scada data* [Master thesis - tu delft repository].

MATLAB. (2019). *Estimating remaining useful life (rul) | predictive maintenance*. https://www.youtube.com/watch?v=Dd_4rbWYgI4&t=430s accessed: 12.01.2024.

McMorland, J., Collu, M., McMillan, D., & Carroll, J. (2022). Operation and maintenance for floating wind turbines: A review. *Renewable and Sustainable Energy Reviews*, *163*, 112499. https://doi.org/10.1016/j.rser.2022.112499

Meango, T. J.-M., & Ouali, M.-S. (2018). Failure interaction models for multicomponent systems: A comparative study. *SN Applied Sciences*, *1*(1), 66. https://doi.org/10.1007/s42452-018-0063-2

Meyer, J. (2022, September 6). *How the population distribution influences the confidence interval* [The analysis factor]. Retrieved June 19, 2024, from https://www.theanalysisfactor.com/how-population-distribution-impacts-confidence-interval/

Nelsen, R. (2006). *An introduction to copulas*. Springer. https://doi.org/10.1007/0-387-28678-0

NREL. (2022). *2022 cost of wind energy review*. https://www.nrel.gov/docs/fy24osti/88335.pdf Accessed: 29.02.2024.

Oakley, J. L., Wilson, K. J., & Philipson, P. (2022). A condition-based maintenance policy for continuously monitored multi-component systems with economic and stochastic dependence. *Reliability Engineering & System Safety*, *222*, 108321. https://doi.org/10.1016/j.ress.2022.108321

Olde Keizer, M. C. A., Flapper, S. D. P., & Teunter, R. H. (2017). Condition-based maintenance policies for systems with multiple dependent components: A review. *European Journal of Operational Research*, *261*(2), 405–420. https://doi.org/10.1016/j.ejor.2017.02.044

Orcel, O., Sergent, P., & Ropert, F. (2021). Trivariate copula to design coastal structures [ADS Bibcode: 2021NHESS..21..239O]. *Natural Hazards and Earth System Sciences*, *21*, 239–260. https://doi.org/10.5194/nhess-21-239-2021

Ossai, C. I., Boswell, B., & Davies, I. J. (2016). A markovian approach for modelling the effects of maintenance on downtime and failure risk of wind turbine components. *Renewable Energy*, *96*, 775–783. https://doi.org/10.1016/j.renene.2016.05.022

Padman, P., Xu, J., Vanni, F., Echavarria, E., & Wilkinson, M. (2016). *The effect of pitch system reliability on wind power generation's levelized cost of energy*. Retrieved April 2, 2024, from https://windeurope.org/summit2016/conference/allfiles2/582_WindEurope2016presentation.pdf

Pishro-Nik, H. (2014). *Introduction to probability, statistics, and random processes*. Retrieved June 8, 2024, from https://www.probabilitycourse.com/

Privault, N. (2018). *Understanding markov chains: Examples and applications*. Springer Singapore. https://doi.org/10.1007/978-981-13-0659-4

Ren, Z., Verma, A. S., Li, Y., Teuwen, J. J. E., & Jiang, Z. (2021). Offshore wind turbine operations and maintenance: A state-of-the-art review. *Renewable and Sustainable Energy Reviews*, *144*, 110886. https://doi.org/10.1016/j.rser.2021.110886

Reuters. (2023). *Climate on track to warm by nearly 3c without aggressive actions, un report finds*. https://www.reuters.com/sustainability/climate-energy/climate-track-warm-by-nearly-3c-without-greater-ambition-un-report-2023-11-20/#:~:text=climate%20summit%20COP28%20with%20the,1.5C%20(2.7F). Accessed: 22.02.2024.

Ross, S. M. (2014). *Introduction to probability models* (Eleventh edition). Elsevier.

Sari, J. ((2008). Multivariate degradation modelling and its application to reliability testing [Publisher: [object Object]]. https://doi.org/10.6100/IR637589

Schwarzkopf, M., Borisade, F., Espelage, J., & Johnston, E. (2021, August 31). *Floating wind o&m strategies assessment* (Corewind D4.2). Ramboll / Cobra / Equinor / Esteyco / FIHAC. Retrieved May 17, 2024, from https://corewind.eu/wp-content/uploads/files/publications/COREWIND-D4.2-Floating-Wind-O-and-M-Strategies-Assessment.pdf

Shafiee, M., & Sørensen, J. D. (2019). Maintenance optimization and inspection planning of wind energy assets: Models, methods and strategies. *Reliability Engineering & System Safety*, *192*, 105993. https://doi.org/10.1016/j.ress.2017.10.025

Shahraki, A. F., Yadav, O. P., Liao, & Haitao. (2017). A review on degradation modelling and its engineering applications. *International Journal of Performability Engineering*, *13*(3), 299. https://doi.org/10.23940/ijpe.17.03.p6.299314

Shen, J., Hu, J., & Ma, Y. (2020). Two preventive replacement strategies for systems with protective auxiliary parts subject to degradation and economic dependence. *Reliability Engineering & System Safety*, *204*, 107144. https://doi.org/10.1016/j.ress.2020.107144

Singh, C., & Billinton, R. (1977). *System reliability modelling and evaluation* (First). Hutchinson & Co. Retrieved June 11, 2024, from https://chanansingh.engr.tamu.edu/system-reliability-modelling-and-evaluation/

Smith, A. (2022, June 19). *UK offshore wind capacity factors* [Energy numbers]. Retrieved June 19, 2024, from https://energynumbers.info/uk-offshore-wind-capacity-factors

Thomas, E. (2024, March 18). *Wind turbines are ageing – what happens next?* [Power technology]. Retrieved June 19, 2024, from https://www.power-technology.com/features/wind-turbines-are-ageing-what-happens-next/

UN Chronicle. (2007). From stockholm to kyoto: A brief history of climate change. https://www.un.org/en/chronicle/article/stockholm-kyoto-brief-history-climate-change Accessed: 22.02.2024.

UNFCCC. (2021). *The paris agreement*. https://unfccc.int/process-and-meetings/the-paris-agreement Accessed: 22.02.2024.

UNFCCC. (2023a). *Cop 28: What was achieved and what happens next?* https://unfccc.int/cop28/5-key-takeaways#end-of-fossil-fuels Accessed: 22.02.2024.

UNFCCC. (2023b). *Un climate change executive secretary at cop28 closing*. https://unfccc.int/news/we-didn-t-turn-the-page-on-the-fossil-fuel-era-but-this-outcome-is-the-beginning-of-the-end-un Accessed: 22.02.2024.

Veers, P., Bottasso, C. L., Manuel, L., Naughton, J., Pao, L., Paquette, J., Robertson, A., Robinson, M., Ananthan, S., Barlas, T., Bianchini, A., Bredmose, H., Horcas, S. G., Keller, J., Madsen, H. A., Manwell, J., Moriarty, P., Nolet, S., & Rinker, J. (2023). Grand challenges in the design, manufacture, and operation of future wind turbine systems. *Wind Energy Science*, *8*(7), 1071–1131. https://doi.org/10.5194/wes-8-1071-2023

Veers, P., Dykes, K., Lantz, E., Barth, S., Bottasso, C. L., Carlson, O., Clifton, A., Green, J., Green, P., Holttinen, H., Laird, D., Lehtomäki, V., Lundquist, J. K., Manwell, J., Marquis, M., Meneveau, C., Moriarty, P., Munduate, X., Muskulus, M., … Wiser, R. (2019). Grand challenges in the science of wind energy [Publisher: American Association for the Advancement of Science]. *Science*, *366*(6464), eaau2027. https://doi.org/10.1126/science.aau2027

Walgern, J., Fischer, K., Hentschel, P., & Kolios, A. (2023). Reliability of electrical and hydraulic pitch systems in wind turbines based on field-data analysis. *Energy Reports*, *9*, 3273–3281. https://doi.org/10.1016/j.egyr.2023.02.007

Wang, P., & Coit, D. W. (2004). Reliability prediction based on degradation modeling for systems with multiple degradation measures [ISSN: 0149-144X]. *Proceedings of the Annual Reliability and Maintainability Symposium*, 302–307. Retrieved May 17, 2024, from https://www.researchwithrutgers.com/en/publications/reliability-prediction-based-on-degradation-modeling-for-systems-

Wang, Y., & Pham, A. (2012). Modeling the dependent competing risks with multiple degradation processes and random shock using time-varying copulas. *IEEE Transactions on Reliability - TR*, *61*, 13–22. https://doi.org/10.1109/TR.2011.2170253

Wang, Z., Wang, R., Deng, W., & Zhao, Y. (2022). An integrated approach-based FMECA for risk assessment: Application to offshore wind turbine pitch system [Number: 5 Publisher: Multidisciplinary Digital Publishing Institute]. *Energies*, *15*(5), 1858. https://doi.org/10.3390/en15051858

Wei, L., Qian, Z., Zareipour, H., & Zhang, F. (2022). Comprehensive aging assessment of pitch systems combining SCADA and failure data. *IET Renewable Power Generation*, *16*(1), 198–210. https://doi.org/10.1049/rpg2.12281

Welte, T. M., Vatn, J., & Heggset, J. (2006). Markov state model for optimization of maintenance and renewal of hydro power components. *2006 International Conference on Probabilistic Methods Applied to Power Systems*, 1–7. https://doi.org/10.1109/PMAPS.2006.360311

Welte, T. M., Sperstad, I. B., Halvorsen-Weare, E. E., Netland, Ø., Nonås, L. M., & Stålhane, M. (2018, May 11). *Operation and maintenance modelling* [Wiley online library] [Pages: 269-303 Publisher: John Wiley & Sons, Ltd]. Retrieved March 4, 2024, from https://onlinelibrary.wiley.com/doi/abs/10.1002/9781119097808.ch7

Wikipedia. (2024). *Copula (probability theory)*. https://en.wikipedia.org/wiki/Copula_(probability_theory) Accessed: 15.04.2024.

WWEA. (2024). *Wwea annual report 2023: Record year for windpower*. https://wwindea.org/AnnualReport2023#:~:text=Bonn%20(WWEA)%20%E2%80%93%20The%20year,year%2C%20more%20than%20ever%20before. Accessed: 31.07.2024.

Zaaijer, M., & Viré, A. (2022, September 28). *Introduction to wind turbines: Physics and technology*.

Zeng, Z., Barros, A., & Coit, D. (2023). Dependent failure behavior modeling for risk and reliability: A systematic and critical literature review. *Reliability Engineering & System Safety*, *239*, 109515. https://doi.org/10.1016/j.ress.2023.109515

Zhang, F., Dai, J., Liu, D., Li, L., & Long, X. (2019). Investigation of the pitch load of large-scale wind turbines using field SCADA data [Number: 3 Publisher: Multidisciplinary Digital Publishing Institute]. *Energies*, *12*(3), 509. https://doi.org/10.3390/en12030509

Zheng, Y., Wei, J., Zhu, K., & Dong, B. (2020). Reliability analysis assessment of the wind turbines system under multi-dimensions [Publisher: SAGE Publications Ltd]. *Advanced Composites Letters*, *29*, 2633366X20966337. https://doi.org/10.1177/2633366X20966337

Zhou, H., Dahlem, E., & Schmitt, A. (2023, December 4). *EU energy outlook to 2060: Power prices and revenues predicted for wind, solar, gas, hydrogen + more* [Energy post]. Retrieved June 20, 2024, from https://energypost.eu/eu-energy-outlook-to-2060-power-prices-and-revenues-predicted-for-wind-solar-gas-hydrogen-more/

A
Appendix A

A.1. Implementation of Alternative Copula

To understand the impact of choosing a different copula for the multiple FM dependent model, the upper-tail dependent Gumbel copula with a correlation coefficient of $\theta \to 1^+$ is implemented. Figure A.1 shows the results of lifetime cost and downtime for the inspection interval range.

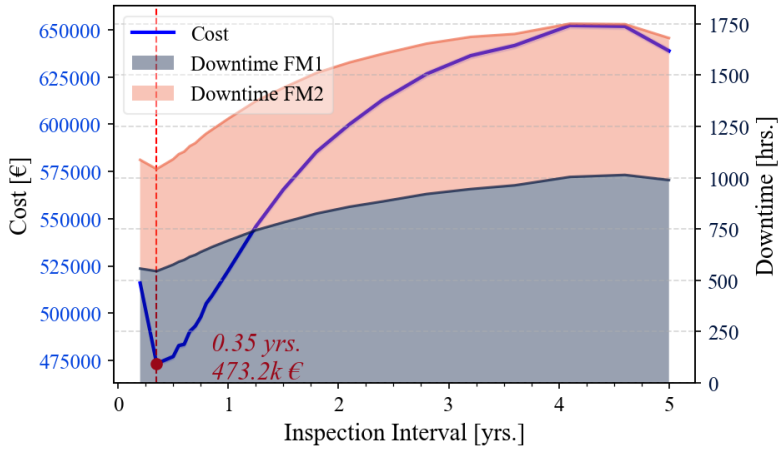

Figure A.1: Implementation of Gumbel copula - Lifetime cost and downtime vs. inspection interval plots

The results show that using an upper-tail dependent copula for an exponential distribution outputs equivalent results to the multiple FM independent model presented in Figure 6.12. The same inspection interval of 0.35 years with a difference of approximately € 5000 in corresponding minimum lifetime costs is obtained. Since exponential distributions have very small probabilities close to their upper tail, this is equivalent to incorporating no dependency between the sojourn times.

A.2. Implementation of Seasonality

As discussed in Section 5.2.2, the effects of seasonality on the results are presented here. Seasonality is accounted for in the model by varying the capacity factors, weather windows and inspection durations for two seasons, summer and winter. Lifetime costs are plotted against inspection intervals and presented in Figure A.2. Figure A.2a uses averaged values of the capacity factor, weather window and inspection durations and Figure A.2b uses varied values for each season. The blue cost curve in Figure A.2a is also visible as the black mean cost curve in Figure A.2b. The black curve is the mean of two curves, the dashed green line showing simulations starting in the summer and the dashed blue line showing simulations starting in the winter. Thus, to implement seasonality, dependency on the start time is also introduced.

Another drawback of this implementation was the limited number of seasons simulated. With just two seasons, the optimum inspection interval was always in the summer. This would output a straightforward maintenance strategy of inspections once a year in the summer. Further, the simulation of many seasons takes a large simulation time. Since using the averaged values of the parameters from the beginning provided the same results, the feature of seasonality was removed from the model.

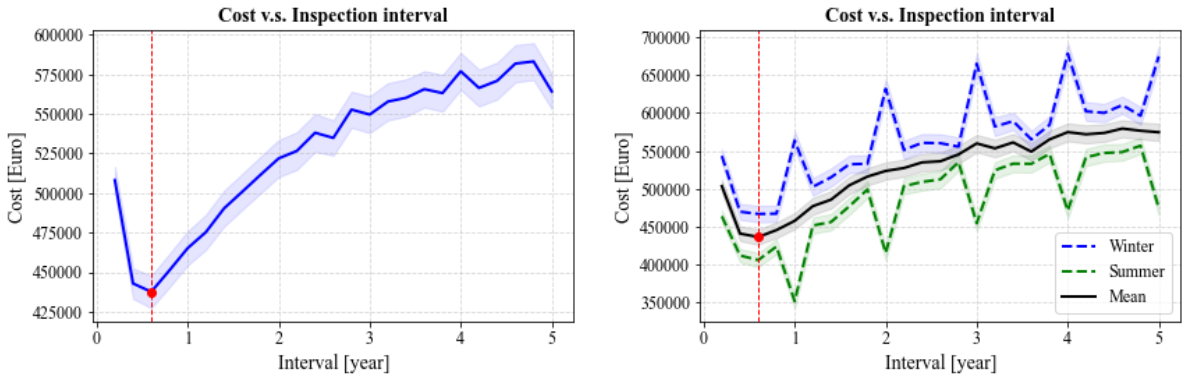

(a) Averaged seasonal parameters

(b) Varied seasonal parameters

Figure A.2: Implementation of seasonality- Lifetime costs vs. inspection interval

A.3. Implementation of the Independence Copula

The comparison of the Clayton copula with the Independence copula in Section 6.2.2.2 depends on the likelihood between the multiple FM dependent model implemented with the Independence copula and the multiple FM independent model. Figure A.3 compares the results of lifetime cost and downtime for the inspection interval range for both cases.

A very good match between both results is obtained. The same optimum inspection interval of 0.35 years with a difference in minimum lifetime costs of € 5100 is observed. This variation in costs is barely 1.06% of the optimum lifetime cost. Further, the downtime for both cases is also observed to match closely with each other.

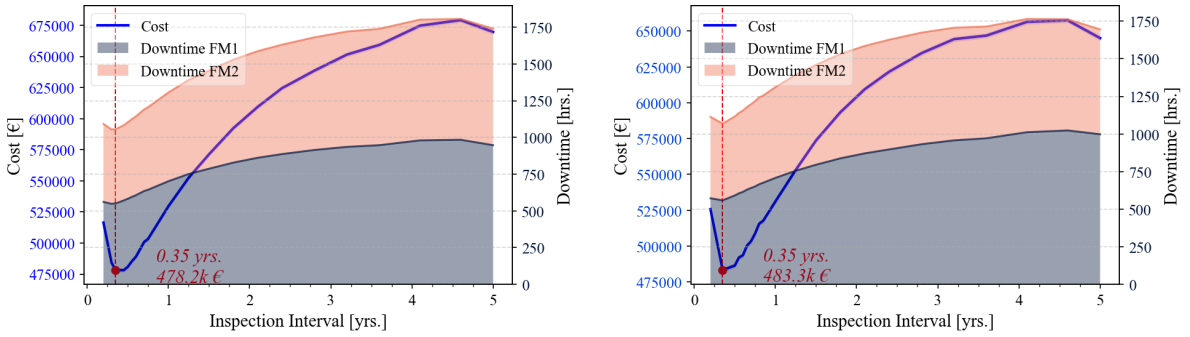

(a) Multiple independent FM model

(b) Multiple dependent FM model - Independence Copula

Figure A.3: Comparison of a) independent model and b) dependent model with Independence copula results - Lifetime costs and downtime vs. inspection interval

This result successfully proves the creation of one generalized model which can simulate both dependent as well as independent failure modes.